The Dissertation Committee for Almas Aitkulov Certifies that this is the approved version of the following dissertation:

Two-Dimensional Study of Chemical Floods for Viscous Oils

Committee:

Kishore K. Mohanty, Supervisor

Gary A. Pope

Mojdeh Delshad

Kamy Sepehrnoori

Marc A. Hesse

Two-Dimensional Study of Chemical Floods for Viscous Oils

by

Almas Aitkulov

Dissertation

Presented to the Faculty of the Graduate School of

The University of Texas at Austin

in Partial Fulfillment

of the Requirements

for the Degree of

Doctor of Philosophy

The University of Texas at Austin

December 2017

Dedication

Dedicated to my parents and my little sister for their love and support throughout my life.

АЛҒА, ҚАЗАҚСТАН!

ALGA, QAZAQSTAN!

Acknowledgements

I would like to express my sincere thanks to my supervisor, Dr. Kishore K. Mohanty for his tremendous support and constant encouragement throughout my studies at the University of Texas at Austin. He has been my professor, supervisor and mentor for 7 years, and supported me like no other. I sincerely thank him for believing in me and my abilities.

I would like to thank Dr. Gary Pope and his research group for their help and valuable advice on this project. One of the main reasons I decided to pursue PhD was your EOR class! I would like to thank Dr. Kamy Sepehrnoori for his support and friendship during my studies. I want to thank Dr. Delshad and Dr. Hesse for their advices and tremendous questions that I have not thought before. I sincerely would like to thank Dr. Lake and Dr. Olson for their support and care throughout my time at The University of Texas at Austin. I thank UT Chemical EOR Industrial Affiliate Project for partial funding of this work.

I want to give special thanks to Barbara Messmore for her help and friendship. I thank my colleagues from Dr. Mohanty's research group for their help and cooperation. I thank Glen Baum, Gary Miscoe and Daryl Nygaard for helping me with equipment. I would like to thank Yu Liang and Jose Parra for their friendship and brotherly support. I especially want to thank Sedef Kocakaplan for her friendship and support during my PhD. Finally I would like to thank my parents, my sister and all my friends for providing me the strength and moral support I always needed for getting me through a very special phase of my life.

Two-Dimensional Study of Chemical Floods for Viscous Oils

Almas Aitkulov, Ph.D
The University of Texas at Austin, 2017

Supervisor: Kishore Mohanty

There is a vast deposit of viscous and heavy oil especially in US North Slope, Canada and Venezuela. Typically, waterflood and thermal methods are used to recover viscous oil. However, waterflood is not very efficient because the water fingers through the oil due to adverse viscosity and thermal methods are inefficient when the depth of the reservoir is high and pay thickness is low. Non-thermal chemical enhanced-oil-recovery (EOR) methods are being developed as alternatives.

The alkaline-surfactant-polymer (ASP) flood has been shown in the past to reduce residual oil saturation to almost zero for light oils. In addition to ASP, a new low-cost chemical EOR technology called alkali-cosolvent-polymer (ACP) flooding has been developed which does not use any synthetic surfactant. ASP/ACP floods for light oils are designed to be stable where the mobility ratio of the oil bank to the ASP slug is kept close to one. For viscous oils, such stable recovery processes may be unreasonably slow due higher oil viscosity. The goal of this work is to study unstable ASP and ACP flooding (i.e., oil to ASP/ACP slug mobility ratio < 1) in secondary and tertiary modes.

ASP/ACP formulations that achieve ultra-low tension were developed. Since achieving high sweep efficiency is challenging in viscous oil reservoirs, ASP/ACP floods were studied in a quarter 5-spot lab model. This research is the first of a kind ASP/ACP study in a multidimensional medium. There are currently no published work available that focuses on studying ASP and ACP in a two-dimensional porous medium. Experimental results were numerically simulated and matched using an in-house simulator UTCHEM. The results of the experiments indicate that tertiary ASP/ACP flood with oil to ASP/ACP slug viscosity ratio between 2 to 4 could recover more than 80% of the oil with a reasonable pressure gradient. This unfavorable mobility of the chemical slug is beneficial considering both oil recovery and pressure drop. The timing of the start of the tertiary flood did not change the cumulative oil recovery very much. However, a shorter waterflood resulted in an earlier oil recovery.

It has been observed in field tests that ASP flooding after polymer flooding is quite effective. It is impossible to compare the effectiveness of ASP floods after polymer floods to ASP floods after waterfloods in the same reservoir. This comparison has been conducted here in a heterogeneous quarter 5-spot, where one half of the sand pack is 10 times more permeable than the other half. One side of the quarter 5-spot model was built to be transparent. The interaction of sweep efficiency and displacement efficiency of ASP flooding was studied through visual observations. The experiments demonstrated that the cumulative oil recovery for the polymer flood-ASP flood combination is significantly higher than that for the waterflood-ASP flood combination. The incremental recovery

efficiencies due to ASP floods are similar for both the cases. Most of the benefit comes from the higher sweep efficiency of the polymer flood over that of the waterflood.

Table of Contents

List of Tables

List of Figures

CHAPTER 1: INTRODUCTION

1.1 Statement of the Problem

Canada, Venezuela, and the United States (US) are countries that have large deposits of viscous and heavy oil. The US Department of Energy estimates that US has around 100 billion barrels of recoverable viscous and heavy oil deposits (DOE, June 2007). The North Slope of Alaska alone contains at least 20 billion barrels of viscous to heavy oil (Hallam and Piekenbrock 1992). The abundance of viscous oil deposits around the world motivates the development of effective recovery methods for viscous oils.

Thermal methods are commonly used for the recovery of viscous to heavy oil. By heating the oil in situ, viscosity can be decreased, and thus, can enable oil to move easier. Thermal methods such as steam flooding, SAGD, etc. are most popular in many reservoirs with thick pay zone and shallow depth. However, when the depth of the reservoir is high and pay thickness is low, thermal methods are inefficient. Furthermore, in a North Slope thermal methods may cause melting of permafrost which would be an environmental hazard (Peyton, 1970). Non-thermal methods can be alternatively used in these situations. A simple non-thermal method such as waterflooding is not efficient in the recovery of viscous oils. During viscous oil displacement, the oil water interface becomes unstable due to significant difference in viscosities of water and oil. Instability at the interface causes water penetrate into more viscous oil in shapes that look like 'fingers' (Engelberts and Klinkenberg, 1951; Van Meurs,1957, Saffman and Taylor, 1958; Chuoke et.al., 1958; De Haan, 1959; Rachford,1964; Peters and Flock,1981; Bentsen and Saeedi, 1981; Riaz and Tchelepi, 2006; Doorwar and Mohanty, 2010, 2015; Luo et. al., 2016; Worawutthichanyakul and Mohanty, 2017). Due to viscous fingering, most of the oil is bypassed and left unrecovered. The chemical

enhanced oil recovery (CEOR) methods can improve oil recovery by increasing both displacement and volumetric sweep efficiencies.

Polymer floods can improve sweep efficiency. Alkaline-surfactant-polymer (ASP) and alkaline-cosolvent-polymer (ACP) floods can improve the oil recovery by increasing capillary number and decreasing mobility ratio at the same time. Thus, both sweep efficiency and displacement efficiency are affected during ASP/ACP floods. Up to now, the displacement efficiency during ASP/ACP floods has been studied and understood very well. However, one of the key aspects of viscous oil recovery is the sweep efficiency of the displacement process, which has not been investigated extensively.

1.2 Research Objectives

ASP or ACP floods can be made more stable by adding enough polymer. Then, the sweep efficiency and the ultimate recovery would be high, but the injection rate would be low because the injection fluid would be very viscous. If only a small amount of polymer is used, then the injection rate would be high, but the sweep efficiency would be low. Thus, these floods should be evaluated as a function of polymer concentration or chemical slug viscosity. Since the sweep efficiency is affected, the formulations should be tested in multi-dimensional porous media (not just core floods). One of the objectives of this research is to perform ASP/ACP floods in a laboratory quarter 5-spot model for a viscous oil and study sweep efficiency and pressure drop as a function of chemical slug viscosity.

Injection rates in viscous oil reservoirs are often limited by small inter-well pressure drops (500-1000 psi) and high oil viscosities. Since not many pore volumes of fluids (about 1-2 PV) can be injected into a viscous oil reservoir (during its project life of about 30-50 year), one key question is the optimum time to start the ASP/ACP flood. If the ASP/ACP flood is started early, then the

injection rate may be too low. If it is started late, then there may be little time to push the oil out during the reservoir life. Another objective of this research is to investigate the effect of the starting time of ASP/ACP floods in viscous oil reservoirs on oil recovery during the project life.

Alkaline-surfactant-polymer (ASP) flooding is an effective technique to improve oil recovery. It has been applied typically after a water flood. Recently, there has been a successful field test where an ASP flood was conducted after a polymer flood. Is the ASP flood after a polymer flood more effective than an ASP flood after a water flood? It is difficult to conduct this experiment in exactly the same location in a field. Another goal of this study was to answer this question in a laboratory heterogeneous quarter 5-spot model.

1.3 Outline of the Dissertation

This dissertation consists of 7 chapters. The first chapter describes statement of the problem, research objectives, and the dissertation outline.

Chapter 2 describes the background information that is relevant for this research. Chapter 3 describes materials, equipment, procedures and calculations used for conducting the phase behavior and sandpack flooding experiments.

Chapter 4 describes experimental methods employed and results of 2D experimental investigation of alkaline-surfactant-polymer flooding for viscous oil recovery.

Chapter 5 describes experimental methods employed and results of 2D experimental investigation of alkaline-cosolvent-polymer flooding for viscous oil recovery.

Chapter 6 describes experimental methods employed and results of 2D heterogeneous experimental investigation of alkaline-surfactant-polymer flooding for viscous oil recovery.

Chapter 7 summarizes the results of this research work and discusses the conclusions.

CHAPTER 2: LITERATURE REVIEW AND BACKGROUND

Chapter 2 discusses the background literature relevant to alkaline-surfactant-polymer and alkaline-colsovent-polymer flooding and other related topics such as surfactant-oil-brine phase behavior, microemulsions, and description of chemicals used in this research.

2.1 Overview of CEOR Methods

Polymer flooding is one of the most used CEOR methods. This technique can significantly improve the sweep efficiency in viscous oils compared to conventional waterflooding. For a long time, it was thought that the upper limit for a successful polymer flooding application was around 150-200 cp oil viscosity (Taber et al. 1997). However, improvements in horizontal well technology increased the range of oil viscosities that can be used in polymer floods. The recent success in the Pelican Lake field scale polymer flooding of heavy oil (1000-2500 cp) is the prime example of the successful implementation of a polymer flooding for more viscous oils (Delamaide et. al., 2014). Studies have shown that under certain conditions polymer floods, not only improve sweep efficiency (Wassmuth et al., 2009), but also displacement efficiency (Li et al., 2014; Koh, 2015).

One of the more recent developments in CEOR is alkaline-surfactant-polymer (ASP) flooding. It can improve the oil recovery by lowering the interfacial tension (Stegemeier, 1977) and decreasing the mobility ratio at the same time (Gogarty et al., 1970). Substantial work at The University of Texas has been done on developing new high-performance surfactants, especially for viscous oils (Flaaten et al., 2008, 2010; Zhao et. al. , 2008; Levitt et al., 2009; Adkins et al., 2010, 2012; Wang et al., 2010; Lu et al., 2012; Gao et al., 2013). In addition, significant work has been conducted on improving polymers, cosurfactants, cosolvents and alkali that can tolerate harsh conditions, such as high salinity and high temperature (Sahni et al., 2010; Kulawardana et al., 2012;Puerto et.al., 2012; Sharma et al., 2014; Zhang et. al., 2015; Liyanage et.al. 2015).

Conventionally, ASP processes are applied to oils with a viscosity less than 50 cp (Sheng, 2013). Only a few SP/ASP chemical floods have been reported for more viscous (>50cp) oils (Bryan and Kantzas, 2007, Kumar and Mohanty, 2010; Zhang et al., 2012;Kumar, 2013). ASP flooding was experimentally shown to work in recovering viscous oils from carbonate rocks (Panthi et al., 2013; Carlisle et.al., 2014). Experimentally, it has been shown that the addition of co-surfactants and cosolvents can enhance ASP processes (Nelson et al., 1984; Sahni et al., 2010). However, there are few ASP field projects or pilots on viscous oils. The sweep efficiency of ASP floods of viscous oil is not well studied.

Most viscous oils are acidic where the total acid number (TAN) is greater than 0.5 mg of KOH/gm of oil. Alkali forms soap after reacting with acidic oils. Soaps are hydrophobic surfactants and can be used to achieve ultra-low interfacial tension (IFT). Most recently, the alkali-cosolvent-polymer (ACP) flood has been developed to combine in-situ soaps and cosolvents in order to achieve ultra-low IFT and a desirable flow behavior (Fortenberry et al., 2013, 2015). New hybrid methods, such as the combination of hot water and ACP floods, for recovering heavy oils are promising (Tagafivar et al., 2016).

2.2 Main Recovery Mechanisms in ASP/ACP flooding

One of the main mechanisms of surfactant floods in chemically enhanced oil recovery (CEOR) is lowering the interfacial tension (IFT) between oil and water. Lowering of the IFT leads to reduction of residual oil saturation.

In general, residual oil saturation is controlled by the dimensionless number capillary number (Nc). It was first introduced by Brownell and Katz (1947). Moore and Slobod (1955) defined it as the ratio of viscous forces to capillary forces and is equal to

$$Nc = \frac{Fv}{Fc} = \frac{v\mu}{\sigma \cos\theta}. \tag{2.1}$$

Here, Fv stands for viscous forces and Fc stands for capillary forces, v is the interstitial velocity of displacing fluid, μ is viscosity of displacing fluid, θ is contact angle measured in displacing fluid, and σ is interfacial tension between displacing and displaced fluids. Furthermore, several other modifications of capillary number were derived in other studies. For instance, Foster (1973) omitted $\cos\theta$ term and changed interstitial velocity to superficial velocity, and thus, introduced porosity into the capillary number definition as follows

$$Nc = \frac{u\mu}{\phi\sigma}. \tag{2.2}$$

In addition, it is often convenient to include the pressure drop term in the capillary number definition. Dombrowsky and Brownell (1954) version of capillary number is written in terms of the potential gradient of displacing fluid

$$Nc = \frac{k\left|\bar{\nabla}\Phi_p\right|}{\sigma \cos\theta}. \tag{2.3}$$

Here $\bar{\nabla}\Phi_p$ is potential gradient of displacing fluid, k is permeability, μ is viscosity of displacing fluid, θ is contact angle measured in displacing fluid, and σ is interfacial tension between displacing and displaced fluids.

During typical waterflooding, capillary number is estimated to be about 10^{-7} and in order to recover more oil capillary number needs to be increased further. Stegmeier (1976) presented the relationship between capillary number and residual saturation; later Lake (1989) named the relationship as the capillary desaturation curve (CDC). Figure 2.1 shows CDC published for several rocks (Stegemeier, 1976).

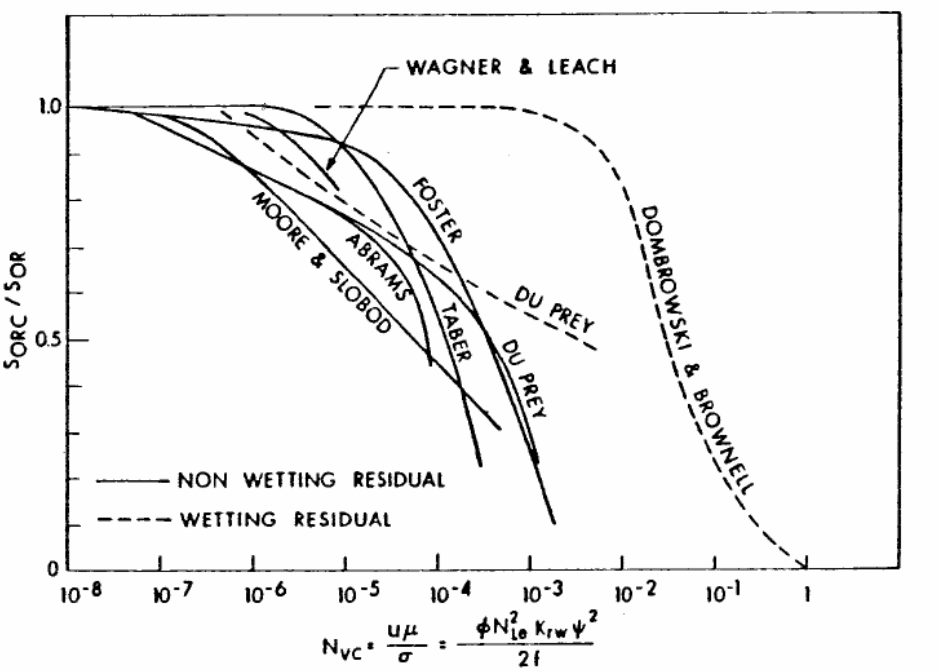

Figure 2.1: Capillary Desaturation Curve (Stegemeier, 1976)

It was determined from several experiments that critical capillary number that would produce additional oil after waterflooding is around 10^{-5} (Mohanty and Salter, 1983; Delshad et al., 1986; Gupta, 1984). To reduce the residual saturation to zero, it is required to increase capillary number at least 1000 times to about 10^{-2}. The way to increase capillary number from typical waterflood values of 10^{-7} to values higher than 10^{-5} is to either increase pressure drop or decrease IFT. Pressure can be increased by increasing injection flow rate or viscosity; however, it is not feasible to increases pressure drop several orders of magnitude due to limited availability of pressure drop in field conditions. The only way to increase capillary number several folds of magnitude is to decrease IFT from about 30 dynes/cm in typical waterflooding to ultra-low values ($<10^{-3}$ dynes/cm) between fluids which is possible to achieve using well designed surfactant formulations (Green and Willhite, 1998).

In order to reach ultra-low values, interaction energy across the interface must be large which can be achieved only if nature of material on both sides of interface is very similar. Since oil and water are very dissimilar in nature, in order to have similar nature at the interface, there

must be a third phase that would have similar concentration of surfactant, oil, and water (Rosen, 1989). Furthermore, ultra-low interfacial tension can be achieved in the three-phase region (Puig, 1979). The presence of surfactant leads to micelle formation. When surfactant concentration in the interface region reaches certain critical concentration called critical micelle concentration (CMC), the surfactants start aggregating into micelles. The solutions where micelles have solubilized phase that is immiscible with solvent are called microemulsions (Green and Willhite, 1988). Formation of a separate microemulsion phase which solubilizes both oil and water creates three phase region of microemulsion, oil and water. The three phase region is very important in surfactant EOR since microemulsion has ultra-low IFT against both water and oil (Green and Willhite, 1998; Delshad et. al., 1996).

2.2 Microemulsions

Definition

Bourrel and Schechter (1988) defined microemulsion as thermodynamically stable transparent or translucent blends of oil, water, surfactants, and other additives. Furthermore, aside from being thermodynamically more stable than ordinary emulsions (macroemuslions), microemulsions also have an order of magnitude smaller drop size compared to macroemulsions. Lastly, microemulsions unlike macroemulsions are independent of mixing and can return to its original state after mechanical disturbance and perturbations in temperature.

2.2.1 Microemulsion Phase Behavior and Transition Parameters

In general, anionic surfactant solution phase behavior is mainly affected by salinity. Increasing the salinity of a surfactant solution decreases the solubility of surfactants in the aqueous phase. Further salinity increase drives anionic surfactants out of the aqueous phase while also solubilizing

some water inside reverse micelles. Thus, at high salinities the phase behavior is represented by two phases: oil-external microemulsion and excess water. At low salinity, behavior is reversed and oil is essentially free of surfactant and some oil is solubilized inside micelles dispersed in the water phase. Therefore, at low salinities, phase behavior is represented by two phases: excess oil phase and water-external microemulsion. At intermediate salinities, three phases could exist: excess oil, middle phase microemulsion, and excess water. Winsor (1954) classified oil-external, middle phase microemulsion (also called bicontinuous), water-external microemulsion as Winsor Type I, II, III respectively. Reed and Healy (1976) stated that microemulsion phase transitions may occur due to changes in salinity, temperature, surfactant and co-solvent (alcohol) molecular structure, composition of oil and dissolved solids in the aqueous phase. For example, increasing surfactant hydrophobicity by increasing hydrophobe chain length causes shift from Type I microemulsion to Type II microemulsion; the trend is reversed when surfactant hydrophilicity is increased. It can be achieved by addition of alkoxy groups such as ethylene oxide into surfactant structure. An increase in pressure typically shifts Type II microemulsion to Type I microemulsion behavior (Skauge and Fotland, 1986). An increase in temperature typically causes shift from Type II to Type I behavior for anionic surfactants (Walker, 2011). Oil composition can be characterized by the equivalent alkane carbon number (EACN). An increase in EACN commonly causes optimum salinity to increase; thus microemulsion behavior shifts from Type II to Type I (Solairaj, 2011). Furthermore, Reed and Healy (1976) found that higher molecular weight alcohols tend to shift microemulsion behavior from Type I to Type II. Lastly, Hsieh and Shah (1976) stated that branched co-solvents tend to be more hydrophilic compared to linearized co-solvents, and thus, optimum salinity is shifted to a higher value which means microemulsion phase behavior is shifted from Type II to Type I behavior.

2.2.2 MICROEMULSION PHASE BEHAVIOR AND INTERFACIAL TENSION

As salinity is increased, IFT between water and microemulsion is increased and IFT between oil and microemulsion is decreased. The point where both IFT's are equal to each other is termed optimum salinity and the solubilization ratio at this salinity is called the optimum solubilization ratio (Reed and Healy, 1976). The middle phase microemulsion has the most favorable condition for oil recovery because both oil-microemulsion and water-microemulsion IFT's are ultra-low. Furthermore, IFT is closely related to solubilization ratio. Solubilization ratio is defined as ratio of solubilized oil (water) volume to surfactant amount in the microemulsion. When solubilization of oil is equal to that of water, IFT reaches minimum. Huh (1979) derived a relationship between oil / water solubilizations and IFT

$$\gamma = \frac{C}{\sigma^2} \tag{2.4}$$

where σ is a solubilization ratio, C is a constant with value equal to 0.3 dynes/cm, and γ is an interfacial tension.

2.2.3 VISCOSITY OF MICROEMULSION

Microemulsion viscosity is one of the most significant parameters affecting surfactant formulation design. In general, surfactants are very prone to forming viscous microemulsions, gels, complexes and liquid crystals under different conditions (Hirasaki, 2011). Depending on the structure of microemulsion, its viscosity can increase an order of magnitude compared to the oil viscosity. In general, viscosity increases to a maximum value at a composition where water and oil contents are equal (Green and Willhite, 1998). Injecting highly viscous microemulsion can lead to high surfactant retention, very high pressure gradients and reduced sweep efficiency. Thus,

overall oil recovery suffers significantly due to surfactant performance and mobility control design (Walker, 2011). Viscosity of microemulsion can be decreased by the following methods such as adding branched surfactants, mixture of surfactant blends (Levitt et al., 2009; Jang et. al. 2016; Tagavifar et. al., 2016), co-solvents, and increasing temperature.

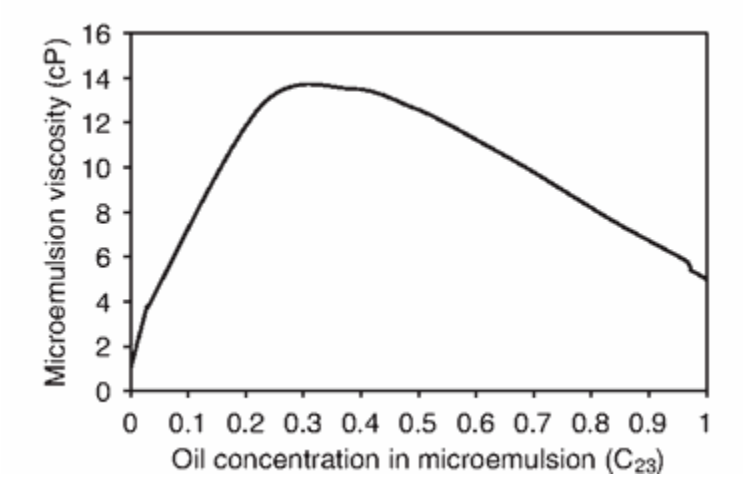

Figure 2.2: Microemulsion viscosity as a function of oil concentration (Sheng, 2011)

2.3 Importance of Mobility Control in CEOR

The main objective of mobility control is to improve sweep efficiency during displacement processes. Bansal and Shah (1977) defined mobility control for the microemulsion processes as changing the properties of the injected fluids such that stable movement of the separate banks is achieved with minimum of mixing and dispersion. In surfactant related CEOR processes main chemicals in ASP slug are very expensive; thus, only small portion of main chemical slug (about 5% to 40% of pore volume) can be injected in economically feasible manner (Green and Willhite, 1998). Typically, main surfactant slug is displaced by less expensive polymer bank, which in turn is displaced by water. It is important to have good mobility control in all three slugs. In main chemical slug, good mobility control is required so that the main slug does not finger through the oil/water bank. Adverse mobility control would cause main slug to finger through the oil/water

bank and have early breakthrough. Furthermore, significant amount of chemicals would be trapped and retained, if mobility control is not properly designed. Dissipation is minimized if there is favorable mobility control between main chemical slug and polymer bank. Lastly, mobility control prevents water drive from fingering through polymer bank into the chemical slug. Therefore, it is very important to have good mobility control during CEOR processes. Mobility control is usually characterized by mobility ratio,

$$M = (k_{rD}/\mu_D)_{S_D} / (k_{rd}/\mu_d)_{S_d} \tag{2.5}$$

where, k_{rD} is the relative permeability of displacing phase, k_{rd} is the relative permeability of displaced phase, μ_D is the displacing phase viscosity, μ_d is the displaced phase viscosity, S_D is the average displacing phase saturation in the region behind displacing front , S_d is the average displacing phase saturation in the region ahead displacing front. Volumetric sweep efficiency generally increases as M is decreased, and M less than one is considered favorable mobility ratio and displacement is stable.

Another important parameter in mobility control design for chemical flooding processes is an estimation of total relative mobility in the stabilized oil bank:

$$\lambda_{rw} + \lambda_{ro} = (\frac{k_{rw}}{\mu_w} + \frac{k_{ro}}{\mu_o})_b \tag{2.6}$$

where, $\lambda_{rw} = \frac{k_{rw}}{\mu_w}$ is the relative mobility of water, $\lambda_{ro} = \frac{k_{ro}}{\mu_o}$ is the relative mobility of oil, k_{rw} is the relative permeability of water, k_{ro} is the relative permeability of oil, μ_w is the water viscosity, μ_o is the oil viscosity.-

Gogarty et al. (1970) obtained the total relative mobility as a function of water saturation as shown in Figure 2.3.

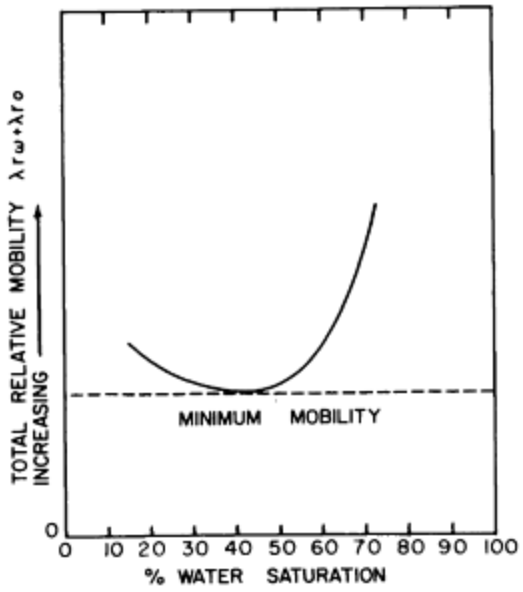

Figure 2.3: Total relative mobility of oil and water versus water saturation (Gogarty et al., 1970)

Gogarty et al. (1970) stated that the relative mobility for the microemulsion bank must be equal or less than minimum total relative mobility of the oil/water bank. Furthermore, the reciprocal of the relative mobility gives the maximum apparent viscosity for oil/water bank (Green and Willhite, 1998). To conclude, in order to have stable displacements, viscosities of both the chemical slug and mobility buffer (polymer drive) must be equal to or higher than the maximum apparent viscosity of the oil/water bank.

2.4 Importance of Salinity Gradient in CEOR

During the ASP flood, there typically exist at least three distinct fluid zones which are the residual oil after waterflooding, followed by ASP slug, and finishing with polymer drive slug. Each of these zones can have different salinities. It is very important to take into account the effect of salinities of each zone on the displacement efficiency (Pope and Nelson, 1978; Nelson and Pope, 1978; Hirasaki et. al 1983. Nelson (1984) presented work on the relationship between salinities of each fluid zone and the performance of the chemical flood. Furthermore, he also introduced the

term called salinity gradient and illustrated its effect on the oil recovery as well as surfactant retention. He conducted several experiments where he changed only the salinity of each slug. This work showed that keeping salinity of the polymer drive slug lower in Type I region while having the leading waterflood salinity and/or the microemulsion salinity at Type II or Type III regions increases chances of passing through the Type III region where ultralow IFT can be achieved. The experimental results showed that the salinity gradient design led to very low residual oil saturation after chemical flood and also significantly lower surfactant retention compared to the constant salinity design flood. The ideal case would be having salinity of all fluid zones in Type III region; however, it is very risky to do that due to factors such as dilution and cation exchange with the formation rock which can easily affect in situ salinity of the fluid. The salinity gradient offers a more robust chemical flood design and decreases risk of missing the Type III salinity window.

2.5 Chemicals Used in ASP

In alkaline-surfactant-polymer flooding alkaline, surfactant and polymer are injected to improve oil recovery. In addition, ASP formulations include co-surfactants, co-solvents and electrolytes.

2.5.1 Primary Surfactant and Co-Surfactant

Surface-active agents, or surfactants, are chemicals that at low concentrations have ability to adsorb onto water-oil interfaces (Rosen, 1989). Furthermore, they can significantly decrease interfacial tension (IFT) between fluids. They are usually organic in nature, and consist of a nonpolar hydrocarbon chain called hydrophobic tail and polar, ionic portion called hydrophilic head (Bourrel & Schechter, 1988). Based on the ionic nature of the head group, surfactants are divided into anionic, cationic, nonionic, and zwitterionic (Lake, 1989). Anionic surfactants are the

most common type of surfactants currently used in CEOR. The reasons are low interfacial tension, low adsorption on reservoir rocks, thermal stability and low cost (Green and Willhite,1998). Nonionic surfactants are used mainly as co-surfactants to improve overall phase behavior of the solution. They have high salinity tolerance, but cannot reduce IFT as good as anionic surfactants (Lake, 1989). Due to strong adsorption on sandstone rocks, cationic surfactants are not used with sandstones; they are used to change wettability of carbonate rocks from oil-wet to water-wet. Zwitteronic surfactants have both positive and negative charges, but they are rarely used due to high cost (Lake, 1989). Over several decades, surfactant formulations were improved continuously to exhibit better qualities such as low cost of manufacturing, improved compatibility with polymers and alkali. Few of the recent developments are discussed next.

From recent developments, branched alcohol propoxy sulfates, internal olefin sulfonates, and branched alpha olefin sulfonates have been identified as high performance surfactants. They exhibit high oil recovery both in sandstone and dolomite, and low surfactant retention (Zhao et. al., 2008; Levitt et al., 2009).

Furthermore, a novel class of surfactants such as Guerbet alkoxy sulfates exhibits substantial improvement in performance. Carboxylation of large Guerbet alkoxylates produces high performance surfactants that can withstand harsh reservoir conditions of high temperature, high salinity, and high hardness (Adkins et al., 2012). Furthermore, addition of alkoxy groups such as propylene oxide and ethylene oxide as extenders to the Guerbet alcohol can be used as a tailoring technique to achieve specific surfactant qualities (Adkins et al., 2010). The addition of EO groups, for instance, enhances hydrophilicity of the surfactant, and thus, increases the optimal salinity. The addition of PO groups has opposite effect of increasing hydrophobicity of the surfactant (Maerker & Gale, 1992).

Wang et al. (2010) used zwitteronic surfactants “Betaine Amphotoreic Surfactants” that can achieve ultra-low IFT without alkali, salts, co-surfactants and co-solvents. In addition, these surfactants can tolerate very high salinity (229,000 ppm), high divalent ion concentrations (21,000 ppm) and high reservoir temperature (up to 98 ^{o}C).

Gao and Sharma (2013) developed novel series of anionic Gemini surfactants that have very high NaCl tolerance (up to 20 wt%) and high CaCl2 tolerance (up to 5 wt%). Furthermore, they found that anionic Gemini surfactants have approximately two or three orders of magnitude lower CMC values and much lower adsorption values compared to other conventional surfactants. This new class of surfactants can also be used as co-surfactant because they can significantly improve aqueous stability and interfacial activity in the mixture with other conventional surfactants.

Lastly, a lot of work was done on finding different blends of two or more surfactants that can work together and achieve synergistic effect on IFT and microemulsion viscosity. Li et al (2014) tested several mixtures of anionic and cationic surfactants. It was found that mixtures of anionic-cationic surfactants produce ultra-low CMC as well as ultra-low IFT and high solubilization ratio. Puerto et al (2014) identified optimal blends of alcohol propoxy sulfates with an internal olefin sulfonate that can have high solubilization suitable for CEOR in the absence of co-solvent.

2.5.2. ALKALI

In general, alkali is used to reduce the surfactant adsorption and to create soap by reacting with crude oil (Nelson, 1984). Addition of alkali increases pH because of its dissociation in the aqueous phase (Green and Willhite, 1998). High pH increases the amount of negatively charged surfaces on the surface of formation rock, which is generally negatively charged for sandstones

and positively charged for carbonates at a neutral pH. An increase in the amount of negative charges on the rock surface reduces surfactant adsorption because negatively charged anionic surfactants are repelled by negatively charged surface of the rock.

In addition, soap is generated when alkali reacts with naphthenic acids in crude oil. Crude oil must have acids in order to produce in situ soap when reacting with alkali. The acid number measurement of crude oil is one way to assess crude oil's ability to form soap. Acid number of crude oil is defined as the amount of potassium hydroxide (KOH) in milligrams needed to neutralize 1 gram of petroleum acid in crude oil (Green and Willhite, 1998). However, an acid number measurement is not an accurate method of quantification of soap in crude oil. The reason is that it measures only free carboxylic groups in crude oil at low temperatures (Yang, 2010). Another similar and more reliable method used to assess crude oil's ability to generate soap is saponification number, which is determined by adding potassium hydroxide (KOH) in crude oil sample and titrating it with hydrochloric acid at an elevated temperature.

Generally, in situ soap produced by reaction of alkali and reactive crude oil is quite hydrophobic; thus, a robust ASP design counters the hydrophobicity of the generated soap by more hydrophilic surfactant addition. Lastly, with good chemical design one might entirely discard use of surfactant in ASP flood and just proceed with alkali-co-solvent-polymer (ACP) flood by employing soap and compatible co-solvent to achieve optimum phase behavior (Fortenberry, 2013).

Most common alkaline agents used in CEOR are sodium carbonate, sodium hydroxide, sodium orthosilicate (Green and Willhite, 1998). Out of these three, sodium carbonate is usually most commonly used due to its ability to propagate further into formation, relatively low cost of manufacturing, and moderate pH. However, sodium carbonates cannot be used in in formations

with high gypsum or anhydrite concentrations. Sodium carbonate will precipitate in the presence of gypsum which will cause permeability damage and loss of majority of alkali. Sharma et al. (2014) have tested sodium metaborate (NaBO2) and ammonium hydroxide (NH4OH) as alternatives for sodium carbonate for application in gypsum containing formations. Through a series of ASP core floods they determined that both of alkalis can propagate through core without loss of alkalinity with pH of 10 and without permeability damage to the formation. Furthermore, he was able to achieve high oil recovery and low surfactant retention. However, sodium metaborate is more expensive compared to sodium carbonate and ammonium hydroxide has some safety concerns related to handling and transportation to surface facilities.

2.5.3 POLYMER

In ASP design, polymers are responsible for mobility control and sweep efficiency. Lower mobility enhances both vertical and horizontal sweep efficiency (Sorbie, 1991; Lake, 1989; Koh et. al., 2017). Polymers are water soluble and increase the viscosity of water. Most commonly used polymers are synthetic partially hydrolyzed polyacrylamide (HPAM) and biopolymer xantan gum. Currently, HPAM and its modifications are widely employed around the world. Not only HPAM increases viscosity of the solution, but it also has suitable rheological behavior. The aqueous solution behaves as a Newtonian fluid at low shear rates; at moderate shear rates it behaves as a shear thinning fluid and at high shear rates it plateaus again into Newtonian behavior. Thus, when injecting at near wellbore region in the field one would expect low viscosity of HPAM since shear rates around the wellbore are very high which in turn increases the injectivity of polymer solution into the formation. As a polymer slug is propagated into the formation, lower shear rates trigger increase in viscosity of the polymer solution thus improving mobility control and sweep

efficiency. Without adequate polymer concentration in ASP slug, the oil recovery suffers due to adverse mobility ratio. In order to have a stable flood, mobility ratio of the chemical slug to oil bank must be equal to or less than one (Gogarty et al., 1967). Mobility ratio is defined as the mobility of displacing fluid over the mobility of displaced fluid. Furthermore, polymers are used as mobility buffer that is injected after the main ASP slug. Injection of polymer drive after the ASP slug will prevent final water drive breakthrough into ASP solution and/or oil bank. However, due to field equipment constraints such as available pressure drop between injector and producer it is much harder to use ASP in viscous oils with favorable mobility ratio. Thus, polymer concentration might be lowered, so that chemical slugs can be injected into the formation at required rate (Gogarty, 1970).

2.5.4 CO-SOLVENT

Co-solvents are alcohols that are added to improve the surfactant formulation by making the primary surfactant sufficiently soluble in the brine. Iso-butanol (IBA), triethylene glycol monobutyl ether (TEGBE), sec-butanol (SBA), isopropanol (IPA), diethylene glycol monobutylether (DGBE) and ethoxylated alcohols are representative co-solvents that are used in surfactant formulation development (Sahni, 2010; Upamali et. al., 2016). Co-solvents have several benefits that enhances overall formulation; however, they have also significant drawbacks.

Co-solvents can minimize development of gels, liquid crystals, emulsions, inhibit separation of polymer-rich phase from surfactants, improve formulation equilibration time, and reduce microemulsion viscosity (Bourrel and Schechter, 1988). Furthermore, co-solvents can also shift optimal salinities. Higher molecular weight co-solvent decreases optimal salinity and lower molecular weight co-solvent increases optimum salinity (Wade et al., 1977). Hsieh and Shah

(1976) found that branched alcohols are more hydrophilic compared to straight-chain alcohols, and thus have higher optimum salinity. Reduction of microemulsion viscosity is one of the most important effects of adding co-solvent because microemulsion viscosities often exceed viscosity of the oil by an order of magnitude at low shear rates (Walker, 2011, 2012). Co-solvents also improve aqueous stability of ASP solution in the presence of polymer which is one of the most important parameter in ASP food design. Lastly, formulation equilibration time is significantly reduced when co-solvent is added. The microemulsion coalescence time is shortened when alcohol is added that in turn decrease equilibration time (Flaaten, 2007).

Co-solvents also have detrimental effects on surfactant formulations. Mainly they can increase IFT at optimum salinity. Salter et al. (1977) determined that IFT increases at optimum salinity as the concentration of low molecular alcohols such as isopropanol increases. Furthermore, co-solvents add extra cost to the final formulation. Sanz and Pope (1995) and others have demonstrated that alcohol free surfactant blends of ethoxylated sulfonate and internal olefin sulfonate can perform as well as formulations with alcohol.

CHAPTER 3: MATERIALS, EQUIPMENT AND CALCULATIONS

Chapter 3 describes the experimental materials, chemicals, equipment used in the experiments. Furthermore, detailed methodology of conducting the experiments and involved calculations used for data analysis are presented.

3.1 Materials

3.1.1 FORMATION AND INJECTION BRINE

The formation brine and injection brine had the same salinity for all experiments. Synthetic brine was developed from a chemical analysis supplied by a company. Furthermore, all divalent ions such as calcium and magnesium were replaced by sodium ions in order to create a softened reservoir brine (SRB) formulation with salinity of 3,164 ppm. The salts were provided by Fisher Chemicals^{TM}. Table 3.1 shows softened reservoir brine composition.

Table 3.1: Softened reservoir brine (SRB) composition

Composition		**Softened Reservoir Brine (SRB)**
Cations		(mg/l)
1	Potassium	9
2	Sodium	1214
Anions		(mg/l)
1	Bicarbonate	147
2	Chloride	1792
3	Sulphate	2
TDS (mg/l)		3164.6
Total Divalent Cation		0
Total Monovalent Cation		1223

3.1.2 ALKALI

The main role of alkali is to reduce surfactant adsorption and create in situ soap by reacting with naphthenic acids in a crude oil. Sodium carbonate ($Na_2 CO_3$) was used as an alkali for the

formulation development. Since solubility of sodium carbonate is around 22 gm/100ml in water at room temperature, only 10 wt% -20 wt% ranged stock solutions were used for the experiment. Lastly, for every new experiment different stock solutions were prepared because after some time sodium carbonate precipitates around the bottleneck area of the glass jar, and thus, altering the concentration of the stock solution.

3.1.3 SURFACTANT AND CO-SURFACTANT

Different surfactants were tried in the phase behavior formulation development out of which Alfoterra™ anionic surfactant (S23-13S-90) provided by Sasol was selected as the main surfactant. Enordet™ internal olefin sulfonate (IOS C15-18) was used as a co-surfactant; it decreased equilibration time. The main surfactant's activity was equal to 79.2% and for the co-surfactant activity was equal to 30%.

3.1.4 POLYMER

A high molecular weight (MW=18 million Daltons) hydrolyzed polyacrylamides (HPAM) Flopaam™ 3630S polymer provided by SNF™ was used for the experiments. Making polymer stock solutions correctly is very important since polymer might not be well mixed, and thus, detrimental polymeric gels might be formed. Furthermore, polymer might relatively quickly degrade as the effect of oxygen exposure. Next paragraph describes the standard procedure for the preparation of polymer stock solutions.

In a wide plastic jar of volume 750 ml, 500 ml of DI water was poured and the required electrolytes was added and stirred by using a stir bar. It is very important to have stir bar that is around 3/4 of the diameter of the jar. Then solution was mixed at ~300 rpm so that the created

vortex would be barely touching the stirring bar. In order to scavenge oxygen from the solution, it was bubbled with Argon for a couple minutes. After bubbling Argon, the required amount of polymer was slowly added into the solution. It is very important to add dry polymer particles exactly to the sides of the vortex in order to ensure proper mixing. After adding polymer, the stock solution was allowed to mix at a high rate until no separate polymer particles were observed. Afterwards, the mixing rate was decreased to around 100 rpm and allowed to mix for 3-4 days. After mixing was finished, the polymer solution was tested for filtration ratio (F.R.) defined by

$$F.R. = \frac{time_{80ml} - time_{60ml}}{time_{200ml} - time_{180ml}} \tag{3.1}$$

where, $time_{200ml}$, $time_{180ml}$, $time_{80ml}$, and $time_{60ml}$ are times elapsed to collect 200, 180, 80, and 60 ml of filtered polymer solution, respectively. In order to ensure that the final polymer solution is homogenous the filtration ratio must be equal to or less than 1.2.

3.1.5 CRUDE OIL

Oil was received from a company and viscosities for oil were measured. Viscosity was about 250 cp. After filtering, reservoir oil was diluted with toluene in order to decrease viscosity to 100 cp by using a quarter power mixing rule,

$$\frac{1}{\mu_{A+B}^{1/4}} = \frac{V_A / Vtot}{\mu_A^{1/4}} + \frac{V_B / Vtot}{\mu_B^{1/4}} \tag{3.2}$$

where μ_{A+B} is viscosity of the final mixture, μ_A is viscosity of oil A, μ_B is viscosity of oil B, and V_A, V_B, $Vtot$ are the volumes of oil A, oil B and the total mixture respectively. The mixed oil mimicked the live oil viscosity of the field oil. ACP work 300cp oil obtained from the different

field was used for ACP experiments. For heterogeneous experiments, 100cp oil was further diluted down to 27 cp by adding octane 15% by weight.

3.1.6 RESERVOIR SAND

Reservoir sand was obtained from a reservoir. It was used for all sandpack experiments. Figure 3.1 shows sand size distribution. Most of the sand size lies between 60 and 400 micron, and the median size is about 200 micron.

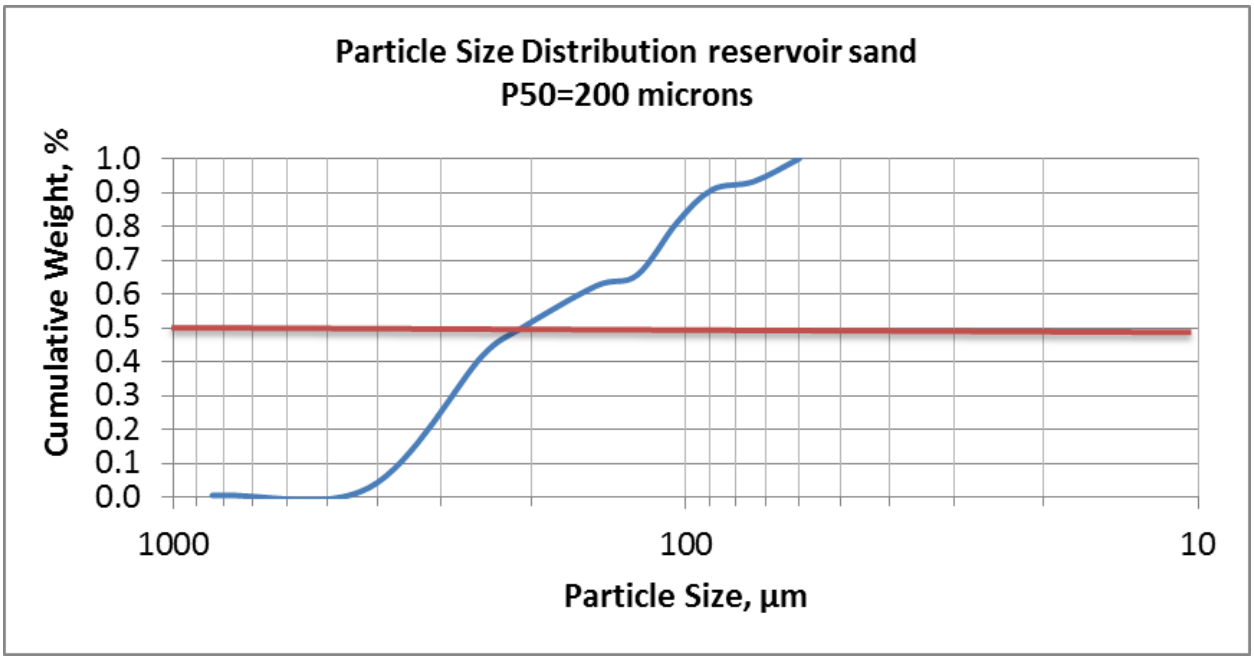

Figure 3.1: Reservoir sand size distribution

3.2 Phase Behavior Equipment and Calculations

3.2.1 PHASE BEHAVIOR EQUIPMENT

Spinning Drop Interfacial Tensiometer

Interfacial tension (IFT) between ASP solution and crude oil was measured with a spinning drop interfacial tensiometer provided by TEMCO. It can measure ultra-low interfacial tension values. Interfacial tension value obtained from the solubilization ratio by using Huh's correlation

(1979) at optimum salinity was confirmed by directly measuring IFT between the crude oil and ASP solution.

Fisherbrand™ Borosilicate Pipettes

Borosilicate pipettes provided by Fisher Scientific™ were used to perform phase behavior analysis. The pipettes have 5 ml of total volume and 0.1 ml graduations. After adding oil, ASP solution was blanketed with argon and sealed by using a propane torch. Worthington propane torch was used to seal the borosilicate pipettes. A high-intensity flame with temperature in air that reaches 3,600 ^{o}F was created through Bernz-O-Matic™ flame nozzle.

For ACP and heterogenous ASP experiments the Ottawa white sand was used. The mesh sizes were: 20/40,40/70, and 100.

Pipette Repeater

Pipette repeater provided by Eppendorf™ was used to dispense accurately oil and ASP solution into the borosilicate pipettes. It can dispense different values ranging from 25 microliters to 1000 microliters.

3.2.2 Phase Behavior Methodology and Calculations

Aqueous Stability

Injection of homogenous ASP solution that does not exhibit any phase separations, cloudiness, and precipitation is very important because otherwise it leads to nonuniform delivery of chemicals and significant phase trapping in the formation. A surfactant solution must be clear or single-phase up to or higher than the injection salinity. This is called the aqueous stability test. In general, aqueous stability test is done by mixing a surfactant formulation which includes the main surfactant, co-surfactant and co-solvent with polymer over wide range of salinities at the

target temperature. There are two methods to change salinity. One way is to fix salinity concentration and change alkali concentration and the other one is to fix alkali concentration and change salt concentration. If the surfactant formulation does not pass aqueous stability test, the contents of the formulation are changed until the formulation is stable over the required range of salinities.

Phase Behavior Screening

After a surfactant formulation (a unique blend of surfactant, co-surfactant, and co-solvent) passed the aqueous stability test, the phase behavior experiments were performed on the surfactant formulation with oil. Initially, no polymer was added into the formulation because polymer has been shown to have little effect on the phase behavior. Pope et al. (1982) stated that the phase behavior sequence was the same with and without polymer over the range of salinities tested except for a limited range of salinities where three-phase region shifts left by a small salinity.

The surfactant formulation was pipetted into borosilicate pipettes and gently tapped on the table so that no trapped air was in the bottom of the pipette. After the aqueous levels recorded, oil was added on top of the surfactant formulation. The amount of oil and the surfactant formulation depends on the chosen water oil ratio (WOR). Generally, initial phase behavior experiments are performed on WOR's equal to one. Next, argon was blanketed on top of the samples, and the pipette sealed with a flame torch. For the first couple of hours, samples were put into an oven at 59 ^{o}C, and the tubes were mixed every 30 minutes. Since temperature of the reservoir of interest was equal to the ambient room temperature, the samples were taken out of the oven and were mixed every 3-4 hours over the next few days until no change in the interface reading was observed.

Microemulsion Viscosity Measurements

The microemulsion viscosity is very important for successful flooding is measured in a rheometer. The rheometer requires at least 0.6 ml of the sample to measure viscosity in a 2° cone and plate geometry. Therefore, after getting successful microemulsion phase behavior in the 5ml borosilicate pipettes, bigger (in volume) samples of the final surfactant formulation along with oil were created. All components' volumes were increased such that ratio of all components stays the same as in the small pipettes and the expected Type III phase volume was at least 1ml in volume. The samples were made in the same salinity range as the pipette samples.

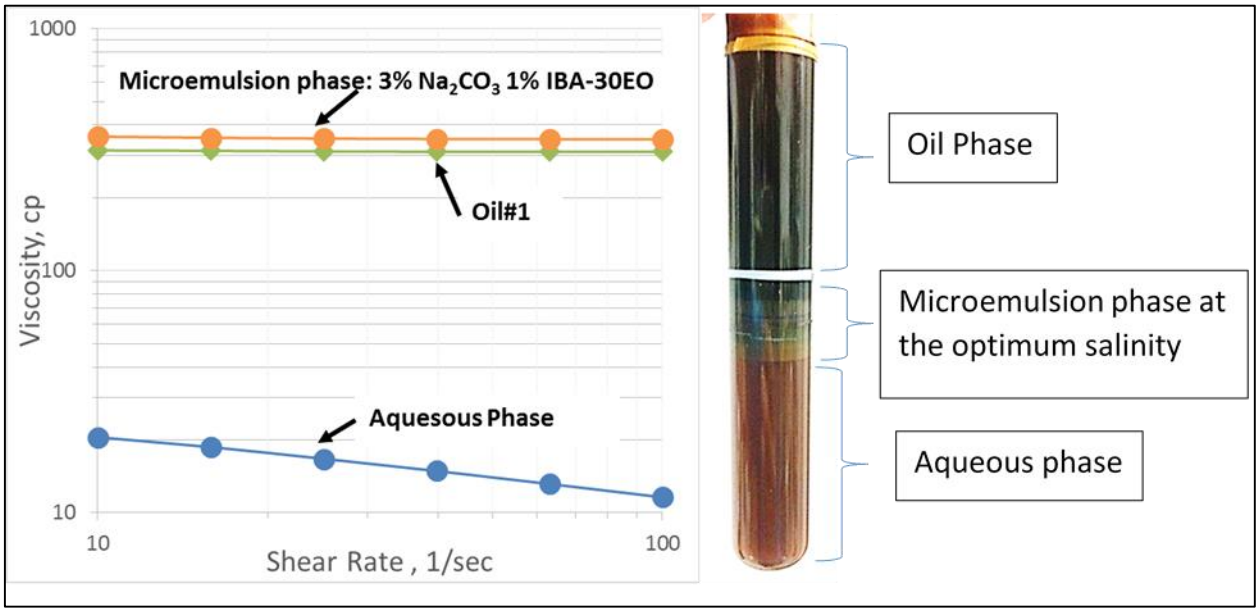

Figure 3.2:Equilibrated Type III microemulsions

Solubilization Plots

The oil or water solubilization ratio is defined as the ratio of volume of oil or water in the microemulsion phase over the volume of surfactant in the microemulsion phase, and expressed by Equation 3.3 for oil and Equation 3.4 for water, i.e.,

$$\sigma_o = \frac{V_o}{V_s} \tag{3.3}$$

$$\sigma_w = \frac{V_w}{V_s} \tag{3.4}$$

where, σ_o is the oil solubilization ratio ,V_o is the volume of oil in the microemulsion phase , σ_w is the water solubilization ratio, V_w is the volume of water in the microemulsion phase, and V_s is the volume of surfactant in microemulsion phase.The oil and water solubilization ratios are calculated over the range of salinities and plotted on solubilization plot shown in Figure 3.3.

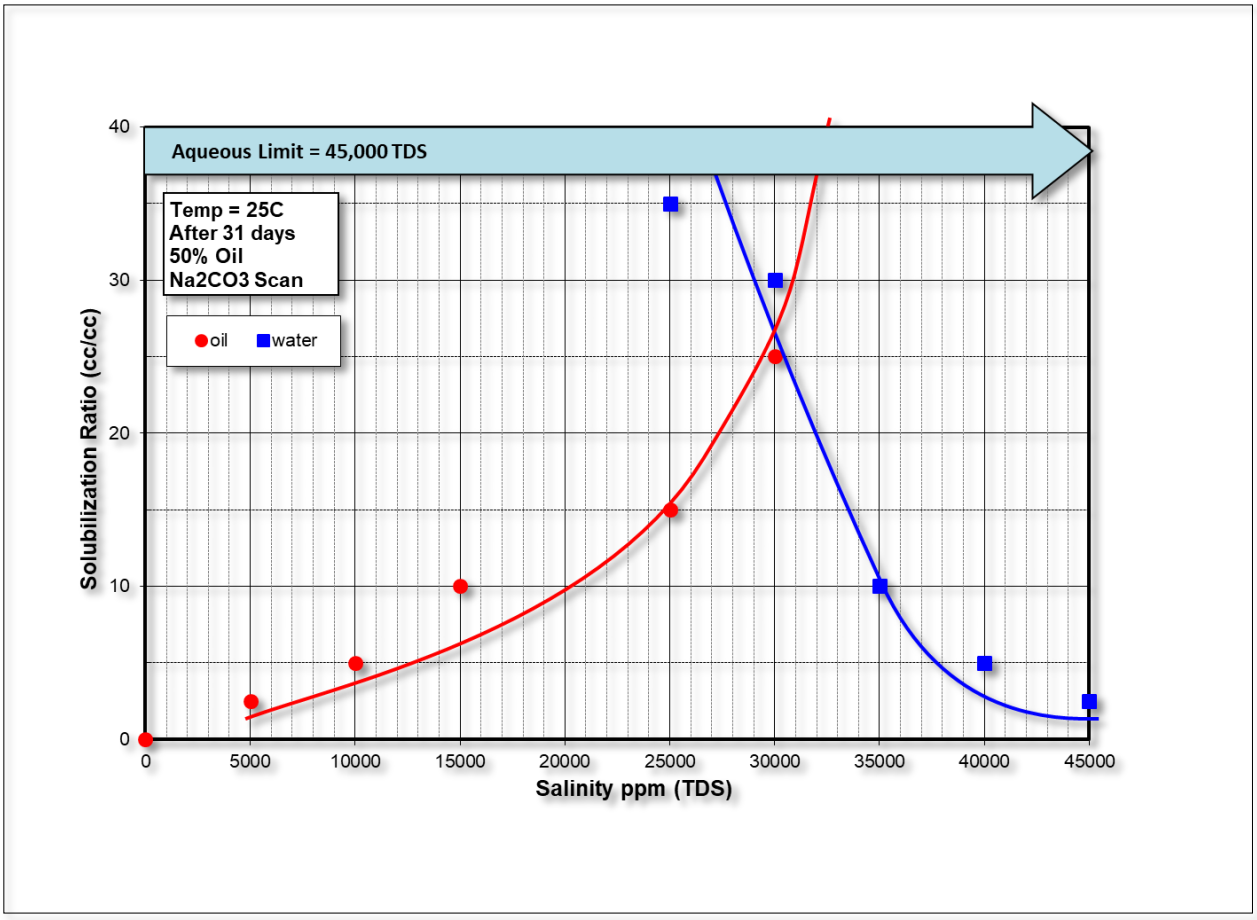

Figure 3.3: Example of surfactant solubilization plot

The point where lines for oil and water solubilization ratios intersect is called the optimum salinity. The lowest IFT is usually achieved at the optimum salinity.

Activity Diagram

One way to see whether oil is reactive is to plot the activity diagram. The reactive crude oil contains naphthenic acids which react with alkali to produce in situ soap. The produced soap is typically hydrophobic; hence, the optimum salinity tends to shift to lower salinities as the concentration of the oil in the phase behavior pipettes is increased. For non-reactive crude oils the optimum salinity does not change with the oil content. The activity diagram is the plot of oil concentration on the x-axis and total dissolved solids concentration or alkali concentration on the y-axis. The activity diagram in Figure 3.4 illustrates how the optimum salinity is lowered as the oil concentration is increased for reactive crude oils.

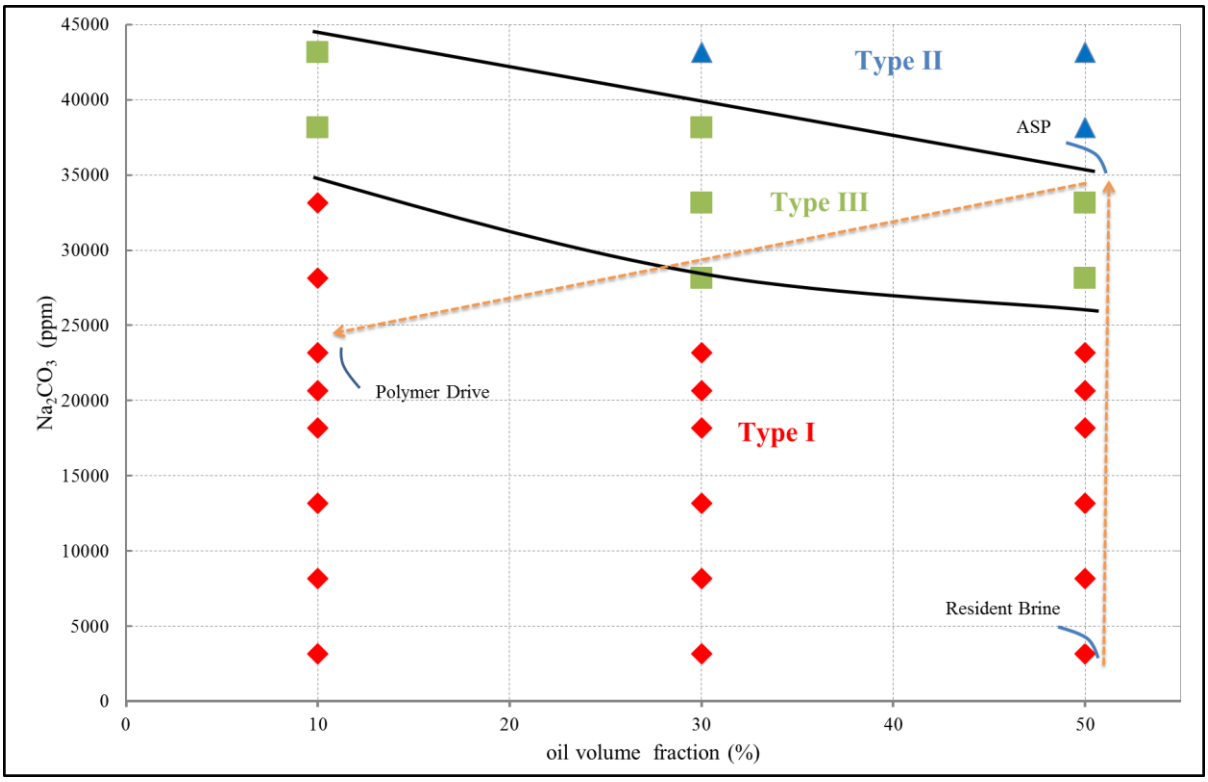

Figure 3.4: Example of activity diagram for reactive crude oil

3.3 Sandpack Equipment and Calculations

3.3.1 THE SANDPACK FLOODING

Brine Tracer Test

Brine tracer test was performed in order to determine the pore volume of the sandpack. It involves injecting higher salinity brine compared to the formation brine. Salinity of the effluent samples were measured and plotted against injected pore volumes. In theory, the midpoint of the S-shaped curve should be equal to 1PV of the sandpack in 1D floods. For 2D floods, measured salinity was used to calculate sweep efficiencies of the quarter five-spot pattern. Many studies showed that the typical sweep efficiency in a five-spot pattern was equal to around 0.7. Using this information, the pore volume was varied such that it matches the sweep efficiency of 0.7 at the breakthrough. The detailed description of the pore volume determination in 1D and 2D floods is presented in the calculations section.

Oil Flood

The oil flooding was conducted in order to saturate the sandpack. The sandpack was placed vertically and injected oil from the top at ~400 psi and displaced water was collected from the bottom of the sandpack. After 2-3 days the procedure was repeated in order to see whether any residual water could come out. The volume of displaced water was equal to the initial oil saturation.

In addition to oil saturation, the oil flooding was conducted to determine the oil permeability. Oil was injected at different flow rates until the pressure drop was stabilized. Then, the pressure drop for each flow rate was used to calculate the effective oil permeability at the residual water saturation.

Water Flood

After the brine tracer test and the oil flooding the waterflooding commences. For 1D floods, the waterflooding was conducted for at least 5 PV in order to ensure no oil was coming out and that pressure drop was stabilized. For 2D floods, the waterflooding was conducted for around 1PV only. The effluent samples were collected at the same time interval by using the fractional collector. The waterflood oil production was recorded, and the residual oil saturation to water was calculated by using mass balance. Lastly, the effective water permeability at the residual oil saturation to water was estimated and used to determine the end-point relative permeability to water.

Chemical Flood

The chemical flood followed waterflooding. Initially, 0.5 PV of ASP slug was injected, followed by polymer drive. The ASP slug is the same for all floods including 2D floods except small variation for the 1D flood in a steel tube experiment. The injection rates of ASP and polymer slugs were 1 ft/day for all type of floods. The effluent samples were collected using the fractional flow collector and oil cut was determined from the collected samples. The oil recovery and residual oil saturations were determined by mass balance from the effluent samples.

Effluent Analysis

The effluent analysis was done on the samples in order to see propagation of the chemical slugs and determine the surfactant retention. Furthermore, viscosity, pH, salinity and the surfactant concentration in each tube were measured.

3.3.2 SANDPACK EQUIPMENT

Steel Tube

The steel tubes provided by Autoclave Engineers^{TM} (3 ft in length and 0.67 inches in diameter) were used for the 1D displacement experiments. These tubes were used as 1D column for the reservoir sand.

Biaxial Type Core Holder

A biaxial type core holder provided by Phoenix Instruments was used to perform the sandpack floods. The reservoir sand was dry packed inside the rubber sleeve of the core holder and vacuumed for a day. Then both radial and axial stresses were applied through injecting water into the confining pressure ports. The maximum working pressure was 5000 psi. The sandpack was tested for leakage before starting the experiment.

Quarter Five-Spot Model Apparatus

A quarter five-spot cell is a cylindrical, stainless steel case designed to hold a sandpack that is 10 inches square and 1 inch thick. The cell is composed of three stainless steel plates that are bolted together. The top and bottom plates are identical and are used to hold an overburden pressure, while middle plate is used to hold sandpack. The quarter five-spot cell has confining pressure ports that are used to apply overburden pressure between rubber sleeves and top and bottom plates. The overburden pressure that can be applied was 2000 psi.

Stainless Steel Accumulator

The stainless steel accumulators provided by TEMCO^{TM} were used as the transfer cylinders for the oil, polymer and ASP slug . They have a floating piston that separates two fluids. Vertically positioned accumulators were pumped in brine/tap water from the bottom end, and fluids on the other side of the piston would be displaced into the sandpack . These accumulators can operate at pressures up to 3750 psi.

Syringe Pumps

Teledyne^{TM} ISCO 500D syringe pumps were used to pump fluids during the experiment. Brine was injected directly into the sandpack through the pump, however, for oil, ASP and polymer injection, pumps were used to inject brine/tap water into the stainless steel accumulator that kept fluids inside. The pumps have total 507 ml volume available inside and can operate at pressure up to 3750 psi.

Pressure Transducer

The pressure transducers from Honeywell^{TM} were used to record pressure drops between inlet and outlet of the sandpack. The pressure measurement ranges between 0-300psi .The pressure transducers convert the measured pressure drop into voltage reading , which in turn is sent to computer and recorded on a excel spreadsheet through Data Acquisition Card (DATAQ).In order to convert back to pressure, the calibration curve between voltage readings and pressure drop was generated before starting the experiment. The example of calibration curve is shown in the Figure 3.5.

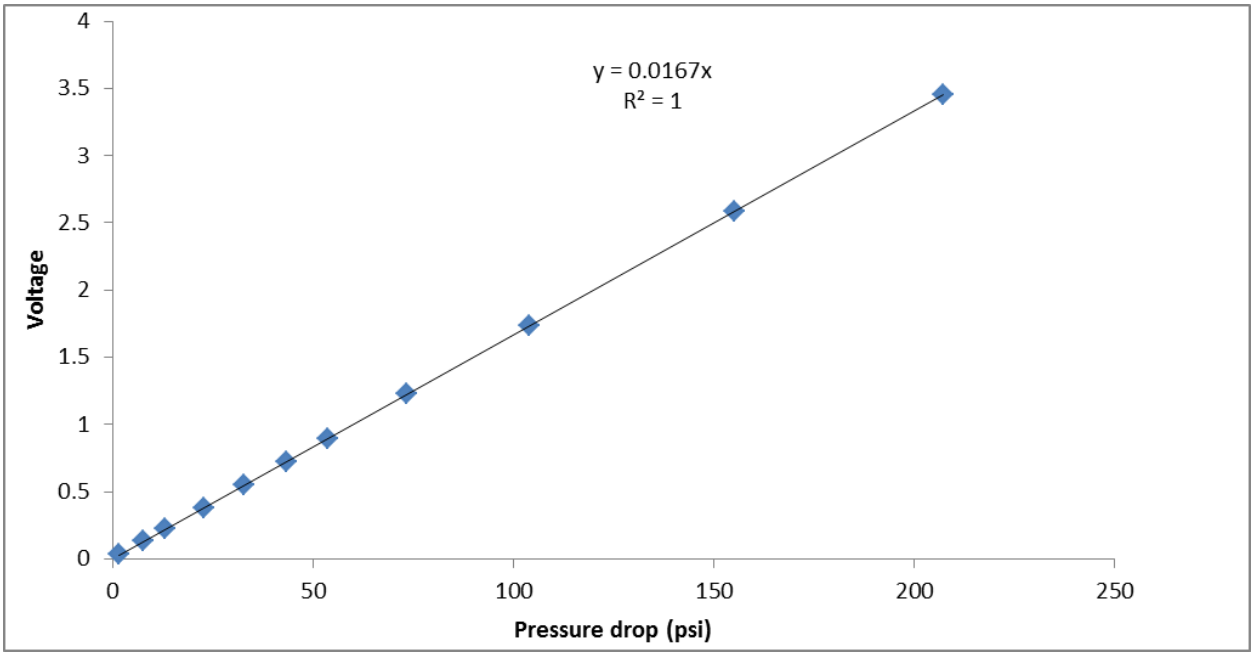

Figure 3.5: The calibration curve between voltage and pressure drop

Fraction Collector

The effluent samples from the sandpack were collected by using ISCO Retriever 500^{TM} fraction collector provided by ISCO Instruments. The fractional collector can hold up to 68 test tubes at the same time. All effluent samples were collected at the fixed time interval.

Refractometer

A portable refractometer RF12, provided by Extech Instruments, was used to measure refractive indices of the effluent samples and bulk solutions. The calibration curve between refractive index and salinity was generated for conversion from refractive indices to salinities of brine and aqueous phase of the effluent samples.

Rheometer

The viscosities of oil, brine, polymer, and ASP slugs were measured by using AR-G2 rheometer provided by TA instruments. The rheometer can measure viscosities using several different geometries such as cone and plate and concentric cylinders. The 2^{o} cone and plate geometry was used to measure viscosities of solutions. The required sample size was about 0.6 ml. The sample is loaded on a peltier plate, and the rheometer rotates cone which contacts fluid on plate. The torque required to rotate the fluid at that particular speed is converted to a viscosity value. The minimum torque that can be applied was about 0.003 $\mu N.m$ and the maximum torque was about 200 $\mu N.m$. In general, viscosities obtained at 0.01 s^{-1} shear rates and above were considered accurate.

High Performance Liquid Chromatograph (HPLC)

The UltiMate^{TM} 3000 HPLC by Dionex was used to measure the dynamic surfactant retention in the effluent samples after sandpack flooding. HPLC can separate different components of a sample by using chromatographic process. Furthermore, HPLC measures retention time of

each separated components. The calibration samples that were prepared from the batch ASP solution were measured. Later, a calibration curve between the surfactant retention time and its concentration was generated. The calibration curve was used to get surfactant concentration in the effluent samples.

pH Meter

The Oakton waterproof pH meter was used to measure pH of the effluent samples and batch solutions. It can measure pH of solutions with +/- 0.01accuracy, and it can also measure temperature of the solutions up 50 °C. The pH meter is calibrated with pH 4, 7, 10 buffer solutions every time before measuring pH of the effluent samples.

Handheld UV Lamp

A handheld UVL-56 ultraviolet lamp provided by Analytik Jena Company was used to better distinguish interfaces between free oil and microemulsions. It emits long wave ultraviolet light at 365 nm wavelength.

Filter Press

A stainless steel OFITE filter press was used to filter stock solutions of oil, polymer, and ASP. Polymer and ASP solutions were filtered by using 1.2 µm Millipore hydrophilic cellulose filter paper at 15 psi argon gas pressure. Oil and brine stocks were filtered by using 1.2 µm and 0.45 µm filter paper respectively.

3.3. 3 SANDPACK FLOOD IN A STEEL TUBE AND CORE HOLDER.

Sandpack Preparation in a Steel Tube

The steel tube sandpack packing started with wetting reservoir sand thoroughly. Then, wetted sand was packed in to 3 feet long steel tube while adding some brine. Extra brine was added

in order to get rid of trapped air. While packing, the steel tube was tapped often in order to dislodge air and ensure tight packing. Excess water was drained from the bottom and after capping the steel tube was flooded from the bottom connection port in order to ensure no air was trapped inside the dead volume zone.

Sandpack Preparation in a Core Holder

The core holder was dry packed. Dry reservoir sand was poured into the core holder while at the same time the core holder was being vacuumed from the bottom. The sandpack was regularly tapped from outside during the whole process. After capping the core holder, it was vacuumed for one day before proceeding with the experiment.

3.3.4 SANDPACK FLOOD IN A 2D QUARTER FIVE-SPOT PATTERN

2D Quarter Five-Spot Pattern Description

Figure 3.6 shows a sketch of the quarter five-spot sand pack and the picture of the actual quarter 5-spot sand pack. The flooding area is rectangular shape with 10”×10”×1”. It is covered on top and bottom with a rubber sheet where confining pressure can be applied. The sandpack is encased with steel.

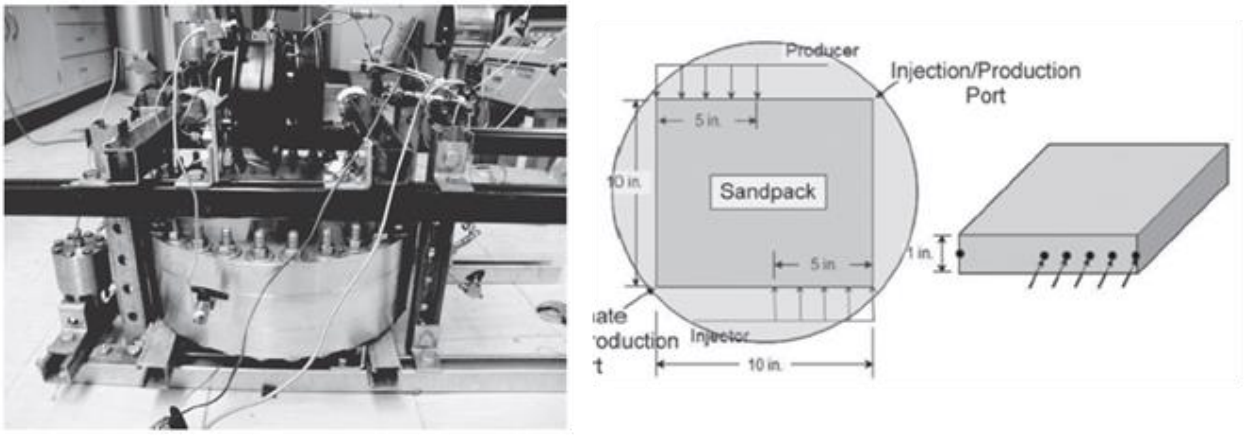

Figure 3.6: A quarter five-spot pattern

2D Quarter Five-Spot Sandpack Preparation

The quarter five-spot pattern was wet packed. The reservoir sand was wetted with excess water and mixed at the same time in order to dislodge trapped air inside the reservoir sand. Then, water wetted sand was spread in small quantities inside the square shaped slot for sand while adding excess of water. Further, extra sand was scraped off from top of the sandpack, and the circular rubber sleeve was put on top of the sandpack. Subsequently, the top steel plate was screwed on. The bottom and top rubber sleeves were used to separate the sandpack and the overburden liquid. The Figure 3.7 shows the top plate and the square shaped slot filled with sand on top of which the rubber sleeve was placed.

Figure 3.7: Top steel plate and middle plate with the sandpack

After closing the five-spot pattern, overburden pressure of 1300 psi was applied. For that purpose top and bottom plates have two injection ports each. Injection ports are used to inject liquid into the hollow space between the rubber sleeves and the inside surface of the plates. Then, the side valves of the 5-spot were opened so that excess amount of water can be leaked out. The compression of the sand from bottom and top ensures creation of tighter sandpack.

3.3.5 SANDPACK FLOOD CALCULATIONS

Pore Volume and Porosity Estimation in a 1D Flood

The sandpack pore volume in a 1D flood was determined by conducting brine tracer test. The brine salinity that was two times of the formation salinity was injected into the 1D sandpack. The injection was carried out until the effluent samples' salinity was equal to injection brine salinity. Then, the brine salinity was normalized and plotted against injected pore volumes. In theory, for the homogenous 1D sandpack the normalized salinity plot should be S shaped and the midpoint of the S-shaped curve should be equal to the sandpack pore volume. However, if a salinity plot does not exhibit symmetry, a better way to get pore volume is to estimate the area behind the salinity curve to calculate the pore volume of the 1D sandpack. Obtained pore volume was divided by total volume to get porosity of the sandpack. The Figure 3.8 shows plot of normalized salinity where the are behind the curve was used since the normalized salinity is not completely symmetric.

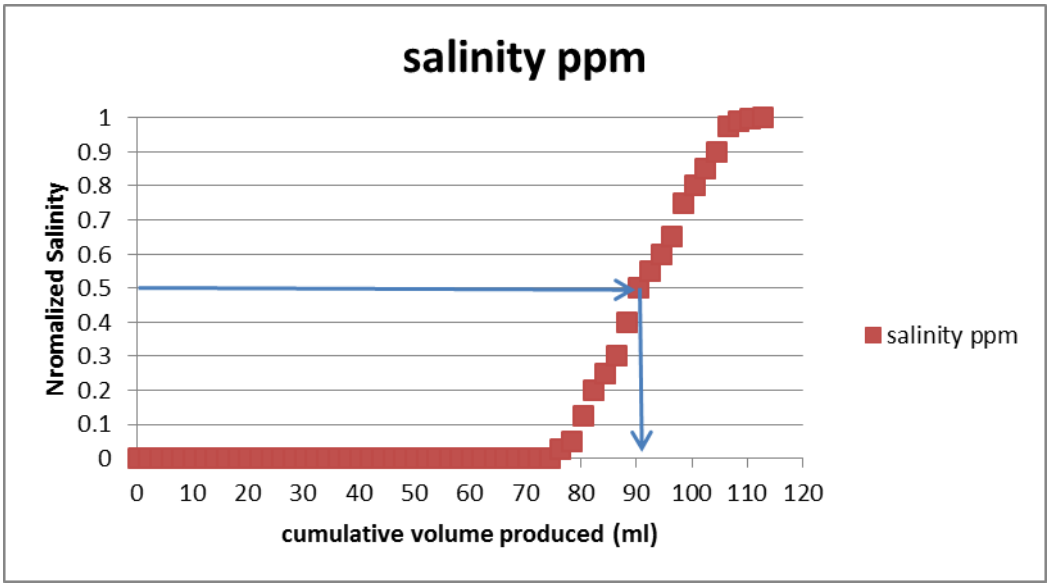

Figure 3.8: Example of estimation of 1D sandpack pore volume

Pore Volume and Porosity Estimation in a 2D Flood

A quarter five-spot pore volume can be estimated with two methods. First, after wet packing the reservoir sand inside the five-spot pattern, the amount of water that would be expelled due to applying overburden pressure was subtracted from the total water that was added during wet packing the sandpack. Obtained value should be equal to the pore volume of the sandpack. This method is less accurate than the second method which is conducting a brine tracer test in the 2D sandpack. It involves determining sweep efficiency in the miscible flood of the homogenous five-spot pattern. Sweep efficiency is calculated as follows

$$E_A = \int_0^{t_D} (1 - \frac{C_D}{C_{D_o}}) dt_D \tag{3.5}$$

where, E_A is the sweep efficiency of the sandpack, t_D is the injected pore volumes, C_D is the normalized salinity at the outlet, and C_{D_o} is the normalized salinity at the inlet which is equal to one.

Habermann (1960) and Dyes (1954) estimated sweep efficiencies for a five spot patterns and found out that the sweep efficiency at breakthrough was typically equal to 0.7 during miscible floods. Furthermore, from Brigham et al., (1965) it was found that breakthrough occurs close to 0.72 PV during the miscible flood.Lastly, the sweep efficiency of the brine flood must not exceeed 1.0 close to the end of the tracer test. Thus, the pore volume was adjusted until the curve of sweep efficiency matched the sweep efficiency at the breakthrough (E_{Abt}) which must be close to 0.7 and the final sweep efficiency (E_{Afinal}) which must be close to value 1.0. Figure 3.9 shows the example of brine tracer test done on the quarter five-spot pattern, it can be seen that E_{Abt} and E_{Afinal} matched reuired values of 0.7 and 1.0 respectively.

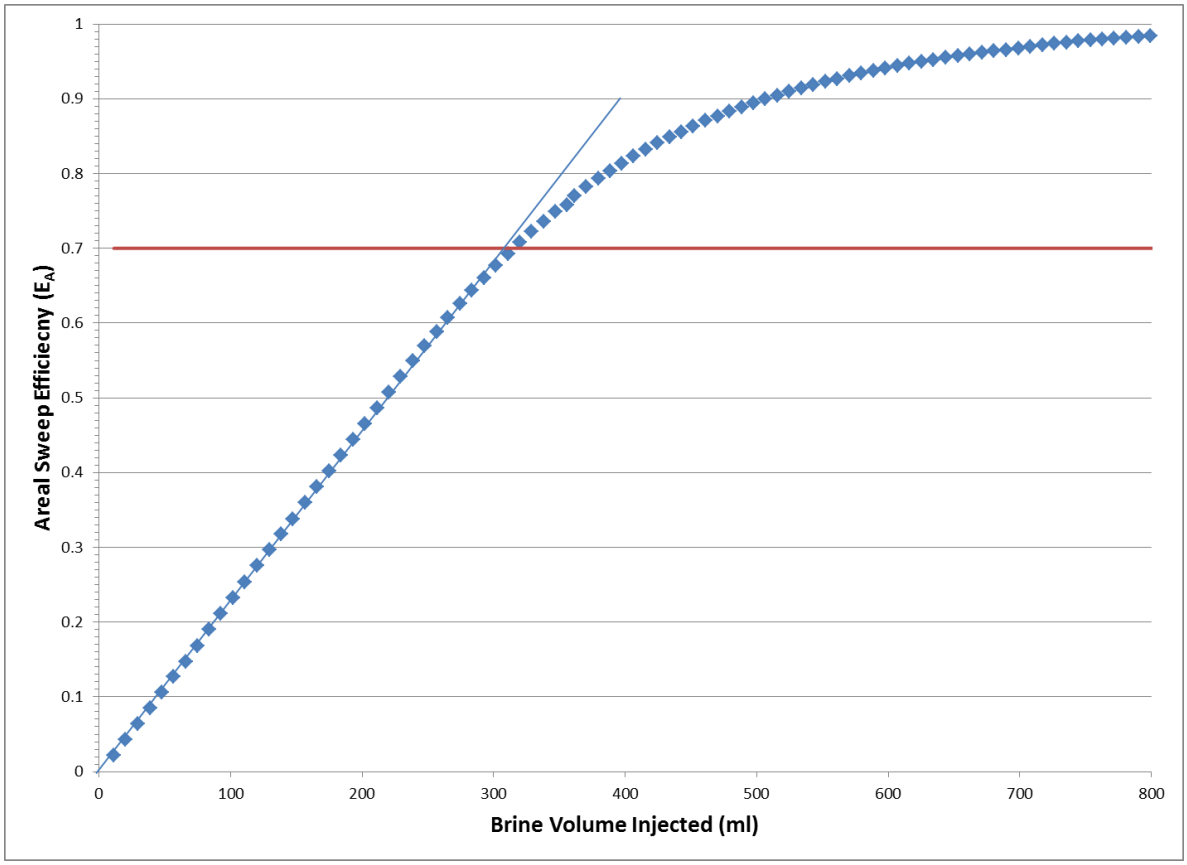

Figure 3.9: An example of pore volume determination in a quarter five-spot pattern

Absolute Water (Brine) Permeability

In order to get absolute water permeability, pressure drop was measured during single phase brine flow when the sandpack was fully saturated by brine only. Absolute brine permeability in 1D flood was calculated by using Darcy's law

$$k_{w@Sw=100\%} = \frac{q_w \mu_w L}{A \Delta P} \tag{3.6}$$

where, $k_{w@Sw=100\%}$ is the absolute water permeability, q_w is the water flow rate, μ_w is the water viscosity, L is the sandpack length, A is the cross-sectional area perpendicular to the flow, and ΔP is the pressure drop across the sandpack.

Effective Oil Permeability

The effective oil permeability was calculated during oil flood when water saturation was at the residual value. The oil flow rate was varied until pressure drop is stabilized at each new oil flow rate. The effective oil permeability at the residual water saturation was calculated as follows

$$k_{o\_eff} = \frac{q_o \mu_o L}{A \Delta P} \tag{3.7}$$

where, k_{o_eff} is the effective oil permeability, q_0 is the oil flow rate, μ_o is the oil viscosity, L is the sandpack length, A is the cross-sectional area perpendicular to the flow, and ΔP is the pressure drop across the sandpack.

Effective Water Permeability after Waterflood

Effective water permeability was calculated at the end of the waterflood when no oil was being produced and pressure drop stabilized across the sandpack at the constant flow rate. The effective water permeability at the residual oil saturation to the water was calculated as follows

$$k_{w\_eff} = \frac{q_w \mu_w L}{A \Delta P} \tag{3.8}$$

where, k_{w_eff} is the effective water permeability, q_w is the water flow rate, μ_w is the water viscosity, L is the sandpack length, A is the cross-sectional area perpendicular to the flow, and ΔP is the pressure drop across the sandpack.

End Point Oil/Water Relative Permeability

The endpoint oil relative permeability was determined by dividing the effective oil permeability at the residual water saturation by the base permeability. The base permeability was

chosen to be the absolute water permeability. The end-point oil relative permeability at the residual water saturation was calculated as follows

$$k_{ro} = \frac{k_{o\_eff}}{k_{w@Sw=100\%}} \tag{3.9}$$

where, k_{ro} is the end-point oil relative permeability at the residual water saturation, k_{o_eff} is the effective oil permeability, and $k_{w@Sw=100\%}$ is the absolute water permeability.

The end-point water relative permeability was calculated in the similar way by dividing the effective water permeability at the residual oil saturation to water by the absolute water permeability

$$k_{rw} = \frac{k_{w\_eff}}{k_{w@Sw=100\%}} \tag{4.0}$$

where, k_{rw} is the end-point water relative permeability at the residual oil saturation, k_{w_eff} is the effective water permeability, and $k_{w@Sw=100\%}$ is the absolute water permeability.

Initial Oil Saturation

Initial oil saturation was calculated from the mass balance. At high pressure drop (~400psi) oil was injected into the sandpack that was initially fully saturated with the formation brine, and the displaced water was collected until no water would come out. The initial oil saturation estimated by

$$S_{oi} = \frac{V_{water\_produced}}{V_p} \tag{4.1}$$

where, S_{oi} is the initial oil saturation, $V_{water\_produced}$ is the volume of produced that is also equal to volume of oil in the sandpack, and V_p is the pore volume of the sandpack

Cumulative Oil Recovery

Cumulative recovery was estimated from the oil recovered in the effluent samples. De-emulsifier was added to the effluent samples so that oil solubilized in the microemulsion would be separated from the microemulsion. The oil recovery was estimated as follows

$$N_p = \frac{\Sigma V_{oil}}{V_p} \tag{4.2}$$

where, N_p is the cumulative oil produced, V_{oil} is the effluent oil volume in the produced sample, and V_p is the pore volume of the sandpack

Oil Cut

Oil cut, which is a fraction of oil in the total volume produced, was estimated from the oil produced at the outlet, and defined as

$$f_o = \frac{V_{oil}}{V_{oil} + V_{water}} \tag{4.3}$$

where, f_0 is the oil cut in the effluent sample produced, V_{oil} is the effluent oil volume in the produced sample, V_{water} and is the effluent water volume in the produced sample,

CHAPTER 4: 2D EXPERIMENTAL INVESTIGATION OF ALKALINE-SURFACTANT-POLYMER FLOOD FOR VISCOUS OIL RECOVERY

One of the objectives of this research was to perform 2D 5-spot pattern ASP floods in heavy oil. ASP floods can be made more stable by adding enough polymer. Stable flood recoveries would be high, but injection rates would be low in viscous oil ASP floods. The addition of smaller amount of polymer makes the ASP floods more unstable. For unstable ASP floods, the injection rates would be higher, but the sweep efficiency would be lower. Thus, these floods should be evaluated as a function of polymer concentration or ASP slug viscosity. Since the sweep efficiency is affected, the formulations should be tested in multi-dimensional porous media (not just core floods).

Another objective of this research was to investigate the effect of the starting time of ASP floods in heavy oil reservoirs. Injection rates in heavy oil reservoirs are often limited by the small pressure drops (500-1000 psi) available. Since not many pore volumes of fluids can be injected into a heavy oil reservoir (during its reservoir life of about 30-50 years), one key question is the optimum time to start the ASP flood. If the ASP flood is started early, then the injection rate may be too low. If it is started late, then there may be little time to push the oil out during the reservoir life. In the next section, I outline our experimental methods. The following section describes the results.

4.1 Experimental Methods

In this work, I have developed an effective alkaline-surfactant-polymer formulation that produced ultra-low interfacial tension. I identified the formulation using microemulsion phase behavior experiments. Furthermore, I tested the formulation effectiveness in a 1D sandpack flood

experiment. Lastly, I conducted ASP floods in a quarter 5-spot sandpack (2D) to study the effect of mobility ratio and timing of ASP injection on the oil recovery and the pressure drop.

Materials

In this research, I used Alfoterra and Enordet IOS surfactants obtained from Sasol and Shell Chemicals, respectively. Alfoterra surfactants are branched alkyl propoxy sulfates and Enordet IOS surfactants are internal olefin sulfonates. In addition to surfactants, I used Isobutyl alcohol (IBA) a cosolvent which was obtained from Sigma-Aldrich. The alkali used for the microemulsion phase behavior was sodium carbonate from Fisher Scientific.

The oil and the sand for the sandpack experiments were received from the fields that I investigated. The oil had a viscosity of 100 cp at 25 oC and an acid number of 1 mg KOH/gm of oil. I used brine with a salinity of 3,164 ppm as the injection brine for the waterflooding part of the sandpack experiments. The salts used to make the injection brine were obtained from Fisher Scientific.

Phase Behavior Studies

Surfactant phase behavior experiments were performed to identify a surfactant formulation which gives ultralow IFT with the reservoir oil and aqueous stability at the optimum salinity. Aqueous solutions were prepared with 1 wt% of surfactants (a mixture of two surfactants), the injection brine, the co-solvent, and the alkali. In addition, all of the aqueous solutions were prepared and kept at the reservoir temperature (25 ^{o}C) to obtain the aqueous stability limits of the surfactant formulation. Initially, alkali concentration was varied systematically (in a series of pipettes) at a fixed water-oil-ratio (WOR). Then, the process was expanded to different WORs. The samples were equilibrated at the reservoir temperature and the phase volumes were recorded. The oil solubilization ratio in the microemulsion phase was estimated from the decrease in oil

volume divided by the amount of surfactant and similarly the water solubilization ratio. The solubilization ratios were used to calculate interfacial tensions using the Huh equation (Huh, 1979). The microemulsion phase viscosities were measured at shear rates ranging from 1 to 100 sec^{-1}.

IFT Measurements

The microemulsion/water IFT was measured using the Temco spinning drop interfacial tensiometer for the sample at optimal salinity with 50:50 oil and ASP solution. Thus, interfacial tension value obtained from the solubilization ratio by using Huh's correlation at optimum salinity was verified by directly measuring IFT.

1D Sand Pack Flood

A half-foot-long steel tube (diameter = 1.5-inches) was packed with field sand. Estimated porosity was 35.4% and the permeability was 2.2 D for the brine. The pore volume was 61.6 cc. The core was first fully saturated with the formation brine and then flooded with the reservoir oil and placed in a vertical orientation at 25 ^{o}C. The core was then flooded with 3 PV of synthetic formation brine from the bottom at the rate of 1 ft/d and then 2 PV of the same brine was injectedd at the rate of 10 ft/d. The first step represents a waterflood (SRB described in section 3.1) at a typical field rate and the second step is conducted to identify the capillary end effect, if any. The ASP flood consisted of injecting ASP slug (0.5 PV) followed by polymer slugs I & II (each 0.5 PV) at the optimum salinity and at the injection brine salinity, respectively. Lastly, just brine was injected for 3 PV. The ASP slug consisted of 1 wt% surfactant, 1 wt% cosolvent, 3.25 wt% Na2CO3, 0.47 wt% polymer. The polymer slugs I & II contained 0.5 wt% and 0.47 wt% polymer, and 3.25 wt% and of 2.275 wt% of Na2CO3, respectively. Table 4.1 lists the key parameters in

the 1D sandpack flood.

2D Sand Pack Floods

Figure 4.1 shows a sketch of the quarter five-spot sandpack and a picture of the actual quarter 5-spot sandpack. The 10” x10” square-shaped flooding area was 1" thick. This flooded area is covered by rubber sheets at the top and bottom. A confining pressure is applied on the rubber sheets which press against the sandpack. The pack is encased in a steel chamber which can withstand about 2000 psi working pressure. The quarter five-spot pattern was wet packed with sand. The reservoir sand was wetted with excess water and mixed to dislodge trapped air inside the reservoir sand. Then, water-wetted sand was placed in small quantities inside the square-shaped slot while adding an excess of water. At the end, extra sand was scraped off from the top of the sandpack, and the rubber sheet was put on top of the sandpack. Subsequently, the top steel plate was screwed on. The bottom and top rubber sleeves were used to separate the sandpack from the confining liquid. Top and bottom steel plates have two injection ports each for injecting the confining fluid. After closing the five-spot pattern, an overburden pressure of 1300 psi was applied. The compression of the sand from the bottom and the top ensures the creation of a tight sandpack.

All the ASP floods were conducted at a temperature of 25 ^{o}C. The injection fluid was pumped at a constant flow rate of 0.5 ml/min, which is equivalent to 0.8 ft/day, using an ISCO pump. The pressure drop across the sandpack was measured by pressure transducers. Effluent samples were collected in tubes using a fractional collector and the phase volumes were estimated. The produced emulsions during the ASP flood were heated and demulsified with appropriate chemicals for accurate measurement of oil and aqueous phase volumes. Table 4.2 lists the injection fluid sequence for the quarter 5-spot sandpack floods with variation of ASP slug viscosity ratio. The first flood injected a high viscosity ASP slug; Floods 2-4 injected a lower viscosity ASP slug.

Table 4.3 lists the flooding sequence for 2D ASP floods where the amount of waterflood before ASP injection varied.

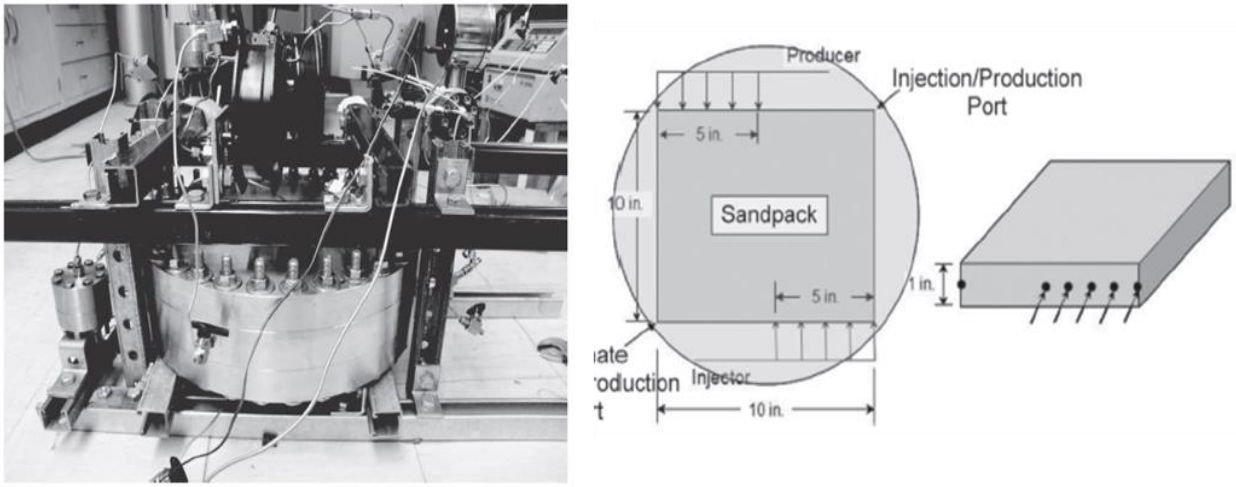

Figure 4.1: The quarter 5-spot sandpack model

Table 4.1: 1D Linear tertiary ASP flood

Flood title	1D ASP Stable
Waterflood extent, PV	5
Soi, %	82
Porosity	0.354
Brine Permeability, Darcy	2.21
Main Surfactant conc.(Alfoterra S23-13S-90)	0.75%
Co-surfactant conc. (Enordet IOS C15-18)	0.25%
Colsolvent conc. (IBA)	1%
AS(P) slug size, PV	0.5
AS(P) viscosity, cp @10s^{-1}	135
AS(P) slug Na_2CO_3, ppm*	32,500
AS(P) polymer conc., ppm	4750
Drive I slug size	0.3
Drive I polymer conc., ppm	5550
Drive I viscosity, cp @10s^{-1}	150
Drive I Na_2CO_3, ppm	32,500
Drive II slug size	1.3
Drive II polymer conc., ppm	4750
Drive II viscosity, cp @10s^{-1}	170
Drive II Na_2CO_3, ppm	22,750

Table 4.1 (continued)

Mobility ratio	<1
Flood mode	Tertiary

* All ASP formulations contain 3,164 NaCl (SRB salinity) in addition to Na_2CO_3 concentration.

Table 4.2: 2D 5-spot tertiary ASP floods with slug viscosity variation

Flood title	ASP VR=0.55	ASP VR=3	ASP VR=10	AS VR=100
Waterflood extent, PV	1.0	1.0	1.0	1.0
Soi, %	88	84	91	92
Porosity	0.326	0.36	0.3	0.32
Brine Permeability, Darcy	~7	~7	~7	~7
AS(P) slug size, PV	0.5	0.5	0.5	0.5
AS(P) viscosity, cp @$10s^{-1}$	180	31	10.8	1
AS(P) slug Na_2CO_3, ppm*	32,500	32,500	32,500	32,500
AS(P) polymer conc., ppm	4750	1800	1000	0
Drive slug size	1.0	1.0	1.0	1.0
Drive polymer conc., ppm	4750	1800	1000	0
Drive viscosity, cp @$10s^{-1}$	180	31	11.6	1
Drive Na_2CO_3, ppm	22,750	22,750	22,750	22,750
Mobility ratio	<1	3.4	11	112
Flood mode	Tertiary	Tertiary	Tertiary	Tertiary

* All ASP formulations contain 3,164 NaCl (SRB salinity) in addition to Na_2CO_3 concentration.

Table 4.3: 2D 5-spot ASP floods with timing variation for VR=3

Flood title	1PV WF ASP	0.5PV WF ASP	Sec. ASP
Waterflood extent	1.0	0.5	0
Soi, %	84	87.7	90.9
Porosity	0.36	0.343	0.354
Brine Permeability, Darcy	7	7	7
ASP slug size, PV	0.5	0.5	0.5
ASP viscosity, cp @$10s^{-1}$	31	31	31
ASP slug Na_2CO_3, ppm*	32,500	32,500	32,500
ASP polymer conc., ppm	1800	1800	1800
Drive slug size	1.0	1.0	1.0
Drive polymer conc., ppm	1800	1800	1800
Drive viscosity, cp @$10s^{-1}$	31	31	31
Drive Na_2CO_3, ppm	22,750	22,750	22,750
Mobility ratio	3.4	3.4	3.4
Flood mode	Tertiary	Tertiary	Secondary

* All ASP formulations contain 3,164 NaCl (SRB salinity) in addition to Na_2CO_3 concentration.

4.2 Results

4.2.1 Phase Behavior and Dynamic IFT

Figure 4.2 shows the solubilization ratios for an alkali-surfactant formulation with a water-oil volume fraction of 30%. The oil and water solubilization ratios are represented respectively as red and blue dots. This formulation contains 0.75% Alfoterra S2313S-90, 0.25% Enordet IOS C15-18, 1 wt% cosolvent (IBA), the injection brine salinity, and varying amounts of Na2CO3 (20,000-44,000 ppm). The optimum surfactant formulation was obtained after several trials with different surfactant blends. With this formulation, I was able to achieve three types of microemulsion phase behavior. At low Na2CO3 concentration (<25,000 ppm), the lower Type-I microemulsion phase forms where the surfactant resides primarily in the water phase and solubilizes some oil. At high Na2CO3 concentration (>43,000 ppm), the surfactant resides primarily in the oil phase and water is solubilized to form the upper Type-II microemulsion phase. When Na2CO3 concentration is between 26,000 and 40,000 ppm, the middle Type-III microemulsion phase forms, where both oil and water are solubilized into the middle phase microemulsion. The salinity at which oil solubilization ratio equals water solubilization ratio is called the optimum salinity. Thus, the optimum salinity is around 37,000 ppm Na2CO3 concentration at a water-oil ratio of 3:7 (or 30 volume% oil).

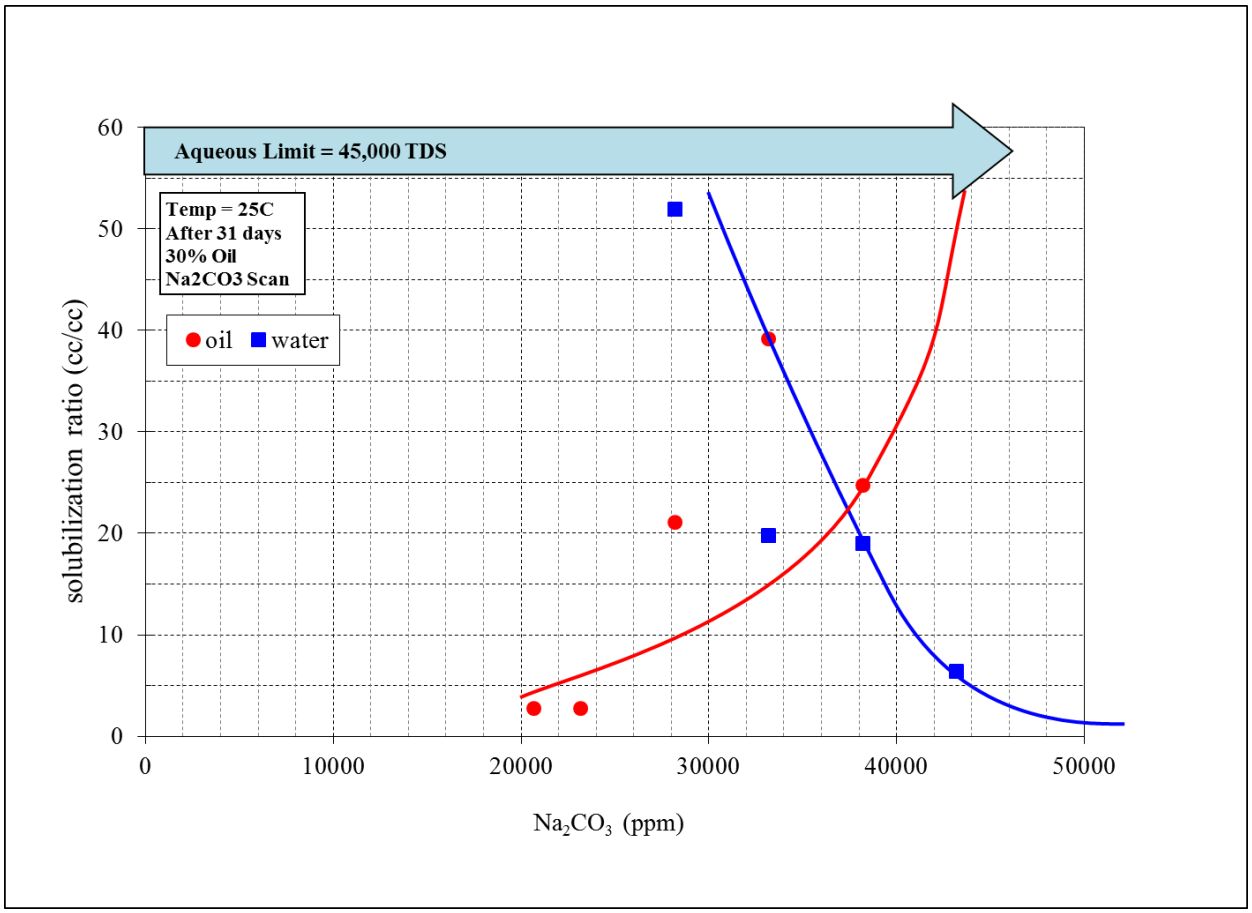

Figure 4.2: Oil and water solubilization ratio for surfactant formulation at an oil volume fraction of 30%

Interfacial tension (IFT) was measured for the alkaline-surfactant formulation at the optimal salinity. An ultralow value of 0.0001 dyne/cm was measured at 50% oil and is consistent with the estimation of IFT from the solubilization ratio (23 in this case) through Huh's equation (1979). These experiments show that this surfactant formulation develops the low interfacial tension with the viscous oil and thus can develop a high capillary number to displace oil from the porous medium.

Figure 4.3 shows the activity diagram where the microemulsion phase behavior is plotted as a function of oil volumetric fraction of 10%, 30%, and 50%. As the oil fraction increases, the three-phase salinity window moves to lower salinity, and thus, the optimum salinity decreases. For

inactive oils, the optimum salinity does not change with the oil fraction. If the oil is active, soap forms by the reaction of oil and Na2CO3; as the oil fraction increases the amount of soap increases. Thus, the soap to synthetic surfactant ratio increases. Since the soap is usually more hydrophobic than the added surfactants, the optimal salinity decreases, as shown in Figure 4.3. During the ASP flood, the salinity of the ASP slug is often at the type III (~35,000ppm) (or slightly into type II), and the salinity of the polymer slug is in the range of type-I salinity (~25,000ppm). In general, the negative slope of the optimum salinity line in the activity diagram is preferred because it ensures that the composition path (the dashed line) during an ASP flood would cross the type III salinity region where ultralow tension can be achieved.

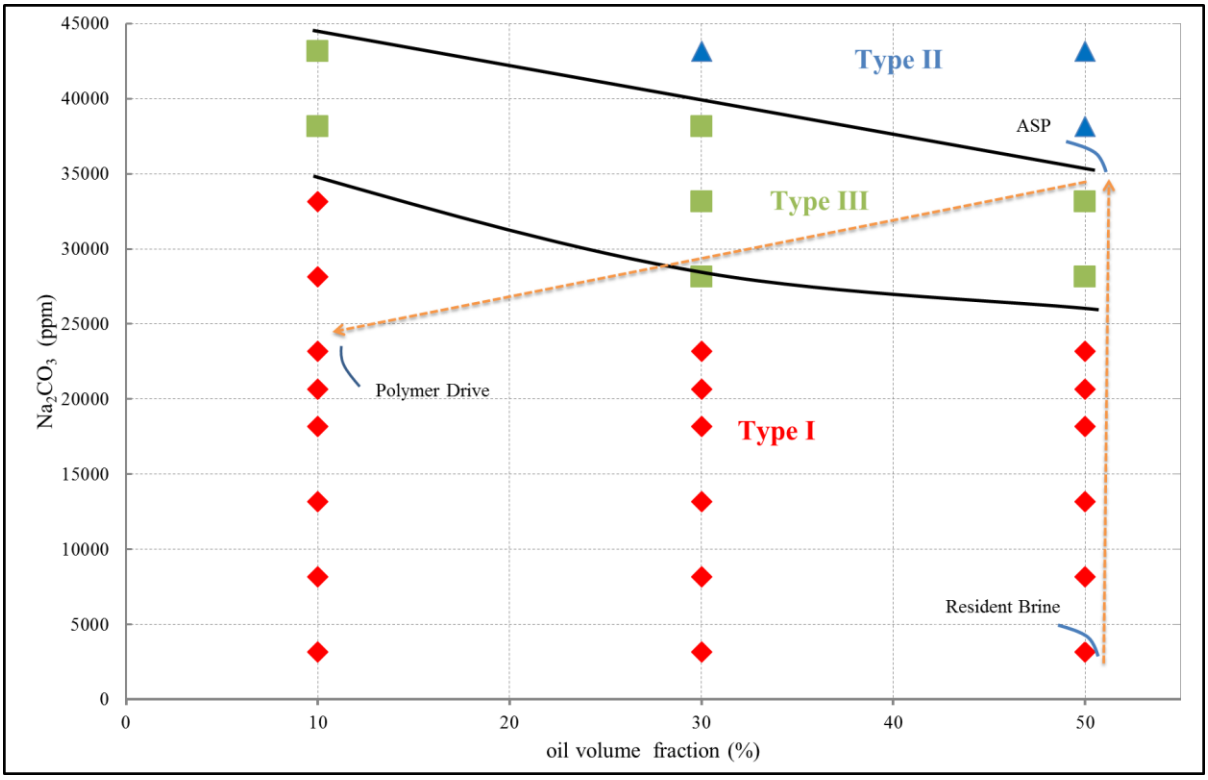

Figure 4.3: Activity diagram showing the phase behavior of viscous oil and the ASP solution at varying oil volume fractions and Na2CO3 concentration

4.2.2 1D ASP STABLE FLOOD

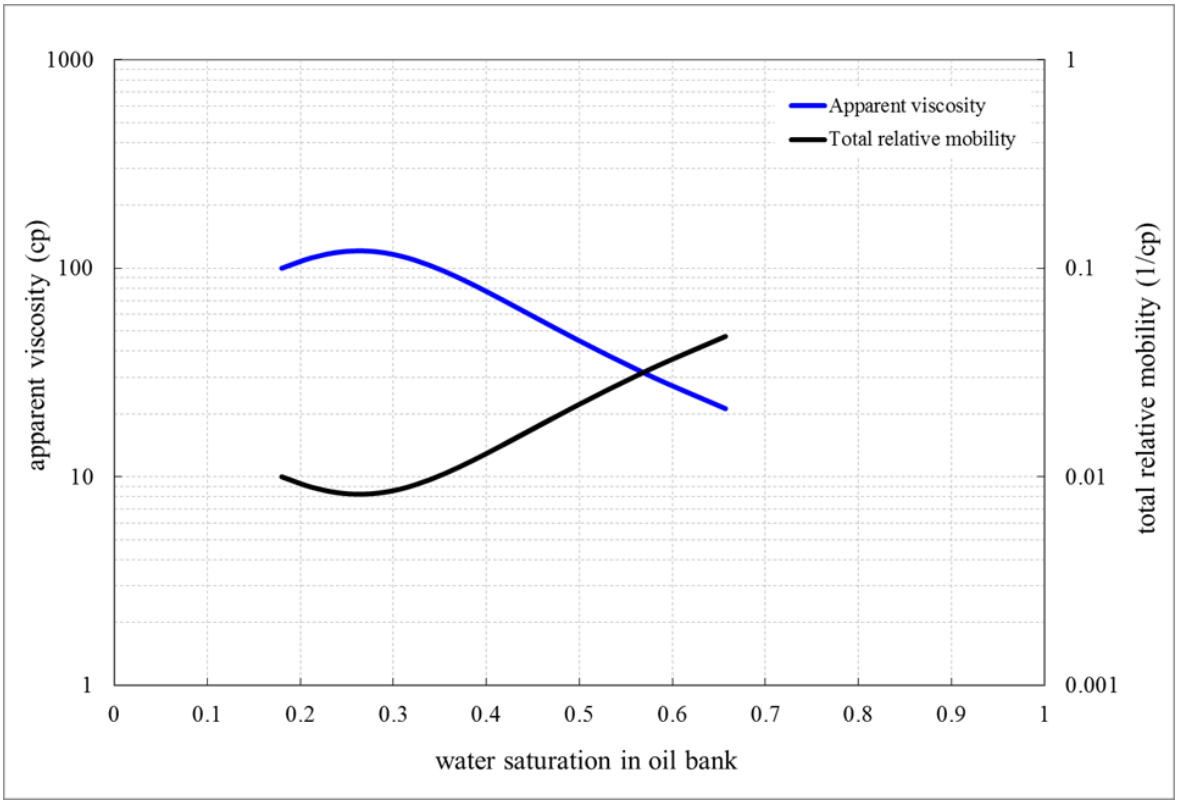

Figure 4.4: Total relative mobility and apparent viscosity of oil water bank

ASP and Polymer Slug Design

The ASP slug was injected for about 0.5 PV followed by the polymer slugs I and II, as listed in Table 4.1. The ASP slug viscosity was 134 cp and the two polymer slug viscosities were respectively 150 and 168 cp (at the 10s-1 shear rate). Figure 4.4 shows total relative mobility and apparent viscosity for the oil bank at different saturations. The minimum total relative mobility was calculated to be 0.0083 cp-1. The maximum apparent viscosity of oil bank, which is equal to the reciprocal of the minimum total relative mobility, was 120 cp. Therefore, the viscosities of ASP and polymer drive must be above 120 cp for a stable displacement of the oil bank. The ASP slug, polymer drive I, and polymer drive II viscosities were above the minimum required viscosity.

Waterflood Performance

Figure 4.5 shows the cumulative oil recovery, the oil cut, the remaining oil saturation and the pressure drop for the 1D ASP sandpack flood. Initially, the oil saturated sandpack at an Swi of 18% was water flooded for 5 PV at an injection velocity of 1ft/d. The waterflood recovered 58% of the original oil in place (OOIP) and decreased the oil saturation from the initial oil saturation of 82% to 34.3%. The pressure drop decreased from about 3 psi to 1.2 psi.

ASP Flood Performance

The oil bank arrived at the outlet at about 0.7 PV after surfactant injection. The oil cut rose to 75% after the surfactant was injected. The oil bank thickness was around 0.5 PV. Most of the oil was recovered by 1.5 PV after the surfactant injection. The chemical flood recovered an extra 35% of OOIP and increased the overall recovery to 93% of OOIP. Furthermore, the chemical flood decreased oil saturation from 34.3% to 5.9%. The tertiary recovery was able to recover 84% of the remaining oil in place (ROIP). The pressure drop decreased from 3.1 psi to 1.28 psi towards the end of the waterflood. After the start of the ASP injection, the pressure drop gradually increased and reached a maximum value of 6 psi at the end of polymer flood. The maximum pressure drop per foot was equal to 12 psi/ft, which would be unsustainable in the field.

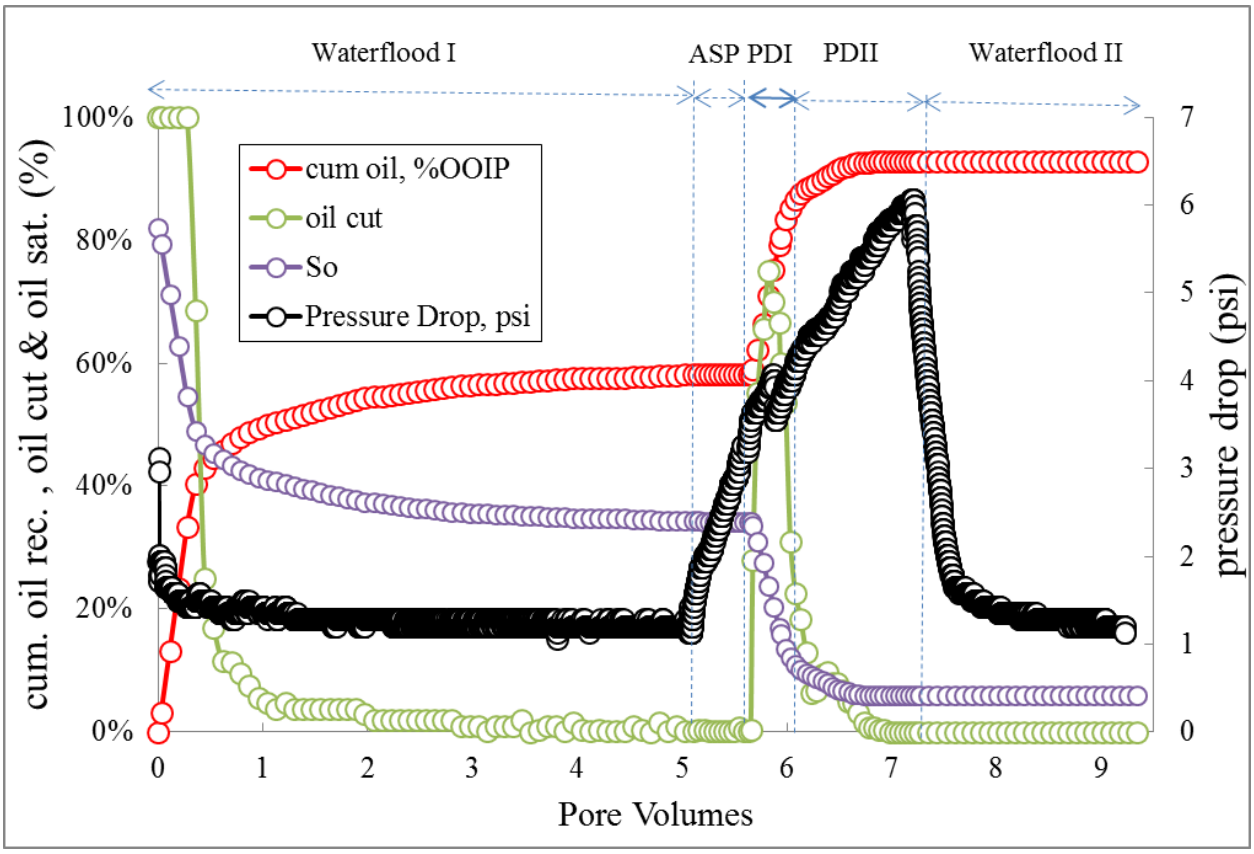

Figure 4.5: Stable ASP core flood cumulative oil recovery, oil cut, oil saturation and pressure drop

The total salinity, pH and viscosity of the effluent water samples were monitored. Figure 4.6 shows that the in situ salinity increased to the type II region due to the ASP slug injection; then decreased and crossed the type III region salinity back to type I region due to the salinity gradient. The pH increased from 8.5 to 11 and stayed at the pH of 11 until the end of the flood. The water viscosity increased due to polymer injection and then decreased during chase water injection. To conclude, the 1D ASP sandpack flood showed that the chemical formulation was effective in mobilizing the oil.

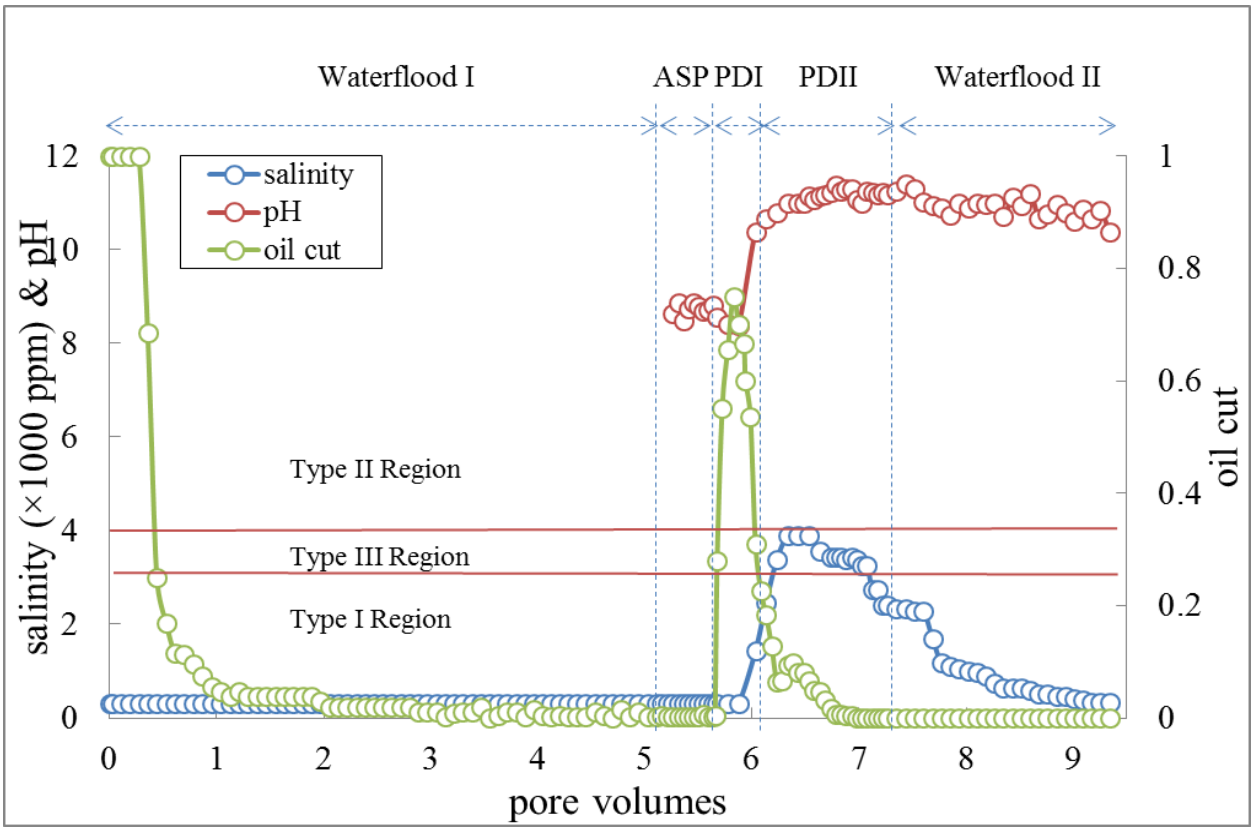

Figure 4.6: Stable ASP core flood the oil cut and the effluent salinity

4.2.3 QUARTER 5-SPOT TERTIARY ASP FLOODS WITH VISCOSITY VARIATION

The 5-spot sandpacks were first saturated with the formation brine. Oil was then injected to achieve the initial oil saturation, which ranged between 0.88-0.92 for four floods in this series. Brine was injected for 1 PV to simulate a short waterflood. Water broke through very fast (at about 0.25 PV), which indicates waterflood was unstable in this multi-dimensional medium. Waterflood recovered ~51% OOIP for the first two floods and ~48% OOIP for the last two floods in 1 PV. This recovery variation reflects the variation in the packing homogeneity as well as the unstable nature of the water flood. The oil saturation decreased from the initial oil saturation to about 0.45. Pressure drop decreased from about ~5 psi initially due to oil flow to ~1.3 psi during water flow (at the remaining oil saturation).

ASP slug was injected for about 0.5 PV followed by the polymer drive slug for about 1 PV. ASP slug compositions were different in the four experiments in the amount of polymers added. The ASP slug consisted of 1 wt% surfactant blends, 1 wt% cosolvent, 3.25 wt% Na2CO3, 0.5 wt% NaCl. The polymer concentrations used were 4750 ppm, 1800 ppm, 1000 ppm, and 0 ppm of HPAM for ASP viscosity ratio (VR) = 0.55, 3, 10, and 100, respectively. All polymer drive slugs contained 2.275 wt% of Na2CO3. 4750 ppm, 1800 ppm, 1000 ppm, and 0 ppm of HPAM were used in the polymer drive for ASP VR=0.55, 3, 10, and 100 floods, respectively. The ASP slug viscosity and the polymer slug viscosity were the same and equal to 180 cp, 30 cp, 10 cp at a shear rate of 6.31 s-1 for ASP VR=0.55, 3, 10 cases.

Figure 4.7 compares the cumulative oil recovery in the three 5-spot tertiary ASP floods. ASP VR=0.55 flood had the most favorable mobility ratio out of the four ASP floods, where 100 cp oil was displaced by the 180 cp ASP slug followed by 1 PV of the 180 cp polymer drive slug. ASP VR=3 had less favorable mobility ratio than ASP VR=0.55 where 100 cp oil was displaced by 0.5 PV of the 30 cp ASP slug, followed by 1 PV of the 30 cp polymer drive slug. ASP VR=10 had the least favorable mobility ratio (out of three floods with polymer) in this series where 100 cp oil was displaced by 0.5 PV of the 10 cp ASP slug, followed by 1PV of the 10 cp polymer drive slug. AS flood was the most unstable flood among the four floods since there was no polymer. ASP VR=0.55 flood recovered 98% OOIP (including waterflood recovery). Most of the oil was recovered. ASP VR=3 flood recovered 90% of OOIP or additional 39% OOIP of oil after the initial waterflood. ASP VR=10 flood recovered 80% of OOIP or additional 32% OOIP of oil after the initial waterflood. Lastly, AS flood recovered total of 55% of OOIP or 7% additional oil in place after initial waterflood. This additional oil could have been recovered by the continuation of the waterflood. Thus the addition of alkali and surfactant did not yield any additional oil. These

experiments show that the viscosity of the ASP slug has an important role in enhancing oil recovery.

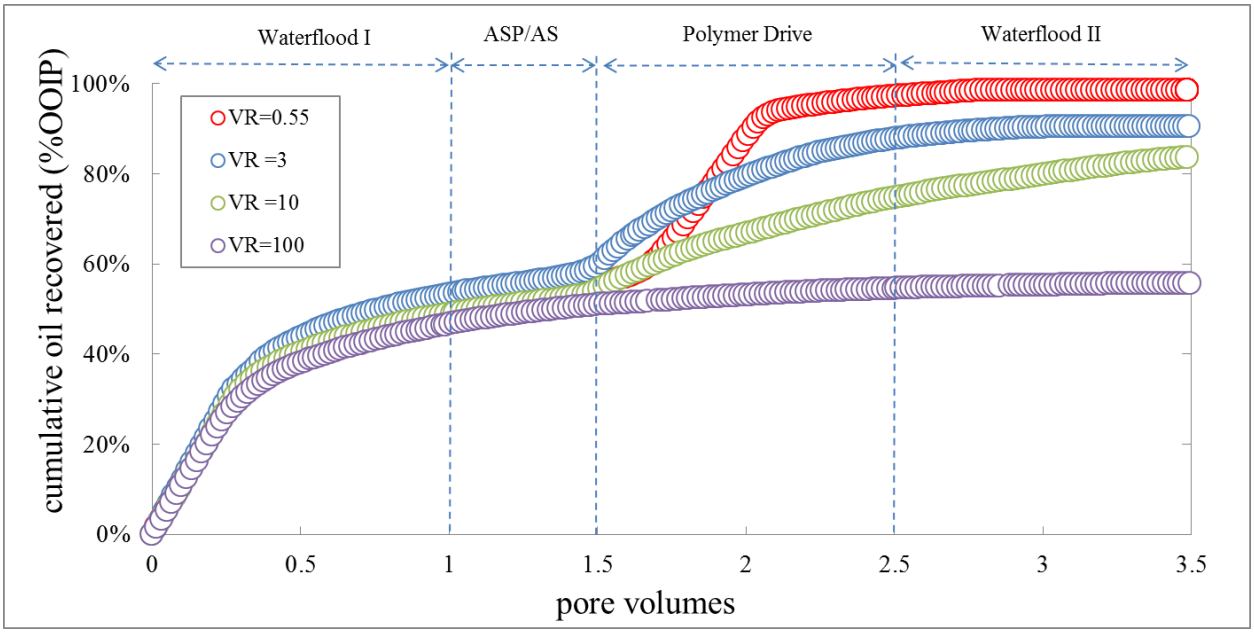

Figure 4.7: Oil recovery for ASP quarter 5-spot floods: variation of chemical slug viscosity (VR=0.5, 3, 10 and 100)

Figure 4.8 shows the oil cut in the waterflood followed by the ASP floods in the quarter 5-spot. The oil cut decreases during the waterflood, then increases during the ASP flood due to the oil bank formation and eventually decreases to zero during the polymer drive for each of the four floods. The maximum oil cut in the oil bank was around 80% for ASP VR=0.55 flood. Maximum oil cut for VR=3 case decreased to 50%. The oil cut could not be sustained at its maximum oil cut; it increased and then decreased due to instability at the back of the oil bank. Oil cut decreased further to 30% for VR=10 case and had a much longer tail of low oil cut compare to the other floods. Lastly, oil bank was not observed for AS flood (after the initial waterflood).

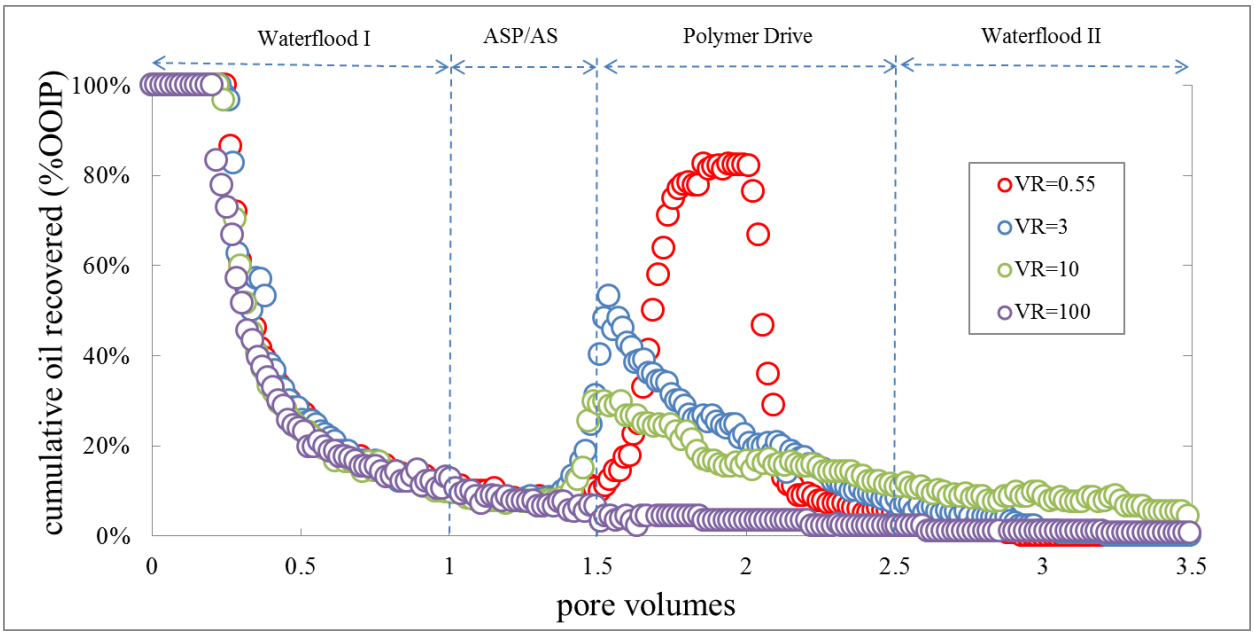

Figure 4.8: Oil cut for ASP quarter 5-spot floods: variation of chemical slug viscosity (VR=0.5, 3, 10 and 100)

Figure 4.9 shows cumulative oil recovery and pressure gradient during the four tertiary ASP floods. Both the cumulative oil recovery and pressure gradient decrease as the viscosity ratio increases, but the pressure gradient decreases faster than oil recovery between viscosity ratio of 1 and 3. The ideal viscosity ratio would be the one which yields high enough oil recovery with low enough pressure gradient. The viscosity ratio of 3 appears to be the optimum (for the quarter 5-spot) where the oil recovery is very high (90%) and the pressure gradient is feasible (5.4 psi/ft). These experiments were performed under constant injection rate, which is not often the case in field applications. Generally, the injection is pressure constrained, and the available pressure drop is limited in viscous oil reservoirs. The optimum ASP viscosity ratio needs to be determined for any field by conducting a realistic stimulation.

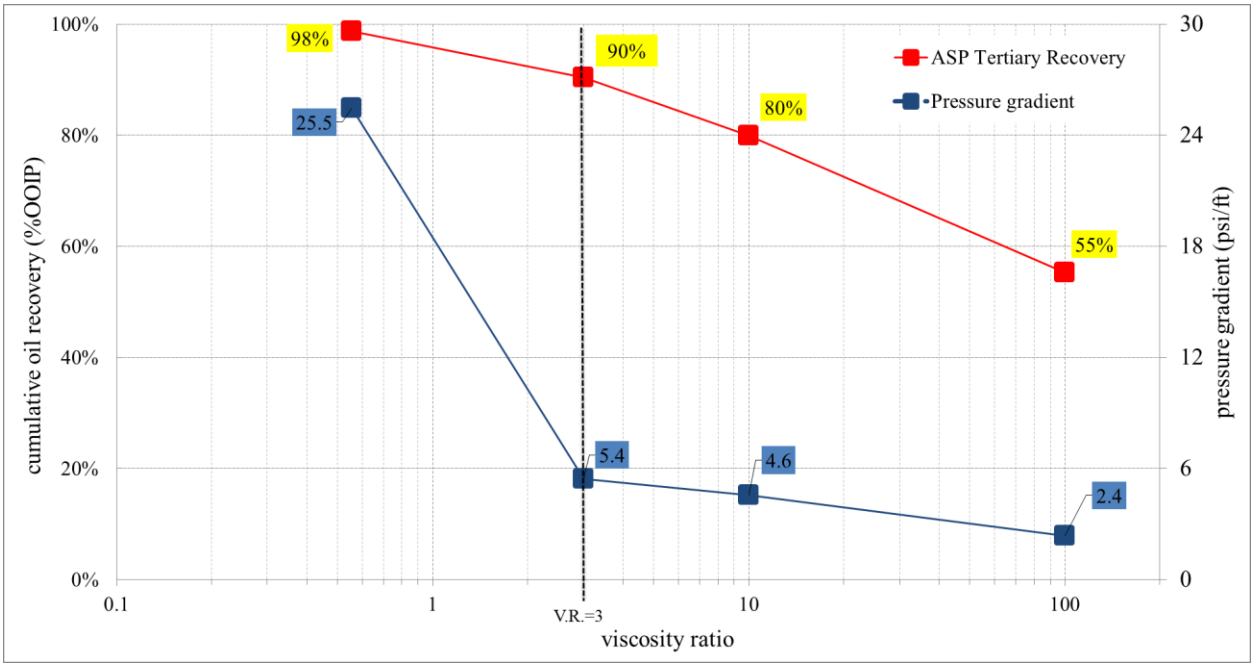

Figure 4.9: Recovery and pressure gradient for quarter 5-spot floods at several viscosity ratios

4.2.4 Quarter 5-spot ASP Floods with Different Starting Times

Two additional floods were conducted with 30 cp ASP slug where the extent of prior waterflood was varied, as described in Table 4.3. Figure 4.10 compares the cumulative oil recovery in the three 5-spot ASP floods at the same viscosity ratio. These floods were unstable because 100 cp oil was displaced by 0.5 PV of the 30 cp ASP slug, followed by 1PV of the 30 cp polymer slug. The main difference between these three floods was the onset of the ASP injection. The ASP floods started after 1PV of the waterflooding, 0.5 PV of the waterflooding and without any waterflooding, i.e., secondary mode. All three floods have similar ultimate recoveries, about 90% of OOIP. The secondary ASP flood recovered oil fastest (in terms of PV injected). These experiments were performed under constant injection flow rate. Generally, the available pressure drop is limited in viscous oil reservoirs. Thus, even though the secondary ASP flood recovered the most amount of oil at a given PVI, it may not recover the highest amount of oil at comparable times under the fixed pressure drop conditions. Figure 4.11 shows oil cuts for the three ASP floods (with the viscosity

ratio of 3). In the secondary flood, the oil cut stayed at 100% for about 0.5 PV and decreased after the breakthrough. The maximum oil cut for tertiary floods were 80% and 50% for 0.5 PV waterflood and 1PV waterflood cases, respectively.

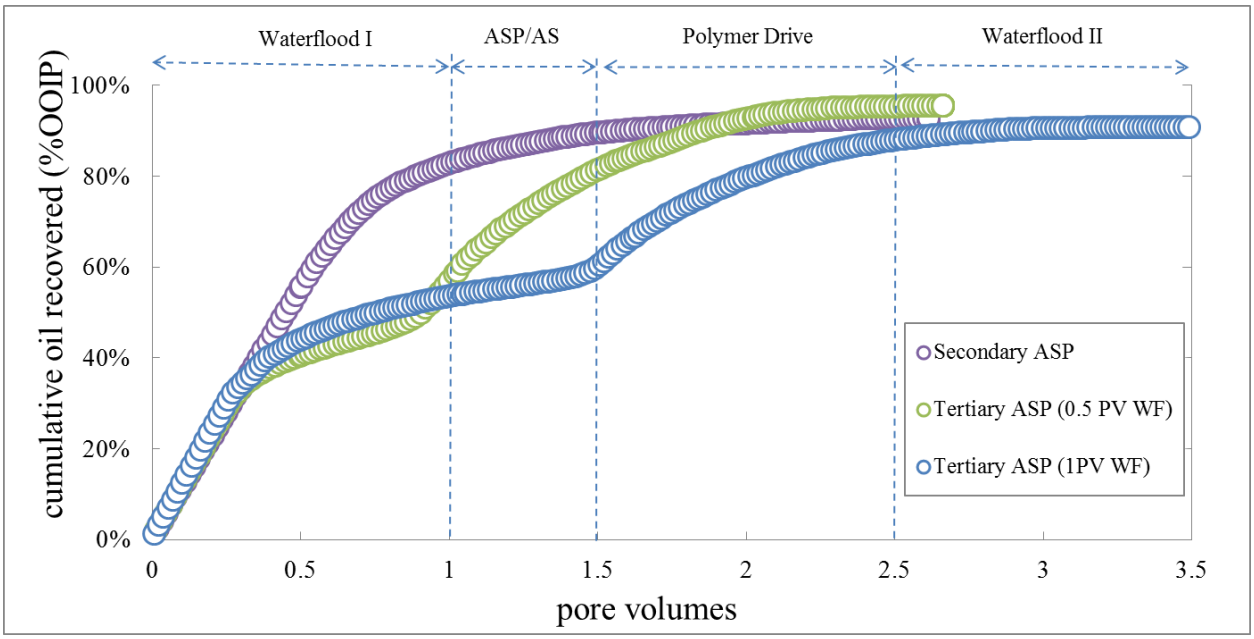

Figure 4.10: Cumulative recovery for secondary and tertiary ASP floods at the viscosity ratio of 3

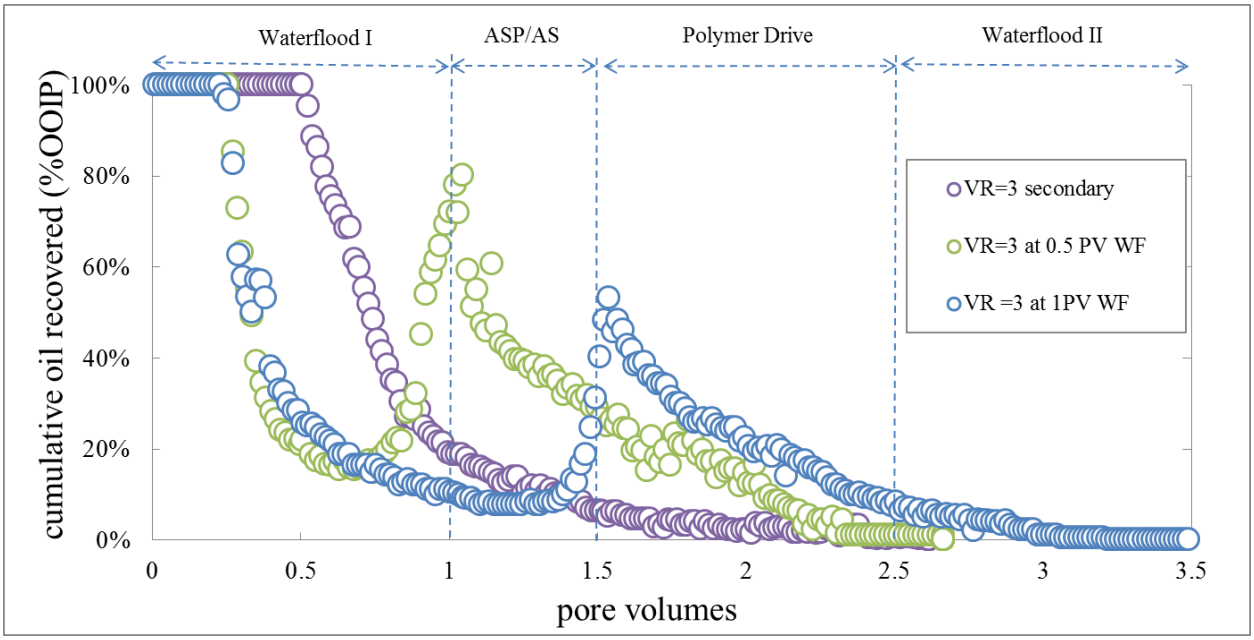

Figure 4.11: Oil cut for secondary and tertiary ASP floods at the viscosity ratio 3

4.2.5 Sweep Efficiency of ASP Floods

After each experiment, the 2D sandpack was opened and analyzed for the distribution of the remaining oil. The injection fluid totally swept the bottom of the sand pack in each case, but the top was not fully swept. Figure 4.12 shows the top of the sand pack at the end of the experiments. Arrows represent injection and production ports. These floods were unstable, and thus, some of the oil was bypassed. The bypassed oil regions look black (or brown) colored. Well-swept regions look light gray (or brown).

Figure 4.12 compares areal sweep patterns for ASP floods with viscosity ratios 3, 10 and AS flood with viscosity ratio 100. For ASP VR=3, the unswept oil zones were mostly concentrated around the closed corners of the 5-spot sand pack with some bypassed regions in the middle of the well-swept area. This indicates that even though the flood was not stable (Mo=3.4), it was still able to sweep most of the sandpack. A further increase in the viscosity ratio to VR=10 (Mo=11), shows drastically decreased areal sweep efficiency. Less than half of the sandpack is well swept on the top. Areal sweep for VR=100 (Mo=112) shows even less sweep and mostly unswept areas. Due to high mobility ratio, even the swept zones look visibly darker indicating higher remaining oil saturations for VR=100 and VR=10 compared to VR=3 case.

Figure 4.12: Areal Sweep Comparison at ASP VR=3, 10, and 100 (from left to right)

Figure 4.13 compares areal sweep efficiencies for ASP floods with different extents of water flood for the same viscosity ratio (3). Qualitatively the areal sweep efficiencies are similar. The left picture was taken after the secondary ASP flood and the right picture was taken after the tertiary ASP flooding with 0.5 PV of initial waterflood. Arrows represent injection and production ports. Bypassed oil zones (black) and well-swept zones (grey) can be seen on top of the sandpack. As expected, unswept oil zones were mostly concentrated around the sides of the 2D cell. Further analysis of the sandpack by computer tomography and direct saturation measurement also confirmed this observation. In all of the 2D ASP floods the bottom of the sandpack was completely swept. This was observed in stable as well as unstable floods and for both the secondary and the tertiary ASP floods. Thus, even in a 1 inch thick sandpack, the gravity effect was significant. That can be attributed to the ultralow IFT achieved in these floods. The capillary forces disappear in chemical floods when ultralow tension develops; thus the aqueous phase segregates to the bottom even in an inch thick sand pack. The vertical sweep efficiency looked larger for the tertiary mode because there is no gravity segregation in the preceding waterflood. All dimensionless number calculation that includes gravity, bond, capillary and trapping numbers indicate that the flood was performed in the transition zone and was not dominated by only one flow region. Thus, sweep efficiency during the ASP flood depends on the timing of the ASP injection.

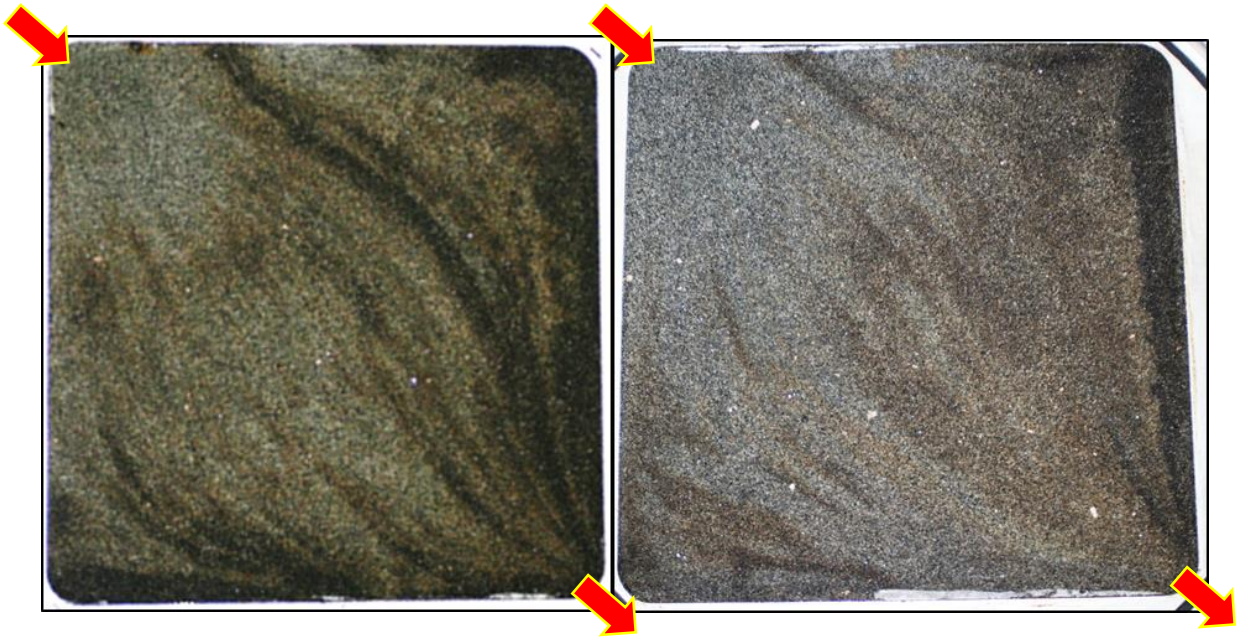

Figure 4.13: Areal sweep comparison for ASP floods: (from left to right) secondary mode and tertiary mode after 0.5 PV waterflood

4.2.6 SIMULATION

The ASP 5-spot sandpack floods were modeled using the University of Texas Chemical Flooding Simulator, UTCHEM (VERSION 9.9) . The key features of ASP modeling are: in-situ soap generation by alkali and oil acid reaction, IFT (as a function of salinity, surfactant, and soap concentration), microemulsion rheology, and polymer rheology. Many critical input parameters were measured in lab. Table 4.4 shows the simulation parameters that were used to history match ASP experiments. The ASP UTCHEM input file details can be found in Appendix A.1. Detailed explanation of ASP flooding simulation and parameters that go into UTCHEM can be found in Mohammadi et al. (2009).

Table 4.4: Key UTCHEM reservoir and fluid property parameters in the ASP simulation model

Parameters	Parameter Values
Components	water, oil, surfactant, polymer, chlorine, calcium, alcohol, carbonate, sodium, hydrogen, and oil acid
Grid	50×50×1
Gridblock size (ft)	0.0167×0.0167× 0.083

Table 4.4 (continued)

Average Porosity	0.354
Average permeability (md)	7,000
Initial water saturation	0.16
Initial salinity (meq/ml)	0.054
Solubilization ratio of surfactant at the optimum salinity	35
Upper Type III Salinity of soap (meq/ml)	1.1
Lower Type III Salinity of soap (meq/ml)	0.5
Huh's IFT model parameters (c, a)	0.3,10
Residual Saturations of water, oil, microemulsion phases at low capillary number	0.16,0.26, 0.16
Endpoints of relative permeabilites water, oil, microemulsion phases at low capillary number	0.025,0.95,0.025
Exponents of relative permeabilities water, oil, microemulsion phases at low capillary number	2.5,2.2,2.5
Water and Oil viscosities (cp)	0.9,100
Oil Acid Number (mg KOH/g Oil)	1
Shear rate at half zero-rate viscosity(s^{-1})	2.7
Polymer rheology exponent	1.6
Injection rate (ft^3/day)	0.0254

A key feature of the ASP flood is the complex interaction between oil and the surfactants (synthetic surfactant and in-situ soap). In-situ soap is generated due to the reaction between the injected alkali and the acid in the oil. It is a natural surfactant which can form microemulsion and reduce interfacial tension. Due to soap being hydrophobic in nature, it always important to find correct ratio of synthetic surfactant to soap in order to have synergistic effect. Thus, in order to find right balance between synthetic surfactant and soap, many phase behavior experiments must be performed. Furthermore, the microemulsion formation is facilitated by the addition of cosolvents. They improve the microemulsion stability and most importantly reduce the microemulsion viscosity.

In order to capture the complex chemical interactions between alkali,surfactant, cosolvent, and oil, the ASP flood modelling was coupled with a full geochemical reaction module.The geochemical reaction module provides an accurate estimate of the soap generation, salinity and concentrations of species involved in chemical reaction during ASP flooding. Table 4.5 shows the reactions described by Luo et al. (2015). It includes the reactions among oil acid, alkali, and water, where $(HA)_o$, $(HA)_w$, *and* A^- are oil acid in oil, oil acid in water, and soap, respectively. During the soap generation a certain amount of alkali is consumed and the pH value is lowered.

Table 4.5: Oil-acid reactions used in the simulation

Species	**Reactions**
$(HA)_w$	$(HA)_o \rightleftarrows (HA)_w$
A^-	$(HA)_w \rightleftarrows H^+ + A^-$

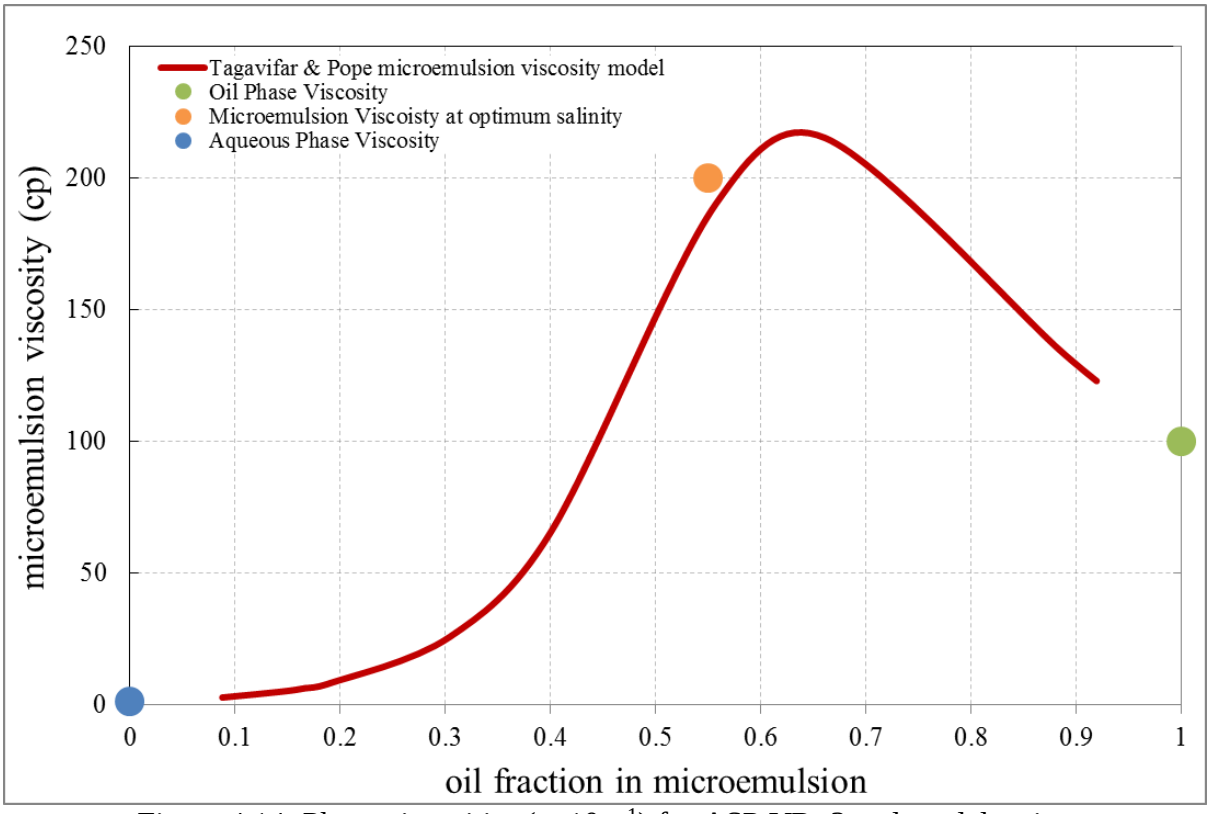

Figure 4.14: Phase viscosities (at 10 s^{-1}) for ASP VR=3 and model estimates

Capturing correct microemulsion viscosity is very important for a successful history match during ASP flooding. There are several microemulsion viscosity models that can be used. The most recent microemulsion viscosity model proposed by Tagavifar et al. (2016) was used to estimate the microemulsion viscosity. The model includes the cosolvent and polymer effect on the microemulsion rheology. It was validated through the accurate laboratory experiments. Figure 4.14 shows the measured microemulsion viscosity at the optimum salinity, the lower aqueous phase viscosity and the upper excess oil viscosity for ASP VR=3 case, represented by points and the model fit represented by a line. The model takes into account the cosolvent effect in reducing the microemulsion viscosity.

The modified Flory-Huggins (Flory, 1953; Delshad et. al., 1996) model takes into account the effect of polymer concentration, water viscosity, salinity and hardness on the polymer viscosity at low shear rates.

$$\mu_p^0 = \mu_w \left[1 + \left(A_{p1}C_p + A_{p2}{C_p}^2 + A_{p3}{C_p}^3\right)C_{SEP}^{S_p}\right] \tag{4.4}$$

where C_p is the polymer concentration either in aqueous phase or microemulsion phase, μ_w is the brine viscosity, A_{p1} , A_{p2} , and A_{p3} are the fitting parrameters obtained from matching measured lab data. The parameter $C_{SEP}^{S_p}$ represents the salinity and hardness effect on the polymer viscosity. The effect of salinity on polymer viscosity is represented by the S_p and is equal to the slope of log-log plot of effective salinity (C_{SEP}) versus $\frac{\mu_p^0 - \mu_w}{\mu_w}$.

The polymer viscosity as a function of shear rate can be modeled by Meter and Bird (1964), i.e.,

$$\mu_{\text{app}} = \mu_\infty + \frac{\mu_{p0} - \mu_\infty}{1 + \left(\frac{\gamma_{eff}}{\gamma_h}\right)^{P_\alpha - 1}} \quad , \tag{4.5}$$

where μ_{app} is the apparent in-situ polymer viscosity, μ_∞ is the polymer solution viscosity at infinite shear rate which I assume to be equal to water viscosity, μ_{p0} is the polymer solution viscosity at zero shear rate, γ_{eff} is the effective shear rate in the reservoir, γ_h is the shear rate at which polymer viscosity is half of the viscosity at zero shear rate, and P_α the power law exponent which depends on polymer concentration. Figure 4.15 shows the experimental data and the model match using Meter's model for polymer viscosity.

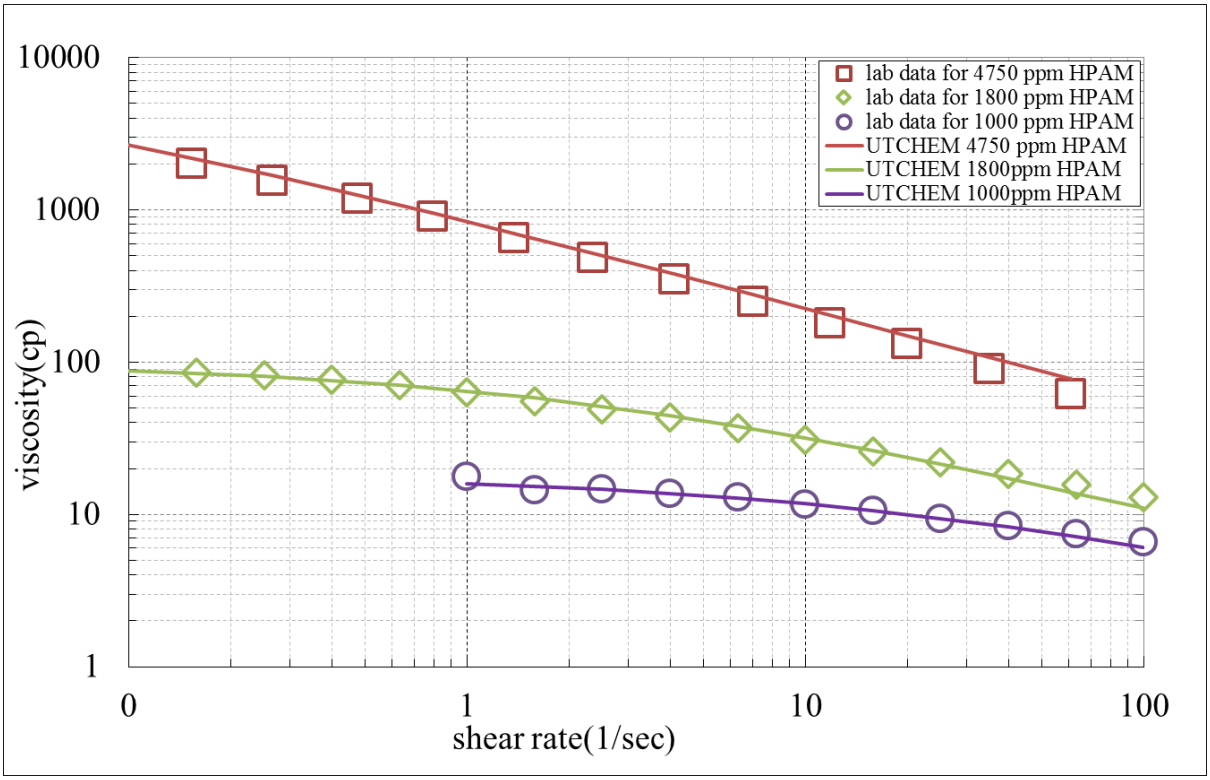

Figure 4.15: ASP slug solution viscosities for ASP VR=0.55, 3, and 10. The data points were measured in lab and lines were computed by UTCHEM

Lab-Scale Simulation by UTCHEM

The quarter 5-spot sand pack was modeled by UTCHEM. The permeability map was created using random distribution with a Dykstra-Parsons (Vdp) coefficient of 0.4 and an average permeability of 7 Darcy. Figure 4.16 shows the permeability map used for lab scale simulations.

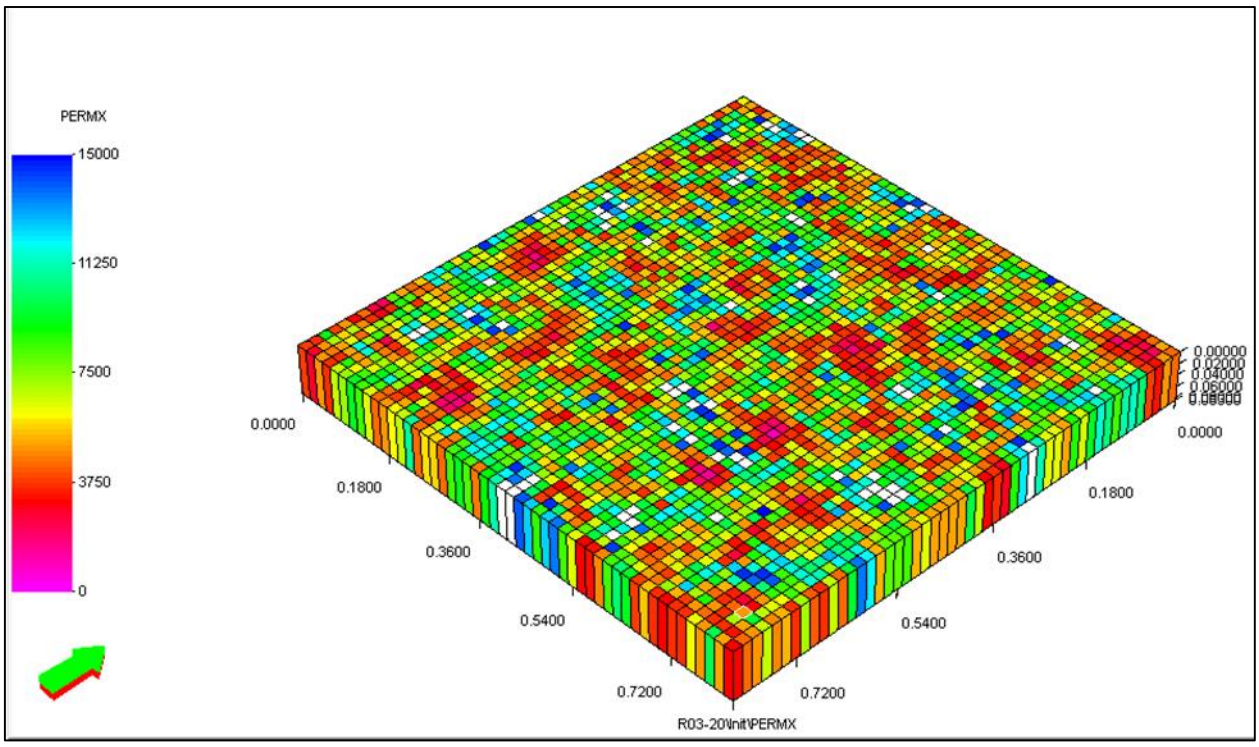

Figure 4.16: Permeability map in mD with Kmean=7,000 mD and Vdp= 0.4

Figures 4.17 and 4.18 show the simulation results for cumulative recovery, oil cut, and pressure drop for ASP flood with a viscosity ratio of 3. Solubilization and capillary desaturation parameters were tuning factors to match the experimental data. The oil recovery was matched well, but the pressure drop was matched only qualitatively. The unstable flow due to adverse mobility ratio, 3-dimensional compositional simulation, numerical dispersion, and uncertainties involved with phase behavior were the main challenges in the matching of the results. Furthermore, the reservoir sand that was used had some fine grains. Fine migration gets exaggerated during viscous ASP flood. Therefore, the pressure drop did not go down after the passage of the oil bank in the experiment.

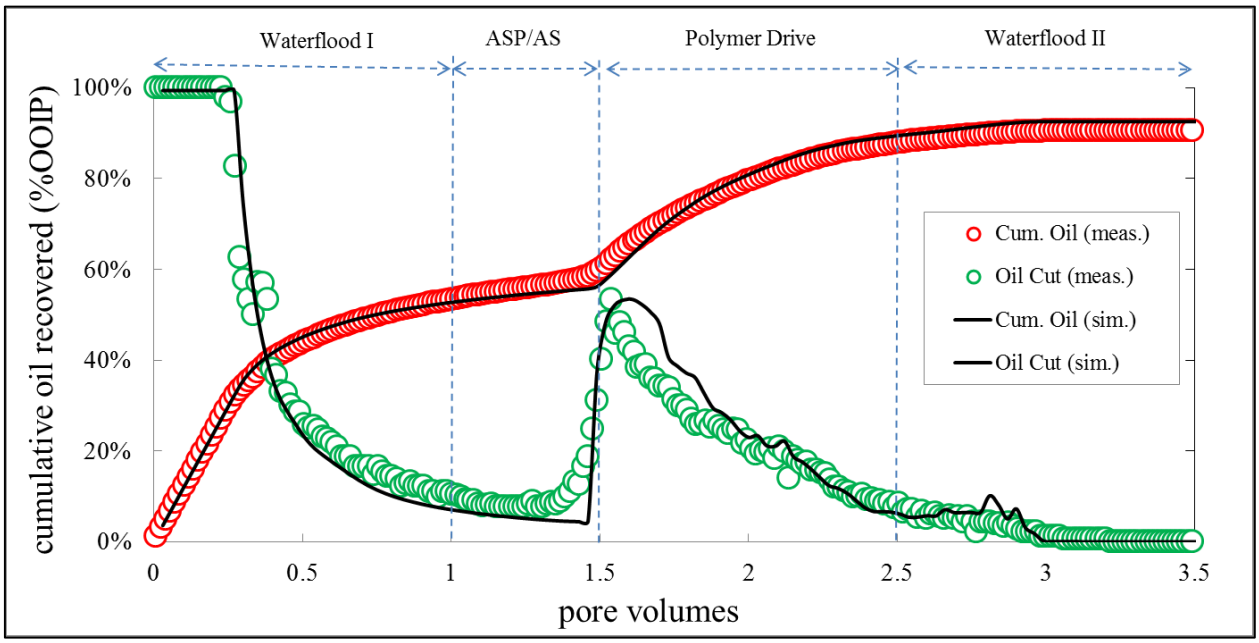

Figure 4.17: Cumulative oil recovery and oil cut comparisons of experimental data and simulation results

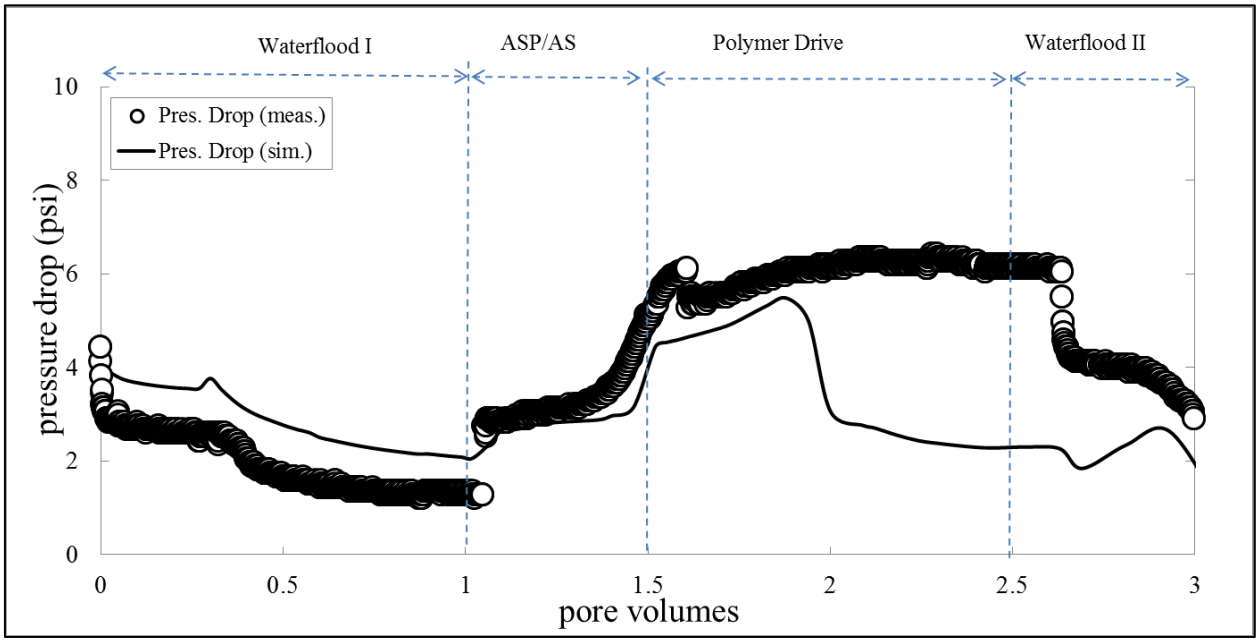

Figure 4.18: Pressure drop during ASP flood experiment and simulation

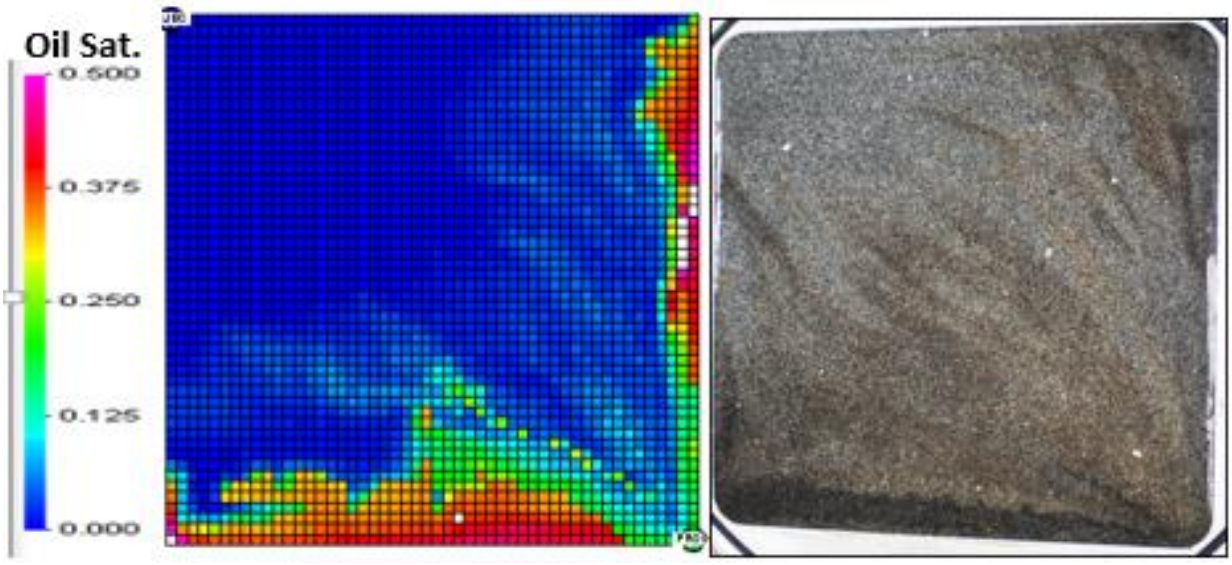

Figure 4.19: Oil saturation distribution at the end of ASP floods for experiments and simulations at VR=3.

The final oil saturation distributions for simulations were compared with the pictures of the sand pack at the end of the experiments. Figure 4.19 shows the final oil saturations on the top of the quarter 5-spot for VR=3 case. Simulations qualitatively match the experimental observations.

In summary, I have conducted several ASP floods in a 2D sand pack to study viscous oil recovery at several viscosity ratios and after variable extents of waterflooding. I have developed an UTCHEM simulation model of the ASP process that is validated with the laboratory experimental data. Such a model can be used at the field scale to develop guidelines for optimum viscosity ratio and starting time for ASP floods.

CHAPTER 5: 2D EXPERIMENTAL INVESTIGATION OF ALKALINE-COSOLVENT-POLYMER FLOOD FOR VISCOUS OIL RECOVERY

One of the key aspects of viscous oil recovery is the sweep efficiency of the displacement process. ASP or ACP floods can be made more stable by adding enough polymer. Then, the sweep efficiency and the ultimate recovery would be high, but the injection rate would be low because the injection fluid would be very viscous. If only a small amount of polymer is used, then the injection rate would be high, but the sweep efficiency would be low. Thus, these floods should be evaluated as a function of polymer concentration or chemical slug viscosity. Since the sweep efficiency is affected, the formulations should be tested in multi-dimensional porous media (not just core floods). One of the objectives of this research is to perform ACP floods in a laboratory quarter 5-spot model for a viscous oil and study sweep efficiency and pressure drop as a function of chemical slug viscosity.

Injection rates in viscous oil reservoirs are often limited by small inter-well pressure drops (500-1000 psi) and high oil viscosities. Since not many pore volumes of fluids (about 1-2 PV) can be injected into a viscous oil reservoir (during its project life of about 30-50 year), one key question is the optimum time to start the ACP flood. If the ACP flood is started early, then the injection rate may be too low. If it is started late, then there may be little time to push the oil out during the reservoir life. Another objective of this research is to investigate the effect of the starting time of ACP floods in viscous oil reservoirs on oil recovery during the project life.

In this work, I developed an alkaline-cosolvent formulation by phase-behavior experiments that produced ultra-low interfacial tension with a viscous oil. I tested the effectiveness of the formulation by conducting a 1D ACP flood in a linear sandpack. Then ACP floods were conducted in a quarter 5-spot sandpack. The viscosity of the chemical slug was varied as well as the starting

time of the ACP flood. These laboratory floods were simulated using UTCHEM, an in-house chemical EOR simulator. The methods and the results are summarized in the following sections.

5.1 Experimental Methods

Materials

Iso-butanol ethoxylates (IBA-xEO) were used as cosolvents and were supplied by Harcros Chemicals. Polymer Flopaam 3630s was provided by SNF Floerger. The alkali used was Sodium Carbonate. Sodium Carbonate and Sodium Chloride were obtained from Fisher Chemical. Oil was received from a field. Oil API gravity is 19 with a viscosity of 320 cp. The total acid number (TAN) is 2.4 mg KOH/gm of oil. The studies were conducted at 25 °C which is close to the reservoir temperature. The formation brine and the water flood injection brine had the same salinity of 40,000 ppm Sodium Chloride.

Phase Behavior Studies

ACP formulations were tested for aqueous stability at 25 °C. The alkali and cosolvents were equilibrated with brine. A chemical is considered aqueous stable when it does not precipitate, or the solution does not become cloudy. Alkali-cosolvent-oil phase behavior experiments were performed to identify the alkali-cosolvent formulation. Aqueous solutions were prepared by mixing 1 wt% cosolvent with DI water, NaCl and alkali. The alkali concentration was varied systematically (in a series of pipettes) keeping the other parameters fixed. The ratio of aqueous solution to oil (WOR) was varied systematically. The samples were equilibrated at 25 °C, and their phase volumes were observed. Occurrence of three phases corresponds to ultralow IFT. This

process allows us to identify alkali concentration ranges of ultralow IFT. Oil, microemulsion, polymer, and ACP solution viscosities were measured using the rheometer AR 2000. A cone-and-plate geometry was used to measure viscosity at different shear rates at a fixed temperature. The alkali-cosolvent formulations that produced ultra-low IFT and other desirable behaviors such as fast equilibration, low microemulsion viscosity, and aqueous stability at injected salinity were selected for ACP chemical floods.

IFT Measurements

The microemulsion/water IFT was determined using the Temco spinning drop interfacial tensiometer. The oil and ACP solution were mixed at the optimum salinity and equilibrated at the experimental temperature until no phase volume change was observed. The equilibrated middle microemulsion phase and the lower aqueous phase were carefully extracted and put into tensiometer. Since tensiometer relies on color contrast between oil and aqueous solution and employs refractive index to calculate IFT, only IFT between dark microemulsion and clear aqueous phase could be measured. The oil-microemulsion IFT could not be measured because both these phases had the same color.

1D Sand Pack Flood

A foot-long steel tube, 1.5 inches in diameter, was packed with Ottawa sand of size 40/70 mesh (average grain diameter ~270 microns). The measured porosity was 32.8%, and brine permeability was ~12 D. The pore volume was 114 cc. The core was first fully saturated with the formation brine and then flooded with the reservoir oil to achieve the initial oil saturation, S_{oi}. Water flood was initiated by injecting formation brine from the bottom at the rate of 1 ft/d; this flood was continued for 4.5 PV. The tertiary ACP flood consisted of injection of an ACP slug (0.5 PV)

followed by a polymer slug (1 PV) which was further followed by a water flood for about 2 PV. The ACP slug consisted of 1.0 wt% cosolvent, 3 wt% Na_2CO_3, and 0.57 wt% polymer in DI water. The polymer slug contained 0.55 wt% polymer and 2 wt% Na_2CO_3 in DI water. Refer to Table 5.1.

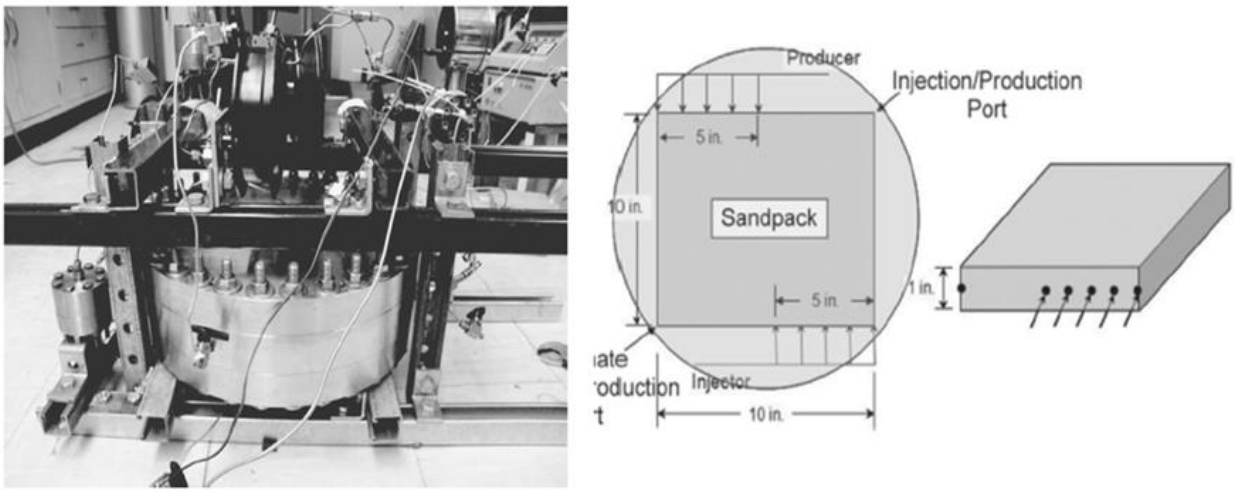

Figure 5.1: The quarter 5-spot sandpack model

2D Sand Pack Floods

Figure 5.1 shows a picture and a sketch of the quarter 5-spot sand pack. It is 10-inch x 10-inch x 1 inch. The sand pack is covered by rubber sheets at the top and bottom over which a confining pressure is applied. The quarter five-spot pattern was wet packed. After closing the five-spot pattern, an overburden pressure of 1300 psi was applied. The compression of the sand from the bottom and the top ensures the creation of a tight sandpack.

All the ACP floods were conducted at a temperature of 25 ^oC (which is also the reservoir temperature). Tables 1 and 2 list the injection fluid sequence for the quarter 5-spot sandpack floods. In Table 5.1, all floods were performed in a tertiary mode. The injection fluid was pumped by an ISCO pump at a constant flow rate of 0.5 ml/min which is equivalent to a maximum interstitial velocity of 0.8 ft/day. The pressure drop across the sandpack was measured by pressure

transducers. Effluent samples were collected in tubes using a fractional collector, and the phase volumes were measured. The produced emulsions during the ACP flood were heated and de-emulsified with appropriate chemicals for accurate measurement of oil and aqueous phase volumes. In Table 5.1, the "1D Stable ACP" stands for the stable ACP flood in the linear 1D sandpack. The ACP VR=2, 4, 12 floods were performed in the quarter 5-spot sandpack at different viscosity ratios (VR). The viscosity ratio is defined as the oil viscosity divided by the ACP slug viscosity. The shear rate of 6.31 s^{-1} was estimated to be the in-situ shear rate; the viscosity mentioned is at this nominal shear rate. In Table 5.2, ACP slug viscosity ratio was kept constant at 4, but the starting time of the ACP flood was varied, i.e., secondary mode and tertiary mode with different extents of water flood.

Table 5.1: 2D 5-spot tertiary ACP floods with slug viscosity variation

Flood title	1D Stable ACP	ACP VR=2	ACP VR=4	ACP VR=12
Waterflood extent, PV	4.5	1.0	1.0	1.0
Soi, %	87	94	90	92
Porosity	0.33	0.354	0.36	0.35
Permeability, Darcy	12	12	12	12
ACP slug size, PV	0.5	0.5	0.50	0.5
Cosolvent conc. %	1	1	1	1
ACP viscosity, cp @6.31s^{-1}	337	160	80	25
ACP slug Na_2CO_3, ppm	30,000	30,000	30,000	30,000
ACP polymer conc., ppm	5730	4000	2950	1500
Drive slug size	1.0	1.0	1.0	1.0
Drive polymer conc., ppm	5580	3700	2700	1350
Drive viscosity, cp @6.31s^{-1}	363	160	80	25
Drive Na_2CO_3, ppm	20,000	20,000	20,000	20,000
Mobility ratio	1	2.3	4.6	14.6
Flood mode	Tertiary	Tertiary	Tertiary	Tertiary

Table 5.2: 2D 5-spot ACP floods with timing variation for VR=4

Flood title	1PV WF ACP	0.5PV WF ACP	Sec. ACP
Waterflood extent	1.0	0.5	0
Soi, %	90	93.1	93.5
Porosity	0.36	0.36	0.35
Permeability, Darcy	12	12	12
ACP slug size, PV	0.5	0.5	0.5
Cosolvent conc. %	1	1	1
ACP viscosity, cp @6.31s^{-1}	80	80	80
ACP slug Na_2CO_3, ppm	30,000	30,000	30,000
ACP polymer conc., ppm	2950	2950	2950
Drive slug size	1.0	1.0	1.0
Drive polymer conc., ppm	2700	2700	2700
Drive viscosity, cp @6.31s^{-1}	80	80	80
Drive Na_2CO_3, ppm	20,000	20,000	20,000
Mobility ratio	4.6	4.6	4.6
Flood mode	Tertiary	Tertiary	Secondary

5.2 Results

5.2.1 PHASE BEHAVIOR AND DYNAMIC IFT

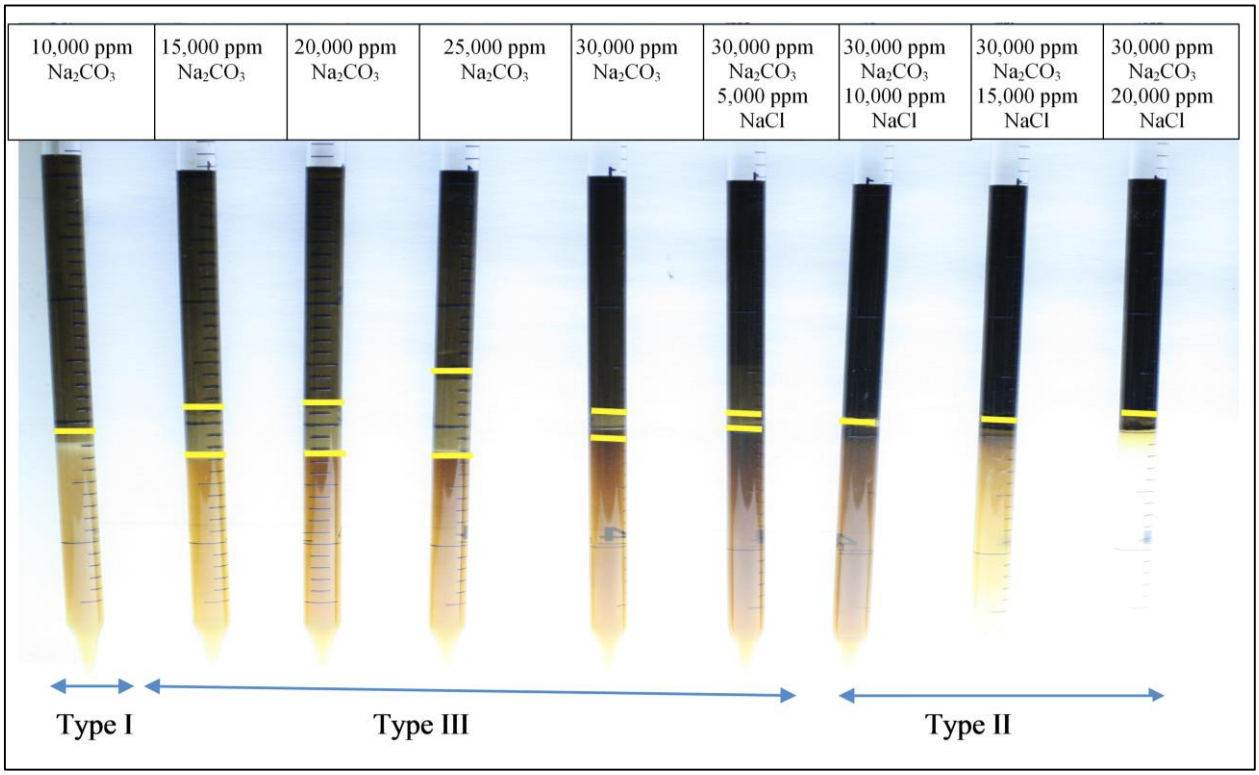

Figure 5.2: Phase behavior of 1 wt% IBA-30EO with oil as the salinity is varied

The phase behavior of IBA ethoxylates was studied with sodium carbonate and oil. Figure 5.2 shows the phase volumes of 1 wt% IBA-30EO with oil as the sodium carbonate concentration is varied at an oil-water volumetric ratio of 50:50 up to 30,000 ppm. After sodium carbonate concentration reaches 30,000 ppm, the sodium chloride is varied. Such phase behavior studies are called salinity scans. At low salinity (≤10,000 ppm), there are 2 phases: the oil phase and the aqueous phase containing soap, cosolvent and solubilized oil. This is Type I microemulsion behavior. As the salinity increases, three phases appear: an oil phase, a water phase and the microemulsion phase containing soap. This is Type III microemulsion behavior. At high salinity (≥40,000 ppm), there are 2 phases: the aqueous phase and the oil phase containing soap and solubilized water. This is Type II microemulsion behavior. The aqueous phase is clear containing

no oil. The samples equilibrated in less than 30 days and no macroemulsions were observed. Similar phase behavior is often observed in ASP formulations, where oil and water solubilization ratios are calculated. Oil solubilization ratio is the oil solubilized per unit volume of synthetic surfactant. High solubilization ratios (>10) lead to ultralow IFT (Huh, 1983). IFT is often ultralow ($<10^{-3}$ dyne/cm) when three phases appear. Such calculations are not made here since there is no synthetic surfactant. The partitioning of cosolvent between the middle microemulsion phase and the bottom aqueous phase is not obvious from the pictures. Thus, oil solubilization ratio on the basis of cosolvent is also not obvious. It is assumed that IFT is ultralow whenever three phases appear, similar to those in ASP systems.

To confirm ultralow IFT, the spinning drop interfacial tensiometer was used to measure the dynamic IFT between equilibrated middle phase microemulsion and the bottom aqueous phase. The IFT values reached 0.0004 dynes/cm in the Type III region. Thus, IFT measurement confirmed that the ACP formulation produces ultra-low values.

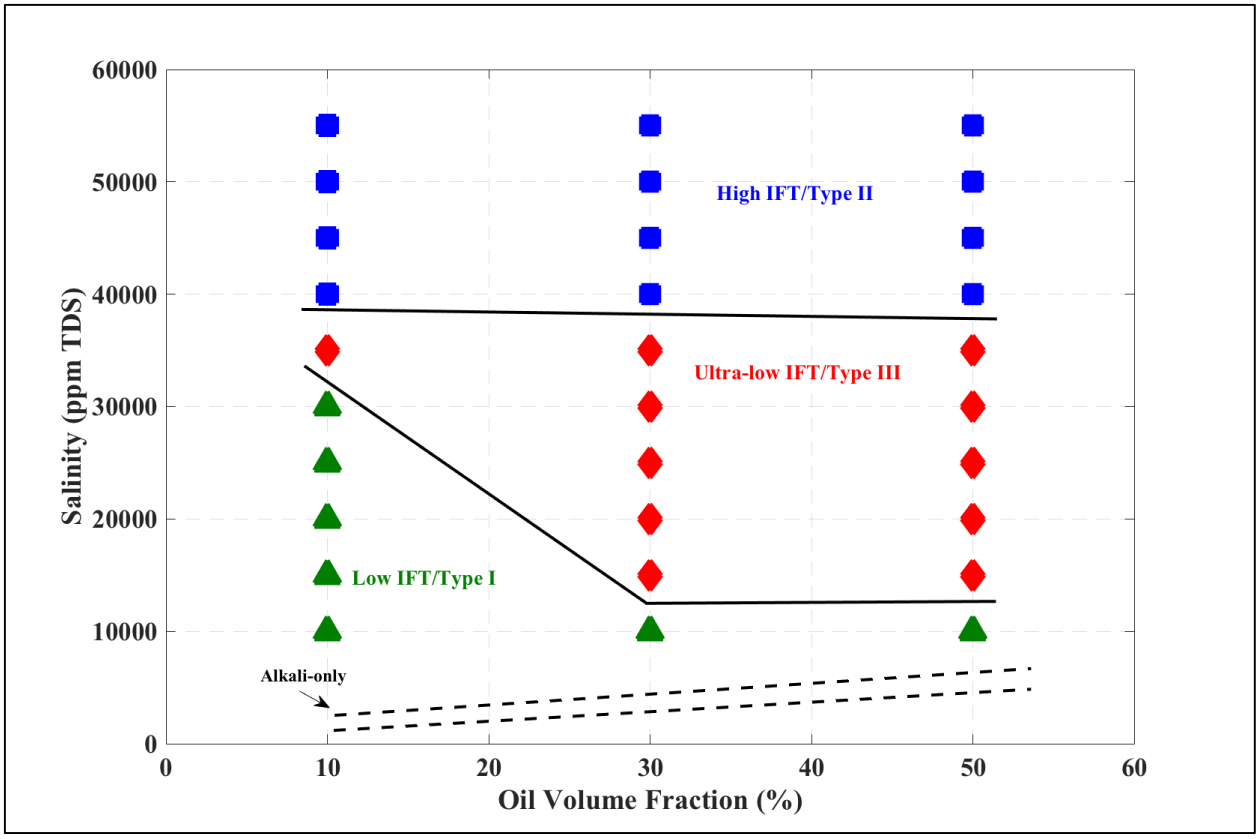

Figure 5.3: Effect of oil-water ratio on phase behavior

Salinity scans were conducted at several oil-water ratios. As the oil-water ratio increases, the amount of organic acid increases and thus the amount of soap increases. The resulting phase behavior is plotted in Figure 5.3. As seen in Figure 5.3, the Type III salinity range changes with the oil-water ratio, especially for the Type I – Type III transition. As the oil-water ratio increases, the salinity for Type I – Type III transition decreases because the amount of soap increases. Figure 5.3 also shows two dashed lines which indicate the Type III region for only alkali (with no cosolvent). This salinity range is much narrower and the transition occurs at a very low salinity. For a robust ultralow tension process, it is important to have a wide salinity range for the Type III phase behavior, which is provided by the cosolvent.

Microemulsion Rheology

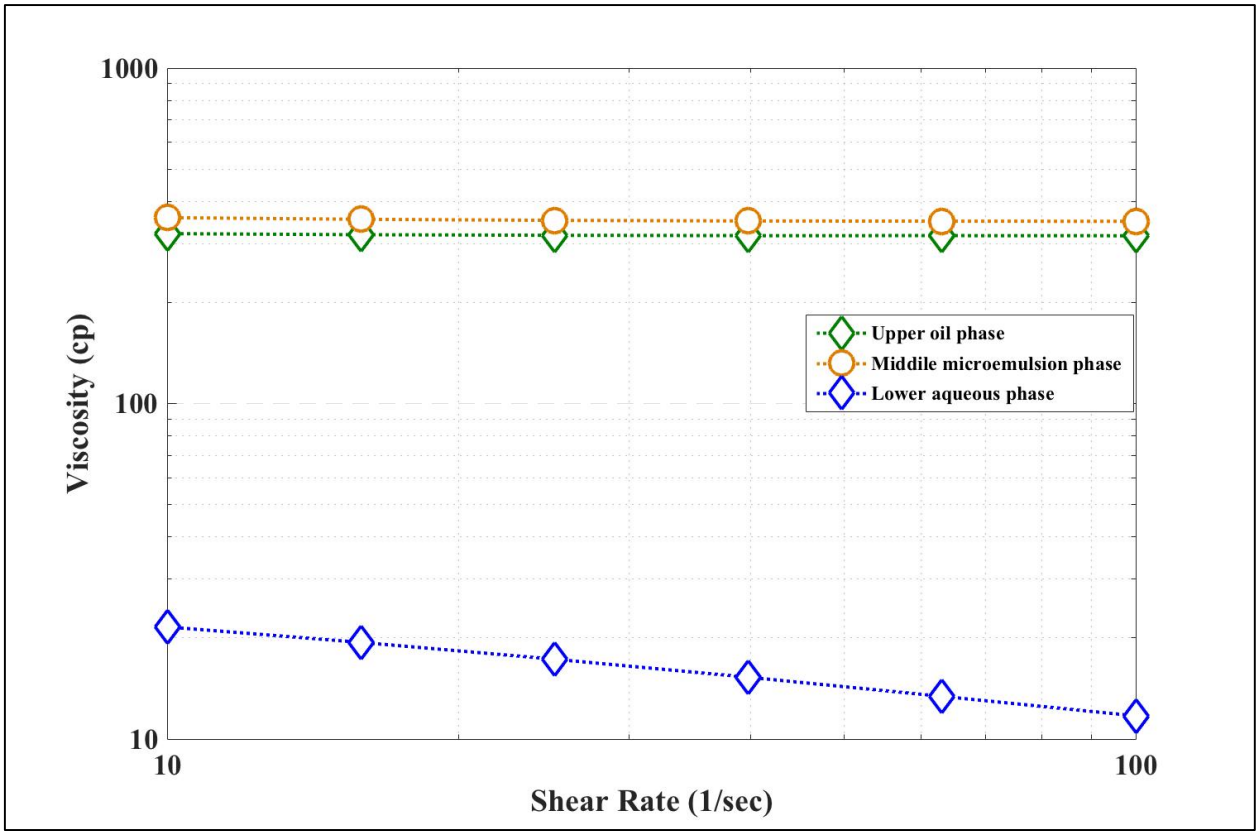

Figure 5.4: Viscosity of microemulsion, oil, and aqueous phases for ACP VR=12 formulation and oil mixture in Type III region

An equal amount of oil and ACP solution with a viscosity ratio of 12 (see Table 5.1 for composition) were mixed in a test tube at a salinity that produces ultra-low IFT Type III phase behavior. Note that polymer was included in this phase behavior experiment. The mixture was shaken several times a day and observed for phase equilibration at the reservoir temperature. This process was repeated until no change in separated volumes was observed. The mixture showed Type III behavior, which consisted of top excess oil, middle microemulsion, and bottom aqueous phases. After the mixture was fully equilibrated, the phase viscosities were measured using a rheometer. Figure 5.4 shows microemulsion, oil, and aqueous phase viscosities. The microemulsion and oil viscosities were similar (350 cp for microemulsion and 330 cp for oil) and

Newtonian (independent of shear rate). Alkali-oil-brine mixtures typically produce macroemulsion phases that are non-Newtonian (Kumar et. Al., 2012). The Newtonian behavior in microemulsions allows easier transport in the reservoir. Having a Newtonian middle phase microemulsion is another advantage of the ACP process over the alkali-only process. The bottom aqueous phase had a lower viscosity (than oil), and this phase was non-Newtonian. The viscosity of the bottom phase was similar to that of original ACP (VR=12) solution (without the addition of any oil). The bottom phase was non-Newtonian because the polymer stayed in this phase. Previous studies have shown that in well-formulated ASP-oil mixtures, polymers stay in the bottom phase and do not partition into the middle phase because the microdomains of the bicontinuous microemulsion phases are too small for polymer molecules (Tagavifar e.al., 2016).

5.2.2 1D ACP STABLE FLOOD

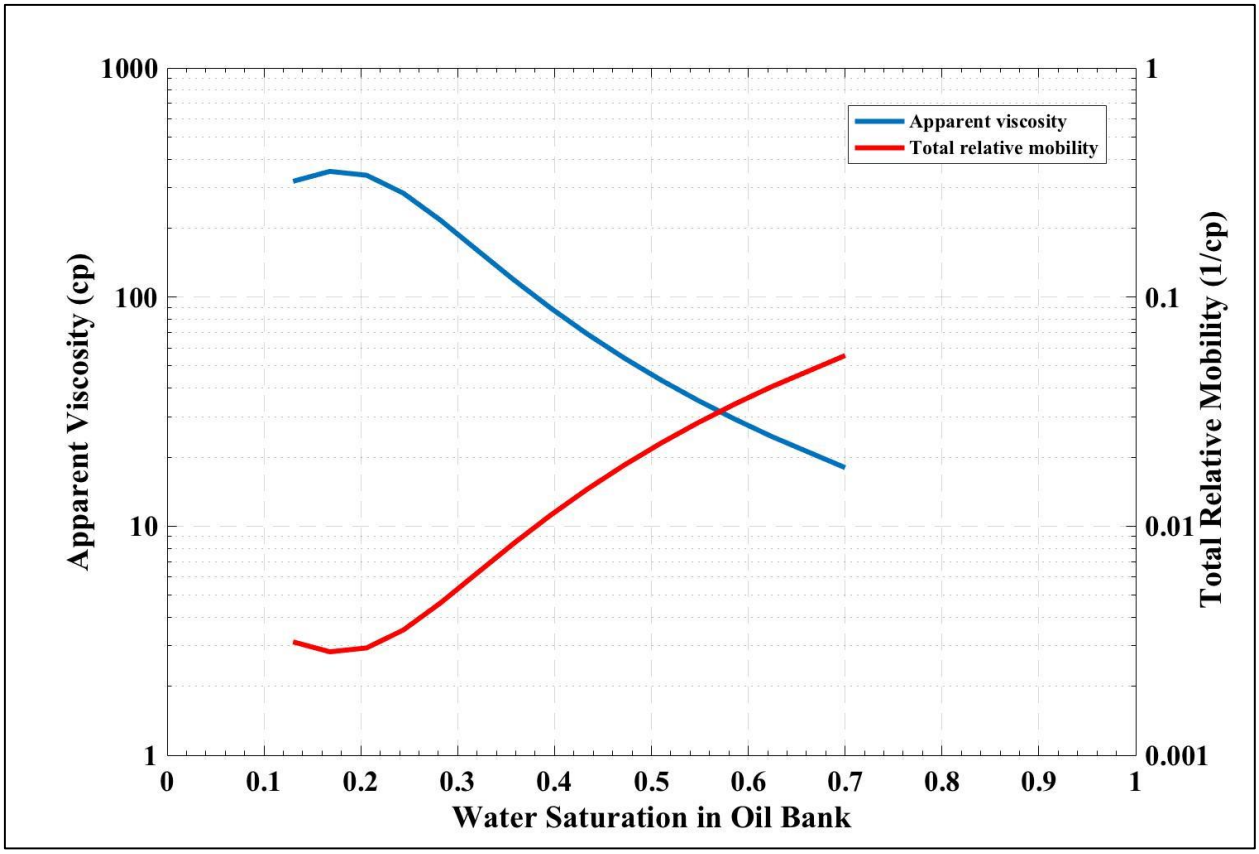

Figure 5.5: Total relative mobility and apparent viscosity

The 1D linear sandpack was oil saturated to an initial oil saturation of 0.87. Water was injected for 4.5 PV at an injection velocity of 1ft/d. Waterflood recovered 62% of the original oil in place (OOIP) and decreased the oil saturation to 0.32. The pressure drop decreased from an initial value of 3.5 psi to 1.5 psi at the end of the waterflood.

After waterflood, the ACP slug was injected for about 0.5 PV followed by the polymer drive slug. The compositions of these slugs are listed in Table 5.1. ACP slug viscosity was 337 cp and polymer drive viscosity was 366 cp at the shear rate of 6.31 s^{-1} (a typical shear rate for core floods). Figure 5.5 shows total relative mobility and apparent viscosity for the oil bank at different saturations. The minimum total relative mobility was calculated to be ~0.003 cp^{-1}, and thus, the maximum apparent viscosity of oil bank was ~330 cp. Therefore, ACP and polymer drive slugs

must have a viscosity above 330 cp for a stable displacement of the oil bank. Viscosities of ACP slug and polymer drive were chosen to be above the minimum required viscosity in this flood.

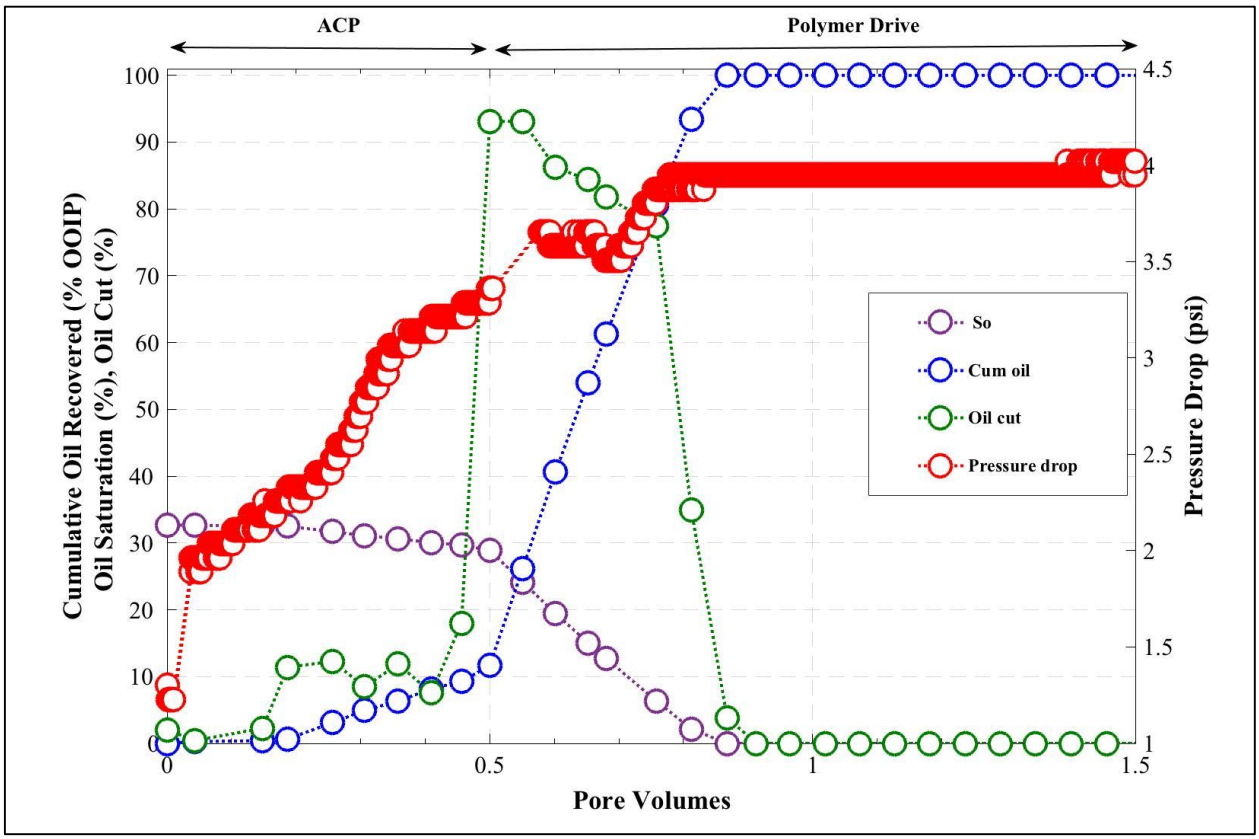

Figure 5.6: Stable ACP core flood cumulative oil recovery, oil cut, oil saturation and pressure drop

Figure 5.6 shows the cumulative oil recovery, oil cut, remaining oil saturation, and pressure drop for the 1D tertiary ACP sand pack flood (after 4.5 PV waterflooding). The oil bank arrived at the outlet at about 0.5 PV after ACP slug injection. Oil cut rose to ~93%. Most of the oil was recovered by 0.9 PV injection. The chemical flood decreased oil saturation from waterflood residual of 32% to 0%. Tertiary recovery was able to recover 100% of the remaining oil in place (ROIP). The chemical flood recovered an extra 38% of OOIP and increased overall recovery to 100% of OOIP. After the start of ACP injection, pressure drop gradually increased and reached a maximum value 4 psi during the polymer flood. The maximum pressure gradient was equal to 4

psi/ft. Salinity and viscosity of the effluent water increased shortly after the oil cut reached its peak and then decreased. The pH increased from 7 to 10.5 and stayed at 10.5 until the end of the flood. Based on the effluent analysis, in situ salinity clearly crossed the type III region salinity where ultralow tension was achieved which mobilized the residual oil. To conclude, 1D ACP sandpack flood showed that the chemical formulation was effective in mobilizing the residual oil.

5.2.3 QUARTER 5-SPOT TERTIARY ACP FLOODS WITH VISCOSITY VARIATION

The 5-spot sandpacks were first saturated with the formation brine. Oil was then injected to achieve the initial oil saturation, which ranged between 0.9-0.94 for the three floods in this series. Brine was injected for 1 PV to simulate a short waterflood. Water broke through very fast (at about 0.03-0.05 PV), which indicates waterflood was highly unstable in this multi-dimensional medium. Waterflood recovered only ~22% OOIP for the first two floods and ~29% OOIP for the third flood. This recovery variation reflects the variation in the packing heterogeneity as well as the unstable nature of the water flood. The oil saturation decreased from the initial oil saturation to 0.65-0.7 in the three floods. Pressure drop decreased from about 6 psi initially due to oil flow to 1.6-1.3 psi during water flow (at the remaining oil saturation) for the three cases.

ACP slug was injected for about 0.5 PV followed by the polymer drive slug for about 1 PV. ACP slug compositions were different in the three experiments in the amount of polymers added. The ACP slug consisted of 1 wt% cosolvent, 3 wt% Na2CO3, 0.5 wt% NaCl. The polymer concentrations used were 4000 ppm, 2950 ppm, and 1500 ppm of HPAM for ACP VR=2, 4, and 12, respectively. All polymer drive slugs contained 2.0 wt% of Na_2CO_3; 3700ppm, 2700ppm, and 1350 ppm of HPAM were used for ACP VR=2, VR=4, and VR=12, respectively. The ACP slug viscosity and the polymer slug viscosity were the same and equal to 160 cp, 80 cp, and 25 cp at a shear rate of 6.31 s^{-1} for ACP VR=2, 4, 12 cases accordingly.

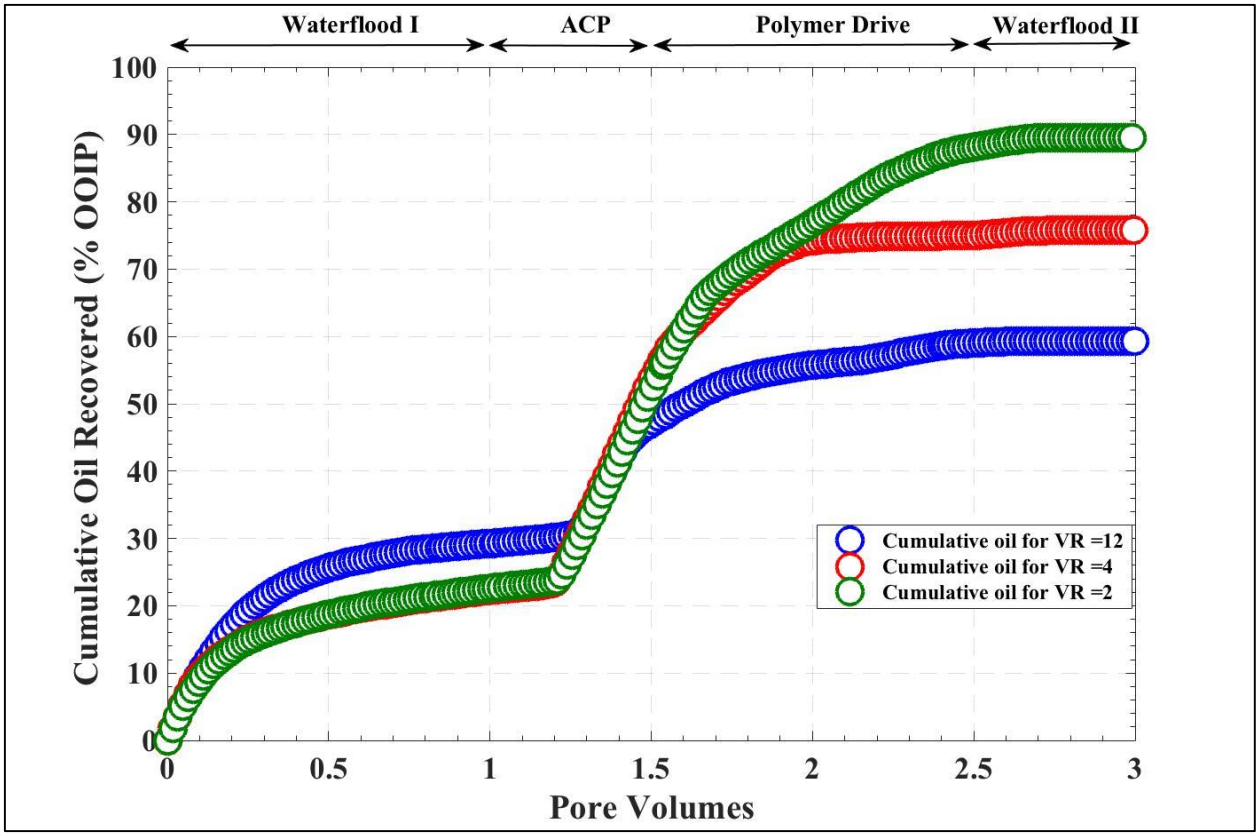

Figure 5.7: Oil recovery for ACP quarter 5-spot floods: variation of chemical slug viscosity (VR=2, 4, and 12)

Figure 5.7 compares the cumulative oil recovery in the three 5-spot tertiary ACP floods. ACP VR=2 flood had the most favorable mobility ratio out of three ACP floods, where 320 cp oil was displaced by the 160 cp ASP slug followed by 1 PV of the 160 cp polymer drive slug. ACP VR=4 had less favorable mobility ratio than ACP VR=2 where 320 cp oil was displaced by 0.5 PV of the 80 cp ASP slug, followed by 1PV of the 80 cp polymer drive slug. Lastly, ACP VR=12 had the least favorable mobility ratio (out of three floods) in this series where 320 cp oil was displaced by 0.5 PV of the 25 cp ASP slug, followed by 1PV of the 25 cp polymer drive slug. ACP VR=2 flood recovered 90% OOIP. ACP VR=4 flood recovered 75% of OOIP or additional 52% OOIP of oil after the initial waterflood. Lastly, ACP VR=12 flood recovered 60% of OOIP or additional 30% OOIP of oil after the initial waterflood.

Figure 5.8 shows the oil cut in the waterflood followed by the ACP floods in the quarter 5-spot. The oil cut decreases during the waterflood, then increases during the ACP flood due to the oil bank formation and eventually decreases to zero during the polymer drive for each of the three floods. The maximum oil cut in the oil bank was around 95% for both ACP VR=2 and 4 floods. Even though they had the same maximum oil cut, VR=2 flood oil cut had a longer tail and sustained about 30% oil cut for an extra 0.5 PV injection. The maximum oil cut was lower, and it sharply decreased to zero (i.e., the oil bank was narrow) for ACP VR=12 flood. While oil cut above 80% was sustained for about 0.4 PV for both ACP VR=2 and VR=4 floods, ACP VR=12 flood had its high oil cut above 80% sustained for only 0.1 PV.

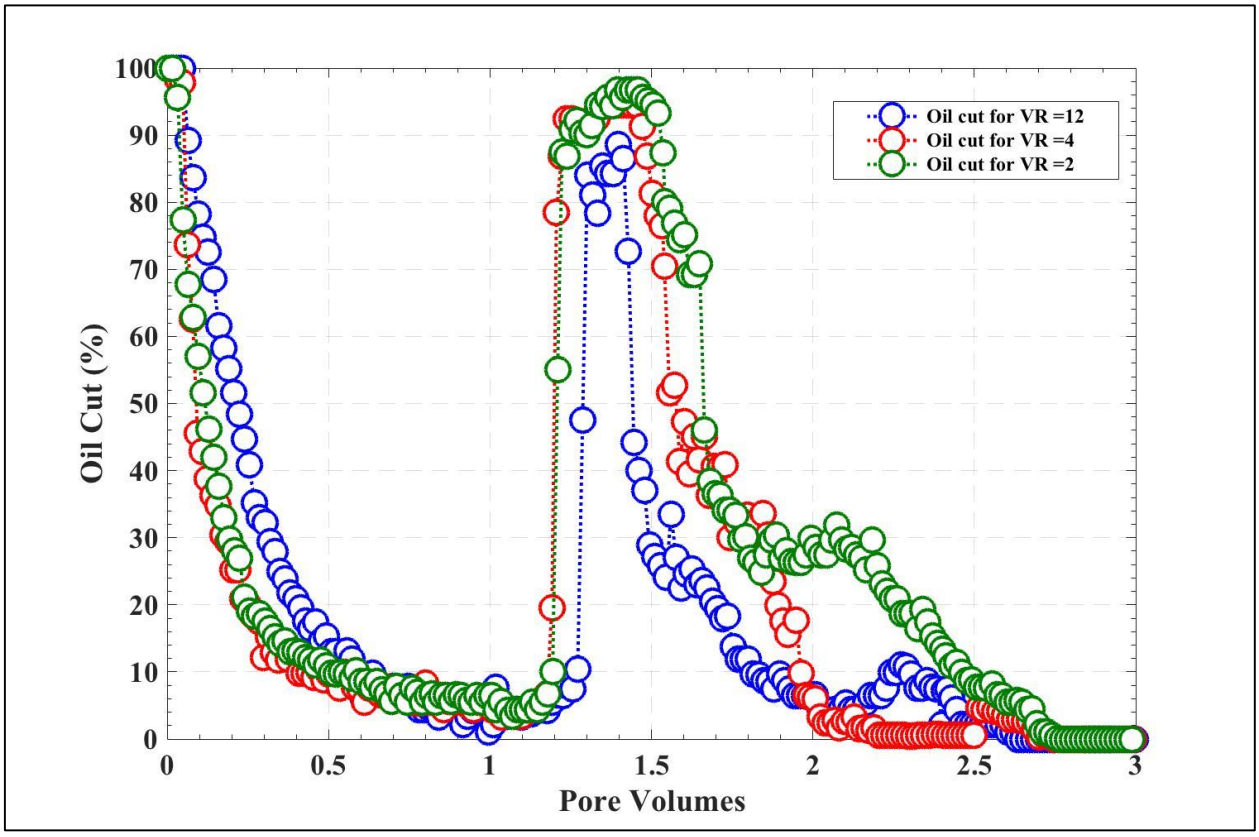

Figure 5.8: Oil cut for ACP quarter 5-spot floods: variation of chemical slug viscosity (VR=2, 4, and 12)

Figure 5.9 shows the pressure gradient during the three ACP floods. This pressure gradient decreases as the viscosity ratio increases. Figure 5.9 also shows the final oil recovery, which decreases as the viscosity ratio increases. The ideal viscosity ratio would be the one which renders high enough oil recovery with low enough pressure gradient. The viscosity ratio of 4 appears to be the optimum (for the quarter 5-spot) where the oil recovery is high (75%) and the pressure gradient is feasible (4.5 psi/ft). These experiments were performed under constant injection rate, which is not often the case in field applications. Generally, the injection is pressure constrained, and the available pressure drop is limited in viscous oil reservoirs. The optimum ACP viscosity ratio needs to be determined for any field by conducting a realistic stimulation.

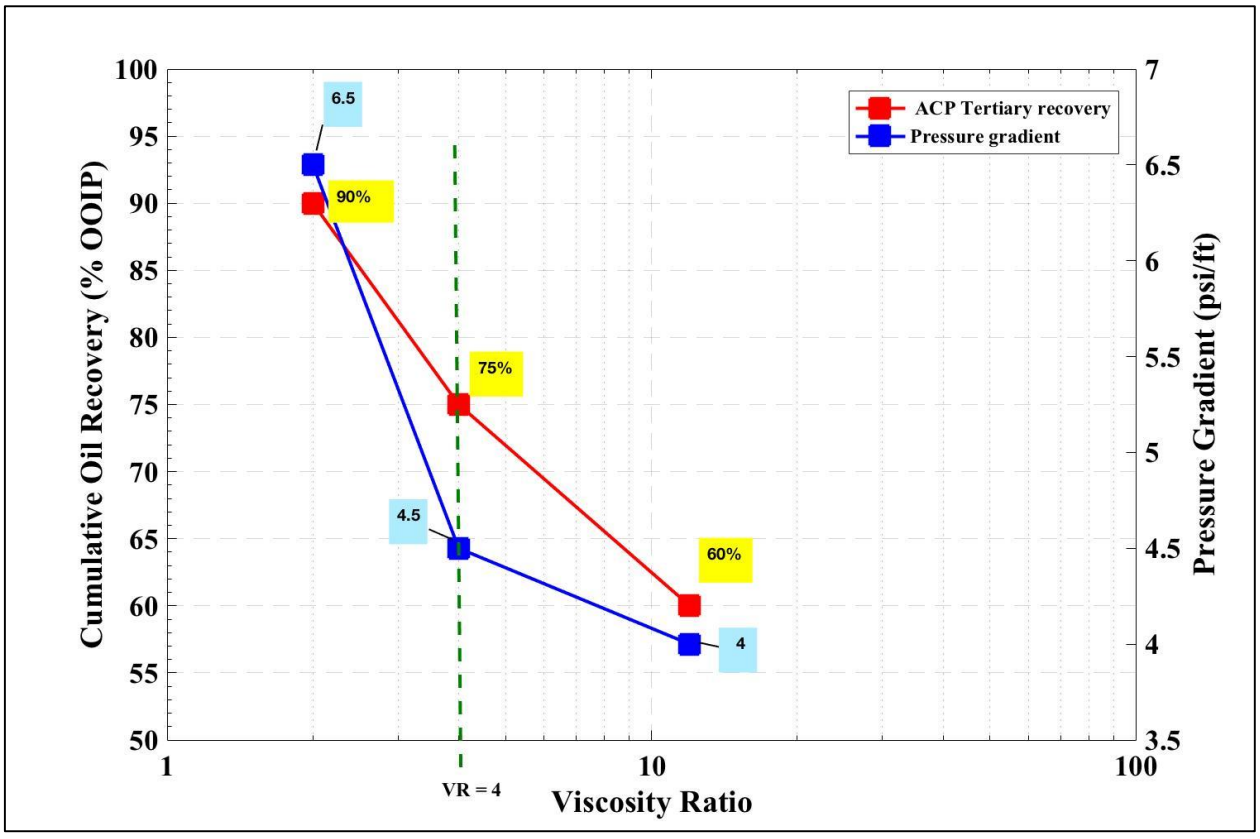

Figure 5.9: Recovery and pressure gradient for quarter 5-spot floods at several viscosity ratios

5.2.4 QUARTER 5-SPOT ASP FLOODS WITH DIFFERENT STARTING TIMES

As listed in Table 5.2, three ACP floods were conducted in the quarter 5-spot model at the same viscosity ratio (4), but with different starting times. Figure 5.10 compares the cumulative oil recovery in the three 5-spot ACP floods. Viscosity ratio 4 was chosen to be the viscosity ratio. ACP floods were run in secondary (before any water flood) and tertiary modes (after 0.5 PV and 1 PV water floods) for the same viscosity ratio. The ultimate recoveries for tertiary ACP flood after 1 PV of water flood was slightly higher compared to secondary ACP flood. The ACP flood after 0.5 PV water flood had a higher ultimate recovery due to a better water flood performance. However, the tertiary oil recovery was the same for both 0.5 PV and 1 PV water flood cases. Earlier the start of the ACP flood, faster was the oil recovered. Figure 5.11 shows oil cuts for the three ACP floods (with the viscosity ratio of 4). In the secondary flood, the oil cut stayed at 100% for about 0.5 PV and decreased after the breakthrough. The maximum oil cut for tertiary floods was the same, around 90%. Thus, maximum oil cut was not affected by the extent of the preceding water flood.

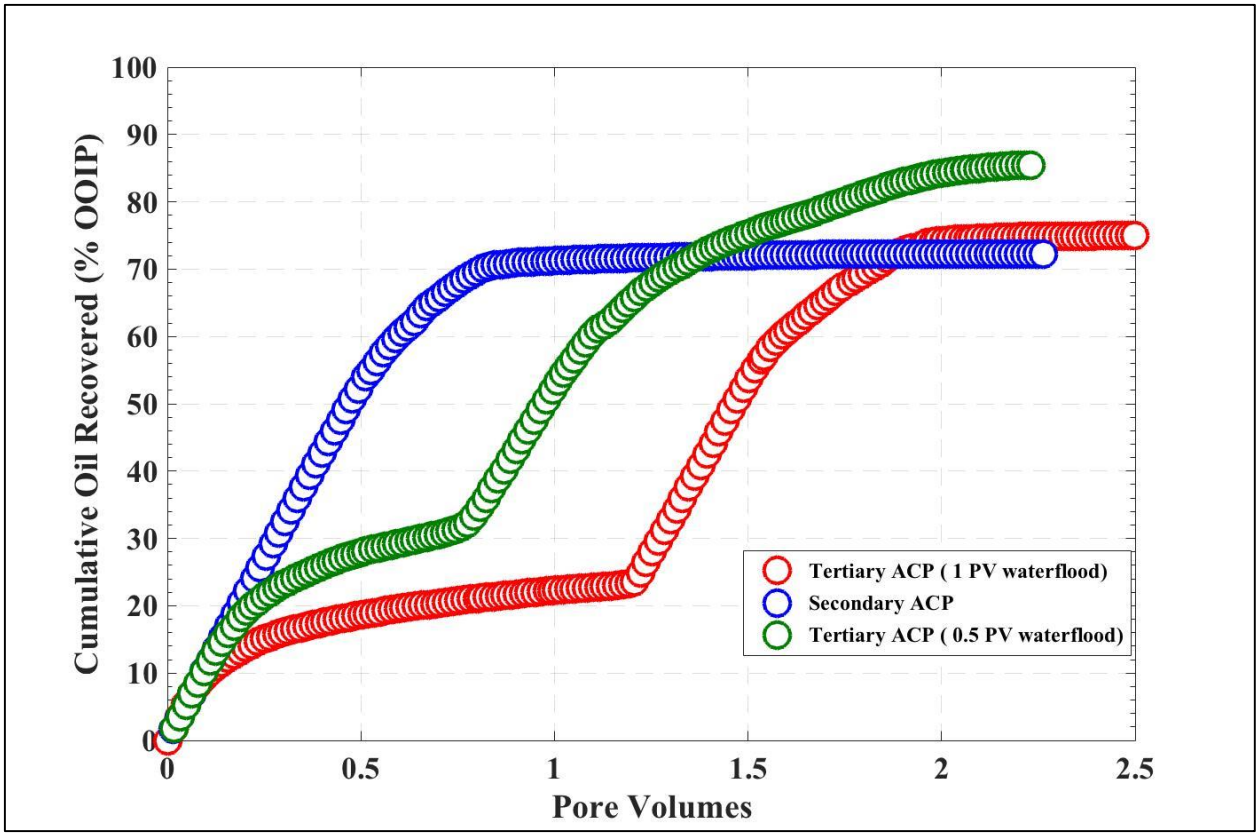

Figure 5.10: Cumulative recovery for secondary and tertiary ACP floods at the viscosity ratio of 4

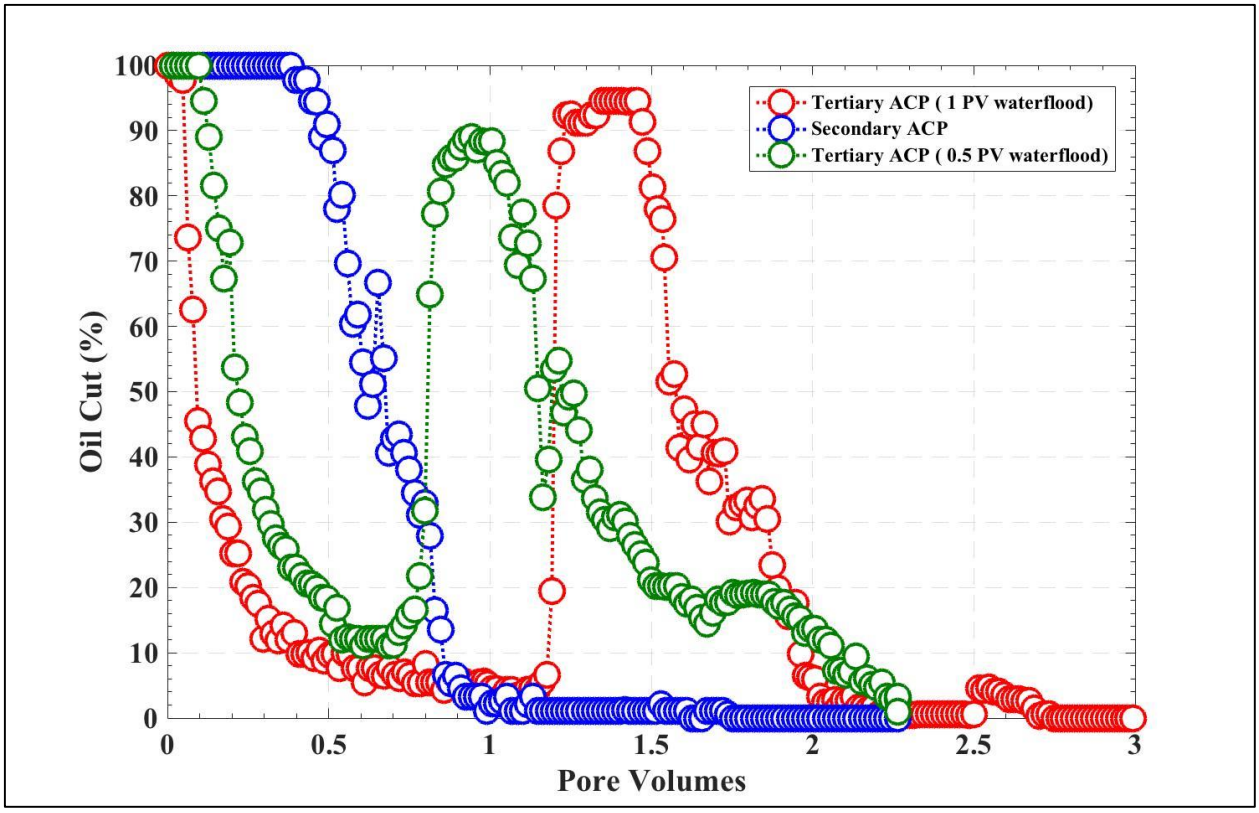

Figure 5.11: Oil cut for secondary and tertiary ACP floods at the viscosity ratio of 4

5.2.5 Sweep Efficiency of ACP Floods

After each experiment, the 5-spot sand pack was opened and analyzed for the distribution of the remaining oil. The injection fluid totally swept the bottom of the sand pack in each case, but the top was not fully swept. Figures 5.12 and 5.13 show the top of the sand pack at the end of the experiments. Arrows represent injection and production ports. These floods were unstable, and thus, some of the oil was bypassed. The bypassed oil regions look black colored in Figures 5.12 and 5.13. Well-swept regions look light or yellow. Some regions look brown indicating partly swept regions.

Figure 5.12 compares areal sweep patterns for viscosity ratios 2, 4, and 12 for the tertiary ACP floods. For ACP VR=2, the unswept oil zones were mostly concentrated around the closed corners of the 5-spot sand pack with some bypassed regions in the middle of the well-swept area. This

indicates that even though the flood was not stable (M^o=2.3), it was still able to sweep most of the sandpack. A further increase in the viscosity ratio to VR=4 (M^o=4.6), shows drastically decreased areal sweep efficiency. Less than half of the sandpack is well swept on the top. Areal sweep for VR=12 (M^o=14.6) shows more irregular sweep with many bypassed regions. Due to high mobility ratio, even the swept zones look visibly darker indicating higher remaining oil saturations for VR=12 compared to VR=2 and VR=4 cases.

Figure 5.12: Areal Sweep Comparison at ACP VR=12, 4, and 2 (from left to right)

Figure 5.13 compares areal sweep efficiencies for ACP floods with different extents of water flood for the same viscosity ratio (4). The areal sweep efficiency gets better with an increase in the waterflood extent. Areal sweep efficiency is directly related to vertical sweep efficiency and cannot be treated separately. Therefore, it is important to also look into vertical sweep efficiency.

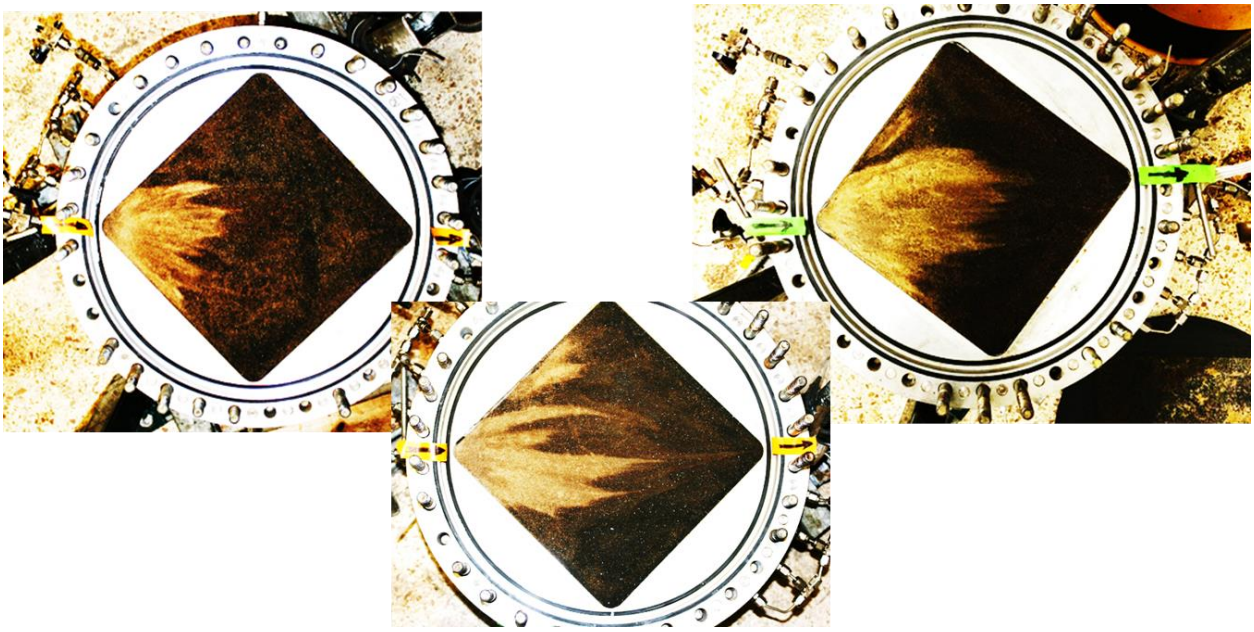

Figure 5.13: Areal sweep comparison for ACP floods: (from left to right) secondary mode, tertiary mode after 0.5 PV waterflood, and tertiary mode after 1 PV waterflood.

After taking the top and bottom pictures, the sandpack was carefully taken out from the 5-spot cell and cut vertically to show vertical cross-sections as shown in Figure 5.14. In Figure 5.14, the left picture was taken after the tertiary ACP flood following 0.5 PV water flood and the right picture was taken after the secondary ACP flood. The fluids were injected from the right bottom corner in these pictures. The vertical sections show vertical segregation of the injected fluid. The capillary forces disappear in chemical floods when ultralow tension develops; thus the aqueous phase segregates to the bottom even in an inch thick sand pack. The vertical sweep efficiency looks larger for the tertiary mode because there is no gravity segregation in the preceding waterflood. All dimensionless number calculation that includes gravity, bond, capillary and trapping numbers indicate that the flood was performed in the transition zone and was not dominated by only one flow region.

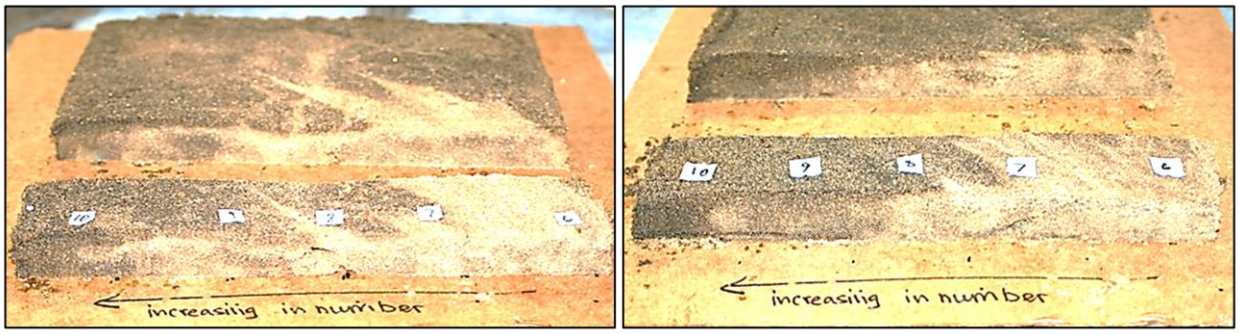

Figure 5.14: Cross section for the sand packs, left for tertiary ACP flood after 0.5 PV of water flood (ACP 0.5 PV WF) and right for secondary ACP flood (Sec ACP)

5.2.6 SIMULATION

The ACP 3D 5-spot sandpack floods were modeled using the University of Texas Chemical Flooding Simulator, UTCHEM (Version 2016) . The Appendix A.2 contains detailed input file used during simulation of the ACP process. A successful simulation of chemical flood depends on many input parameters that must be experimentally measured. Table 5.3 shows the fluid parameters that were measured experimentally and those obtained from the history matching of ACP floods. The key features of ACP modeling are:

- In-situ soap generation by alkali and oil acid reaction,
- IFT as a function of salinity and soap concentration,
- Microemulsion rheology, and
- Polymer rheology.

More information on the specific parameters can be found in Mohammadi (2008).

Table 5.3: Key UTCHEM reservoir and fluid property parameters in the ACP simulation model

Parameters	Parameter Values
Components	water, oil, surfactant, polymer, chlorine, calcium, alcohol, carbonate, sodium, hydrogen, and oil acid
Grid	50×50×5
Gridblock size (ft)	0.0167×0.0167× 0.0167

Table 5.3 (continued)

Average Porosity	0.354
Average permeability (md)	12,000
Initial water saturation	0.06
Initial salinity (meq/ml)	0.684
Solubilization ratio of surfactant at the optimum salinity	20
Upper Type III Salinity of soap (meq/ml)	0.8
Lower Type III Salinity of soap (meq/ml)	0.5
Huh's IFT model parameters (c, a)	0.3,10
Residual Saturations of water, oil, microemulsion phases at low capillary number	0.06,0.36, 0.06
Endpoints of relative permeabilites water, oil, microemulsion phases at low capillary number	0.16,0.5,0.5
Exponents of relative permeabilities water, oil, microemulsion phases at low capillary number	2.2,2.2,2.2
Water and Oil viscosities (cp)	0.9,320
Oil Acid Number (mg KOH/g Oil)	2.4
Shear rate at half zero-rate viscosity(s^{-1})	10
Polymer rheology exponent	1.5
Injection rate (ft^3/day)	0.0254

A key feature of the ACP flood is the in-situ soap generated due to the reaction between injected alkali and the acid in the oil. The soap serves as the natural surfactant to form the microemulsion phase and reduce the interfacial tension. This is different from the ASP flood which includes both the synthetic surfactant and the in-situ soap. The existence of cosolvent accelerates the microemulsion formation, improves the microemulsion stability and reduces the microemulsion viscosity.

To include the geochemical reactions in an ACP flood, I coupled the modeling of ACP flood with a full geochemical reaction module. The geochemical reaction module is described by Luo (2016), which provides accurate estimates of the pH, soap generation, salinity and concentrations of other species. The reactions among oil acid, alkali, and water are given in Table 5.4, where

$(HA)_o$, $(HA)_w$, *and* A^- are oil acid in oil, oil acid in water, and soap, respectively. It is noted that the soap generation consumes a certain amount of alkali and reduces the pH value.

Table 5.4: Oil-acid-relevant reactions used in the simulation

Species	Reactions
$(HA)_w$	$(HA)_o \rightleftarrows (HA)_w$
A^-	$(HA)_w \rightleftarrows H^+ + A^-$

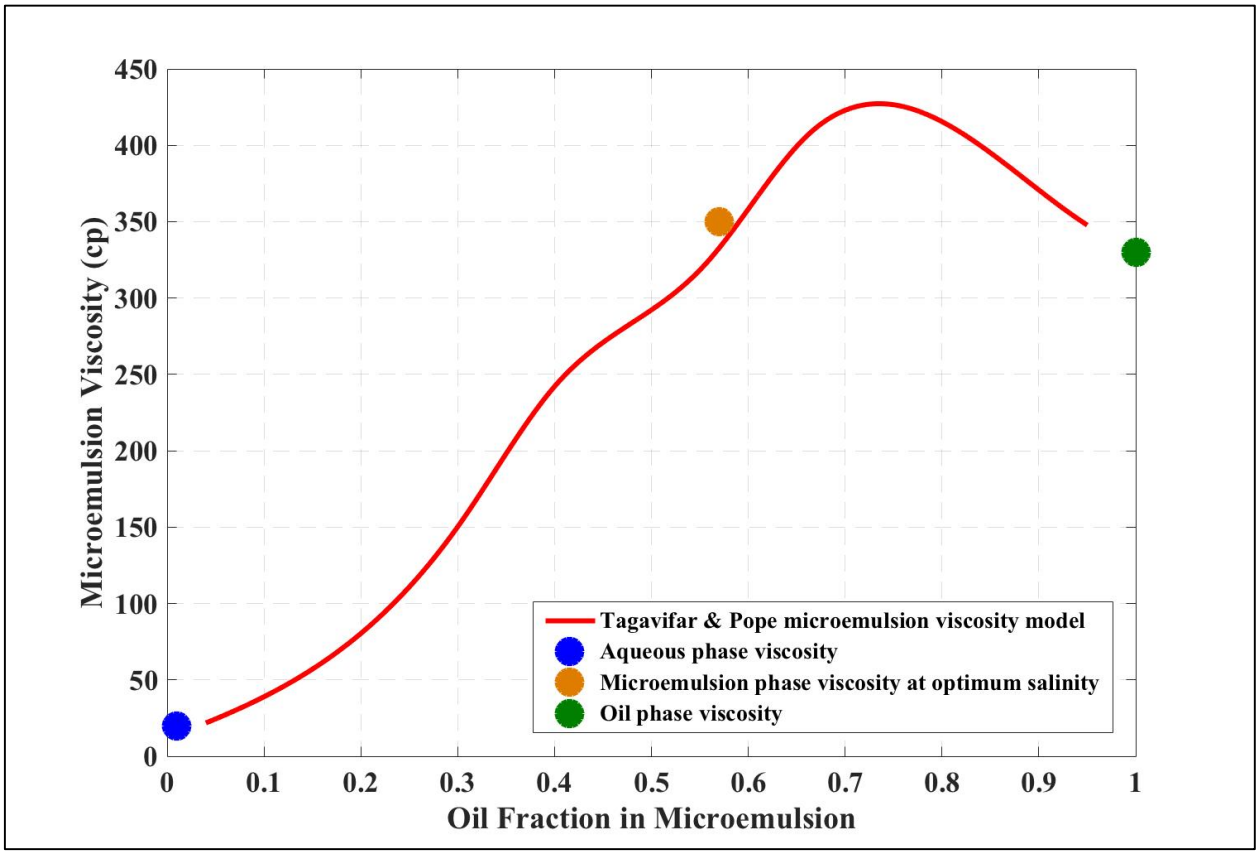

Figure 5.15: Phase viscosities (at 10 s^{-1}) for ACP VR=12 and model estimates

The ACP process is different from alkaline flooding in two ways: the predictability of transport and rheology. Alkaline flooding is extremely hard to simulate properly because unlike in ACP and ASP processes, where microemulsions are created, alkaline flooding mostly creates macroemulsions. Macroemulsions are thermodynamically unstable emulsions and have unpredictable transport and rheology. On the other hand, microemulsions are thermodynamically stable and follow predictable phase behavior and rheology. In this work, the model proposed by

Tagavifar (2016) was used to estimate the microemulsion viscosity. The model includes the cosolvent and polymer effect on microemulsion rheology. It was validated through accurate laboratory experiments. Figure 5.15 shows the measured microemulsion viscosity at the optimum salinity, the lower aqueous phase viscosity and the upper excess oil viscosity for ACP VR=12 case, represented by points and the model fit represented by a line. The cosolvent effect is implicitly incorporated in this graph by reducing the peak of the microemulsion viscosity.

Polymer viscosity was modeled by the rheological model proposed by Meter and Bird (1964), i.e.,

$$\mu_{\text{app}} = \mu_{\infty} + \frac{\mu_{p0} - \mu_{\infty}}{1 + \left(\frac{\gamma_{eff}}{\gamma_h} \right)^{P_{\alpha}-1}} \quad , \tag{4.6}$$

where μ_{app} is the apparent in-situ polymer viscosity, μ_{∞} is the polymer solution viscosity at infinite shear rate which I assume to be equal to water viscosity, μ_{p0} is the polymer solution viscosity at zero shear rate, γ_{eff} is the effective shear rate in the reservoir, γ_h is the shear rate at which polymer viscosity is half of the viscosity at zero shear rate, and P_{α} the power law exponent which depends on polymer concentration. Figure 5.16 shows the experimental data and the model match for polymer viscosity.

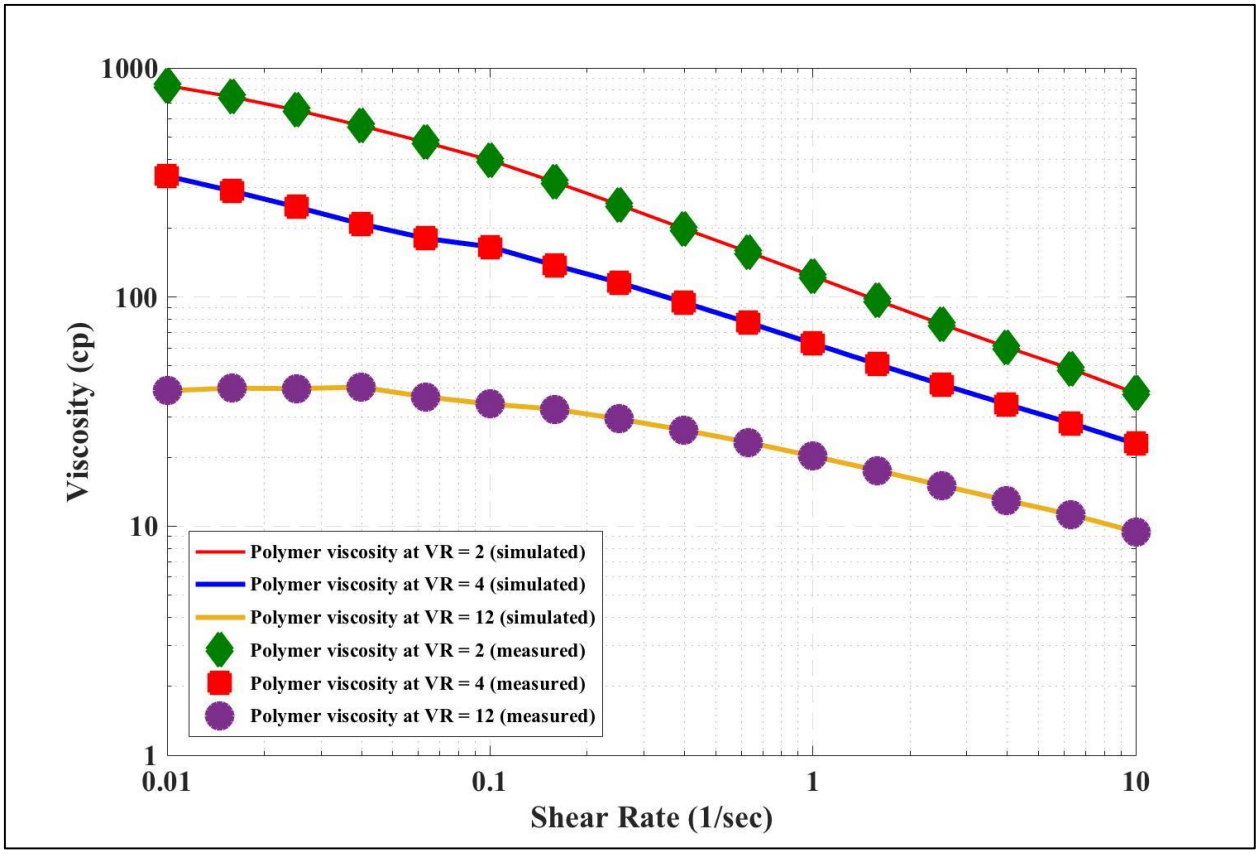

Figure 5.16: ACP slug solution viscosities for ACP VR=2, 4, and 12. The data points were measured in lab and lines were computed by UTCHEM

Lab-Scale Simulation by UTCHEM

The quarter 5-spot sand pack was modeled by 50×50×5 gridblocks. The permeability field was modeled with a Dykstra-Parsons (Vdp) coefficient of 0.4 and an average permeability of 12 Darcy. Dimensionless correlation lengths were chosen to be λ_{Dx}= λ_{Dy}= 0.5 (or correlation length of 5 inches in x and y directions) and λ_{Dz}= 0.2. Figure 5.17 shows the permeability map used for lab scale simulations.

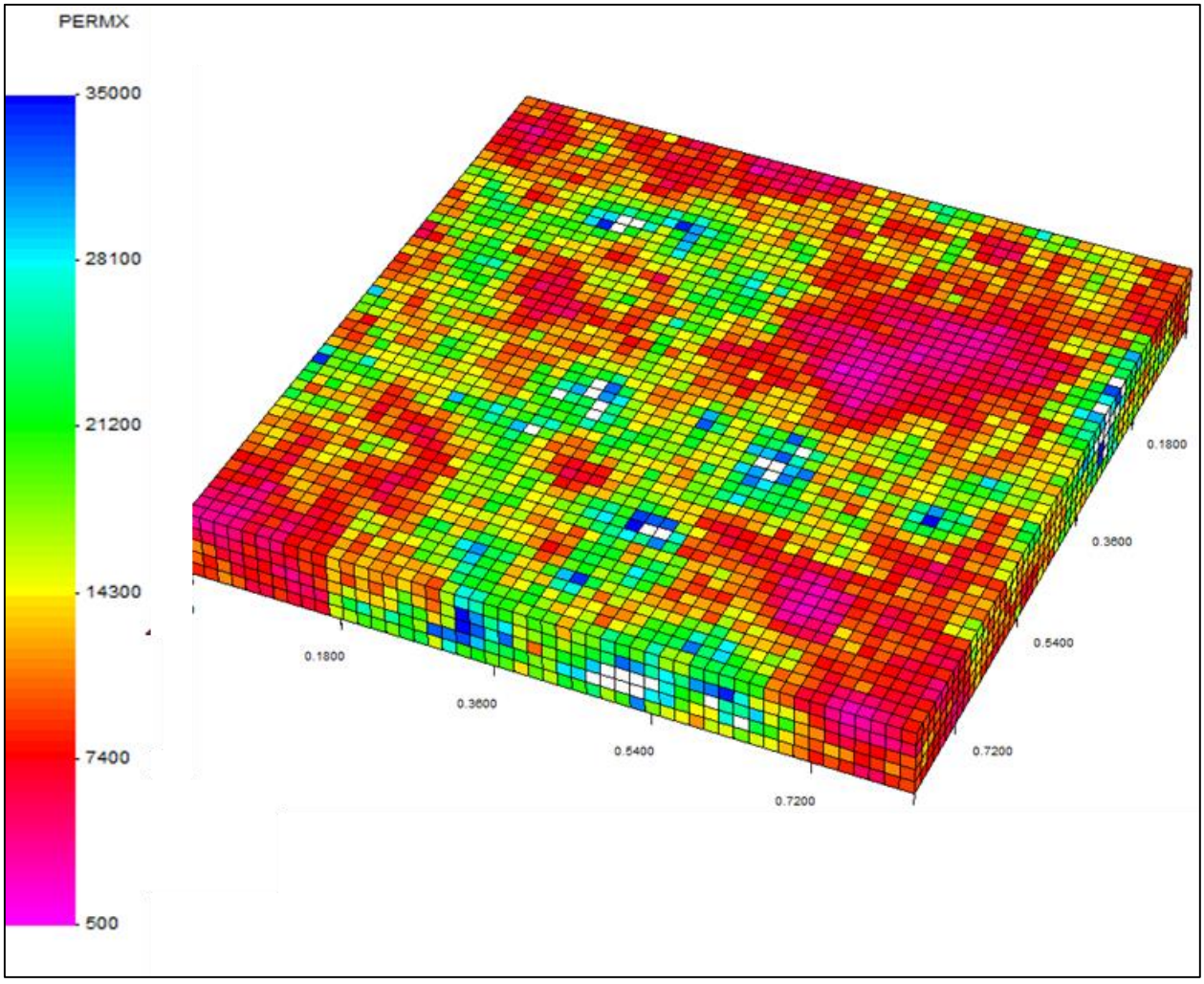

Figure 5.17: Permeability map in mD with Kmean=12,000 mD and Vdp= 0.4

Figures 5.18 and 5.19 show the simulation results for cumulative recovery, oil cut, and pressure drop for ACP flood with a viscosity ratio of 2. Solubilization and capillary desaturation parameters were tuning factors to match the experimental data. The unstable flow due to adverse mobility ratio, 3-dimensional compositional simulation, numerical dispersion, and uncertainties involved with phase behavior were the main challenges in the matching of the results.

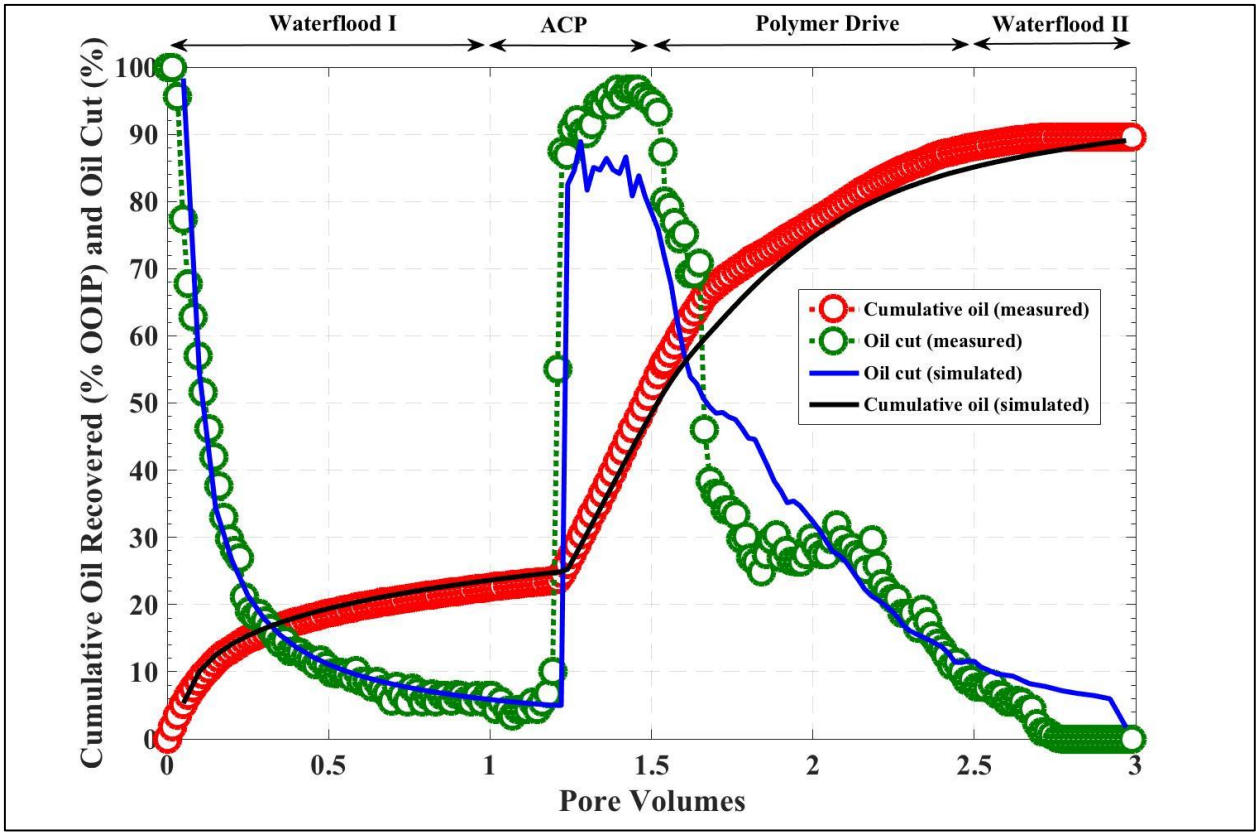

Figure 5.18: Cumulative oil recovery and oil cut comparisons of experimental data and simulation results

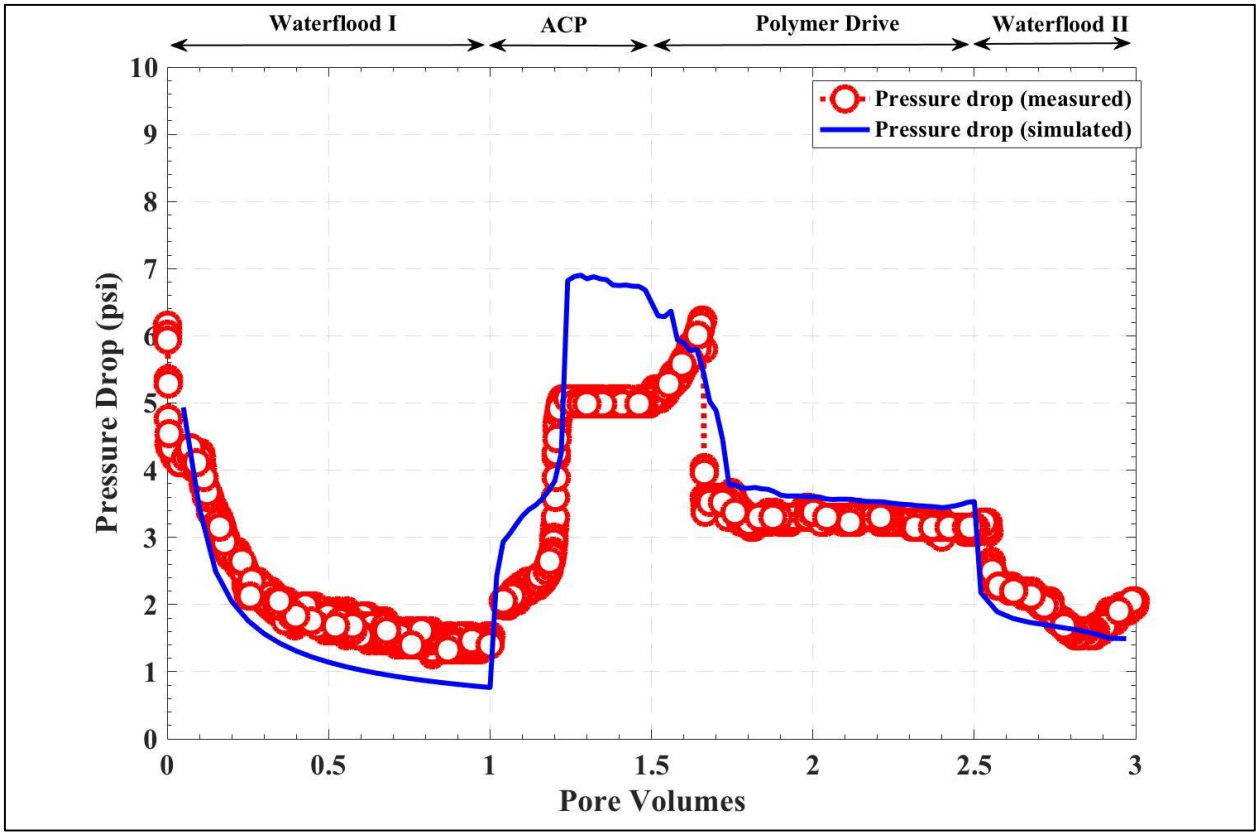

Figure 5.19: Pressure drop during ACP flood experiment and simulation

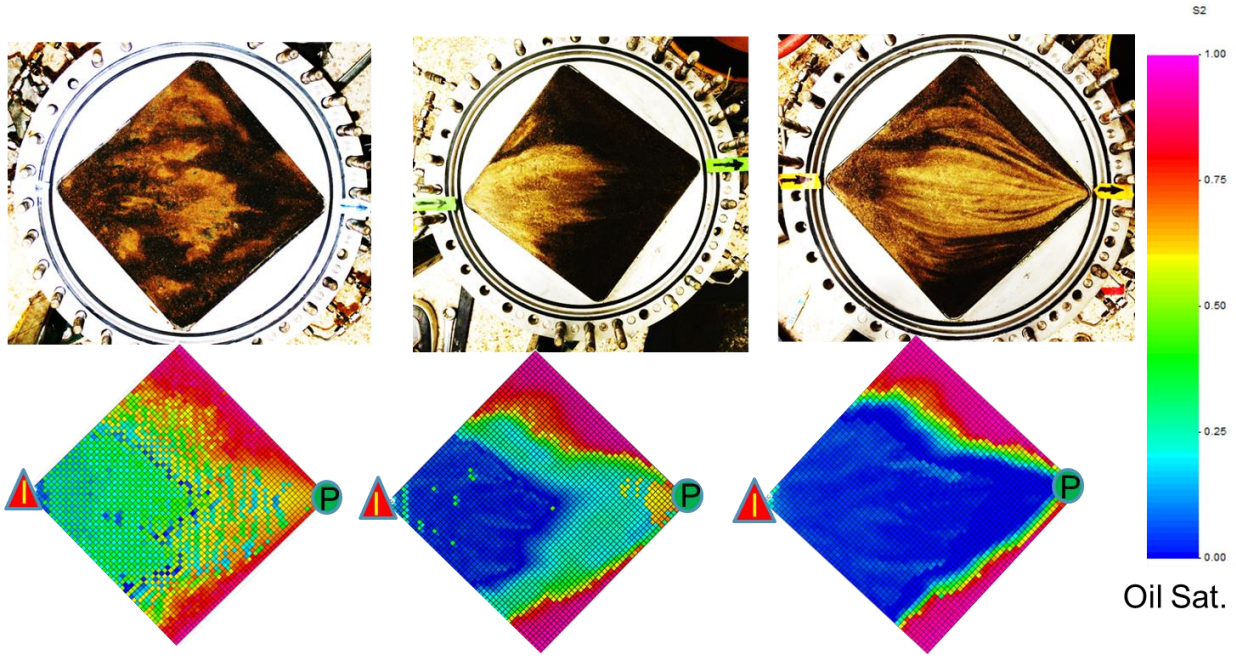

Figure 5.20: Oil saturation distribution at the end of ACP floods for experiments and simulations at VR=12, 4, and 2

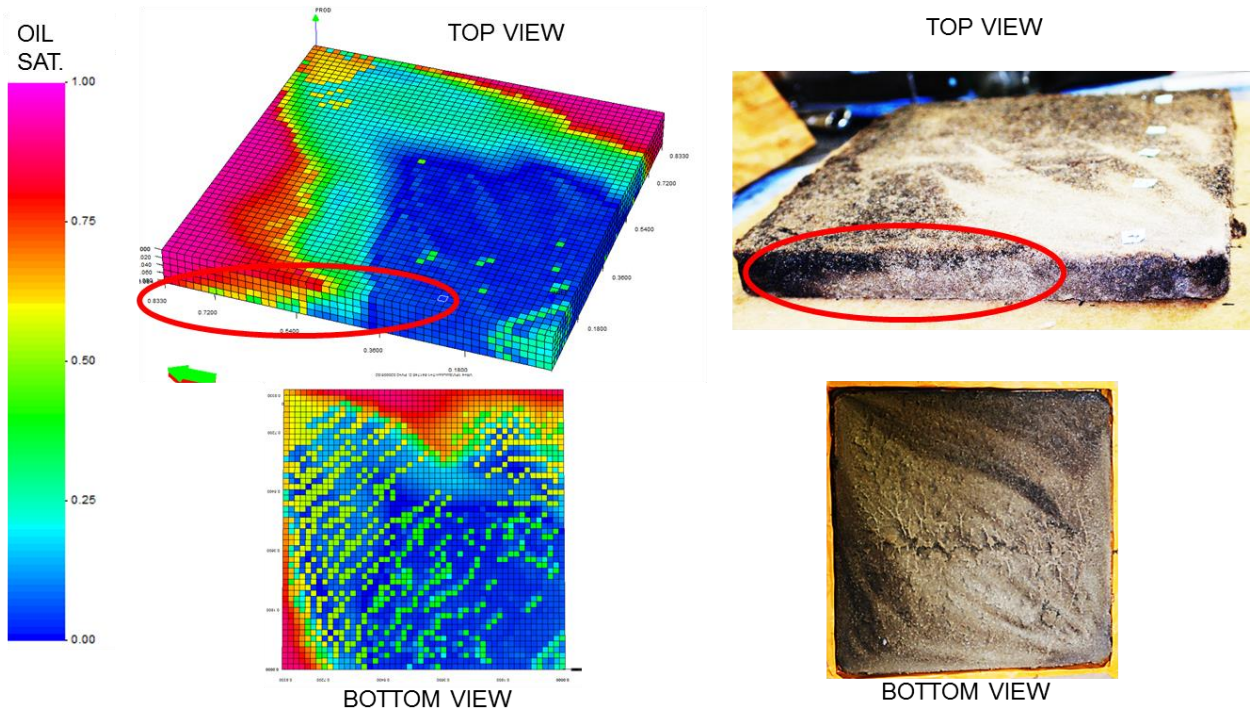

Figure 5.21: Oil saturation distribution at the end of ACP floods for experiments and simulations at VR=12, 4, and 2

Furthermore, the final saturation distributions for simulations were compared with the pictures of the experiments. Figures 5.20 and 5.21 shows the final oil saturations at different viscosity ratios on the top, bottom and side of the quarter 5-spot. Simulations qualitatively match the experimental observations. Thus, the top areal sweep, the vertical and bottom sweep were qualitatively matched and verified with experimental observation.

Thus, I have developed an UTCHEM simulation model of the ACP process that is validated with the laboratory experimental data. Such a model can be used at the field scale to develop guidelines for optimum viscosity ratio and starting time for ACP floods.

CHAPTER 6: POST-WATERFLOOD ASP VS. POST-POLYMER ASP IN A 2D HETEROGENOUS SANDPACK

In this work, an alkaline-surfactant-polymer formulation was developed that produced ultra-low interfacial tension with a 27cp oil. Oil-surfactant-alkaline phase behavior experiments were conducted. Using the chosen formulation ASP flood was conducted in a heterogeneous quarter 5-spot pattern to study the interaction of sweep efficiency and displacement efficiency of ASP flooding through visual observations.

6.1 Experimental Methods

Materials

Alfoterra S23-13S-90 and Enordet IOS C 15-18 surfactants were obtained from Sasol and Shell Chemicals, respectively. Alfoterra surfactants are branched alkyl propoxy sulfates and Enordet IOS surfactants are internal olefin sulfonates. In addition to surfactants, I used Isobutyl alcohol (IBA) a cosolvent which was obtained from Sigma-Aldrich. The alkali used for the microemulsion phase behavior was sodium carbonate from Fisher Scientific. The ASP formulation that was used in this study had same alkali, surfactant and cosolvent concentrations as the ASP formulation in presented in Chapter 4.

The oil and the sand for the sandpack experiments were received from the fields investigated. The oil had a viscosity of 27 cp at 25 ^{o}C and an acid number of 1 mg KOH/gm of oil for ASP flood. The oil viscosity of 27 cp was obtained by addition of 15% octane to 100 cp oil that was use for homogenous ASP experiments. I used brine with a salinity of 45,000ppm (sodium chloride) as the injection brine for the waterflooding part of the heterogenous ASP sandpack experiment. The

salts used to make the injection brine were obtained from Fisher Scientific.

Phase Behavior Studies

Surfactant phase behavior experiments were performed to identify a surfactant formulation which gives ultralow IFT with the reservoir oil and aqueous stability at the optimum salinity. Aqueous solutions were prepared with 1 wt% of surfactants (a mixture of two surfactants), the injection brine, the co-solvent, and the alkali. In addition, all of the aqueous solutions were prepared and kept at the reservoir temperature (25 ^{o}C) to obtain the aqueous stability limits of the surfactant formulation. Initially, alkali concentration was varied systematically (in a series of pipettes) at a fixed water-oil-ratio (WOR). Then, the process was expanded to different WORs. The samples were equilibrated at the reservoir temperature and the phase volumes were recorded. The oil solubilization ratio in the microemulsion phase was estimated from the decrease in oil volume divided by the amount of surfactant and similarly the water solubilization ratio. The solubilization ratios were used to calculate interfacial tensions using the Huh equation (Huh, 1979).

Effluent Analysis

The effluent analysis was done on the samples in order to see propagation of the chemical slugs and determine the surfactant retention. Furthermore, viscosity, pH, salinity and the surfactant concentration in each tube were measured.

Apparent Sweep Determination

The bottom layer pictures of sandpack were loaded to image analyzer program. Each color was assigned certain range of pixels. Total sum of pixels for certain color were used to calculate apparent areal sweep efficiency.

Local Oil Concentration Determination

Each sand block was extracted carefully from the sandpack and was but into glass jars. The mass of sand block was recorded. Then toluene was added such that estimated total oil concentration in the mixture would be below 3%. The mixture of sand, effluents and toluene was thoroughly mixed and the mixture was loaded into cuvette and absorption was measured using UV-Vis spectroscopy. The absorption numbers were converted to oil concentration in the mixture by using pre-determined calibration curve. Extra care was taken during creation of calibration curve.

Transparent Heterogeneous 2D Sand Pack

Figure 6.1 shows a sketch of the quarter five-spot sandpack and a picture of the actual quarter 5-spot sand pack that was used for a heterogenous ASP flood. The 10" x10" square-shaped sand pack was 1" thick. This flooded area is covered by rubber sheets at the top. The bottom of the sand pack was covered by transparent plexiglass. Between the top of the sand pack and the top steel plate there was a thin rubber sheet and water to impose overburden pressure. Figure 6.2 shows more pictures of the heterogeneous quarter 5-spot used for ASP floods. Instead of bottom steel plate I used completely transparent plexiglass cover that has the same geometry as the steel plate. The plexiglass cover can hold up to 3000psi. The overburden pressure is applied only from one side instead of both sides as in the steel 5-spot cell. Thin hollow square shaped rubber sleeve covers the sides where plexiglass and steel are almost in contact; thus, it creates good barrier and seal from leaking. To further enhance the tightness of the packing, a steel ring was screwed on top of the plexiglass plate. The transparent plate was at the bottom of the sand pack in all experiments. Due to heterogeneity, it was decided to saturate the transparent sand pack completely with oil from

the beginning.

Before applying the final confining pressure, the overburden pressure was varied on the sand packs where stepwise increases and decreases in overburden pressure were applied. The overburden sequences helps to ensure a tighter pack. A confining pressure of 300 psi was applied on the top rubber sheet which presses against the sand pack.

The quarter five-spot pattern was wet packed with sand. Initially the transparent cover was placed at the bottom. The reservoir sand was wetted with excess oil and mixed to dislodge trapped air inside the sand. Then, oil-wetted sand was placed in small quantities inside the square-shaped slot while adding some amount of oil. At the end, extra sand was scraped off from the top of the sandpack, and the rubber sheet was put on top of the sandpack. Subsequently, the top steel plate was screwed on. The top rubber sleeve was used to separate the sandpack from the confining liquid on one side. After closing the five-spot pattern, and performing the overburden cycle, an overburden pressure of 300 psi was applied and left to stabilize for several days. The compression of the sand from the top ensures a tight sand pack.

Heterogeneous 2D Sand Pack ASP Floods

All the ASP floods were conducted at a temperature of 25 ^{o}C. The injection fluid was pumped at a constant flow rate of 0.5 ml/min, which is equivalent to 0.8 ft/day, using an ISCO pump. The pressure drop across the sand pack was measured by pressure transducers. Effluent samples were collected in tubes using a fractional collector and the phase volumes were estimated. The produced emulsions during the ASP flood were heated and demulsified with appropriate chemicals for accurate measurement of oil and aqueous phase volumes.

Table 3.1 lists the injection fluid sequence for the quarter 5-spot sand pack floods. ASP HET1 was the post-water flood ASP flood and ASP HET2 was the post-polymer flood ASP floods. In

ASP HET1, water was injected first for 2.4 PV. Then 0.5 PV of the ASP slug was injected. This ASP slug was followed by a 2 PV polymer drive. In ASP HET2, first polymer solution was injected for 2.4 PV. That was followed by 0.5 PV ASP slug and 2PV polymer drive. The compositions of ASP slug and polymer drive was identical in the 2 floods. The difference was the initial water flood in ASP HET 1 and the initial polymer flood in ASP HET 2.

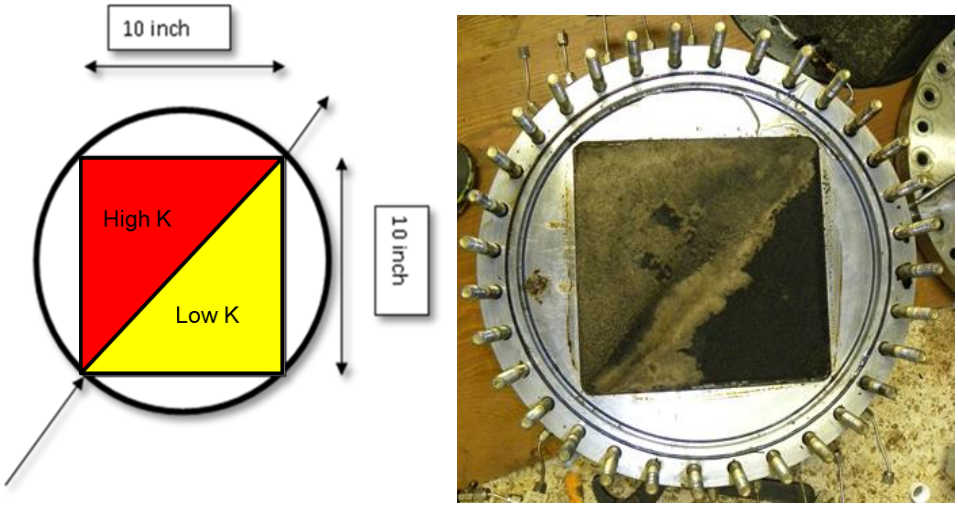

Figure 6.1: Sketch of the quarter five-spot sandpack and a picture of the actual quarter 5-spot sandpack after the finished flood

Figure 6.2: The transparent quarter 5-spot sandpack model

Table 6.1: 2D 5-spot tertiary heterogeneous ASP floods

Flood title	ASP HET1	ASP HET2
Waterflood/Polymer flood extent, PV	2.4	2.4
Soi, %	100	100
Porosity	0.36	0.36
Brine Permeability 100-120 mesh sand, Darcy	~2	~2
Brine Permeability 20-40 mesh sand, Darcy	~20	~20
ASP slug size, PV	0.5	0.5
Main surfactant conc.% (Alfoterra S2313S-90)	0.75	0.75
Cosurfactant conc. % (Enordet IOS C 15-18)	0.25	0.25
Cosolvent conc. % (IBA)	1	1
Oil viscosity, cp	27	27
Ininital Waterflood/Polymer viscosity, cp @6.31s^{-1}	0.9	5
Ininital Waterflood/Polymer salinity (ppm NaCl)	45,000	45,000
Initial Polymer for ASP HET2 , ppm	----------	785
ASP viscosity, cp @6.31s^{-1}	50	50
ASP slug Na_2CO_3, ppm	30,000	30,000
ASP polymer conc., ppm	2400	2400
Polymer Drive slug size	2.0	2.0
Polymer Drive polymer conc., ppm	2250	2250
Polymer Drive viscosity, cp @6.31s^{-1}	50	50
Polymer Drive Na_2CO_3, ppm	15,000	15,000
Flood mode	Tertiary	Tertiary

6.2 Results

6.2.1 PHASE BEHAVIOR

Figure 6.3 shows the solubilization ratios for an alkali-surfactant formulation with the oil volume fraction of 50%. The oil and water solubilization ratios are represented respectively as red and blue dots. The salinity is increased by adding Na_2CO_3. This formulation contains 0.75%

Alfoterra, 0.25% Enordet, 1 wt% cosolvent, and varying amounts of Na_2CO_3 (0-45,000 ppm). The optimum surfactant formulation was obtained after several trials with different surfactant blends. With this formulation, I was able to achieve three types of microemulsion phase behavior. At low Na_2CO_3 concentration (<20,000 ppm), the lower Type-I microemulsion phase forms where the surfactant resides primarily in the water phase and solubilizes some oil. At high Na_2CO_3 concentration (>43,000 ppm), the surfactant resides primarily in the oil phase and water is solubilized to form the upper Type-II microemulsion phase. When Na_2CO_3 concentration is between 20,000 and 40,000 ppm, the middle Type-III microemulsion phase forms, where both oil and water are solubilized into the middle phase microemulsion. The salinity at which oil solubilization ratio equals water solubilization ratio is called the optimum salinity. Thus, the optimum salinity is around 30,000 ppm Na_2CO_3 concentration at a water-oil ratio of 1:1 (or 50 volume% oil).

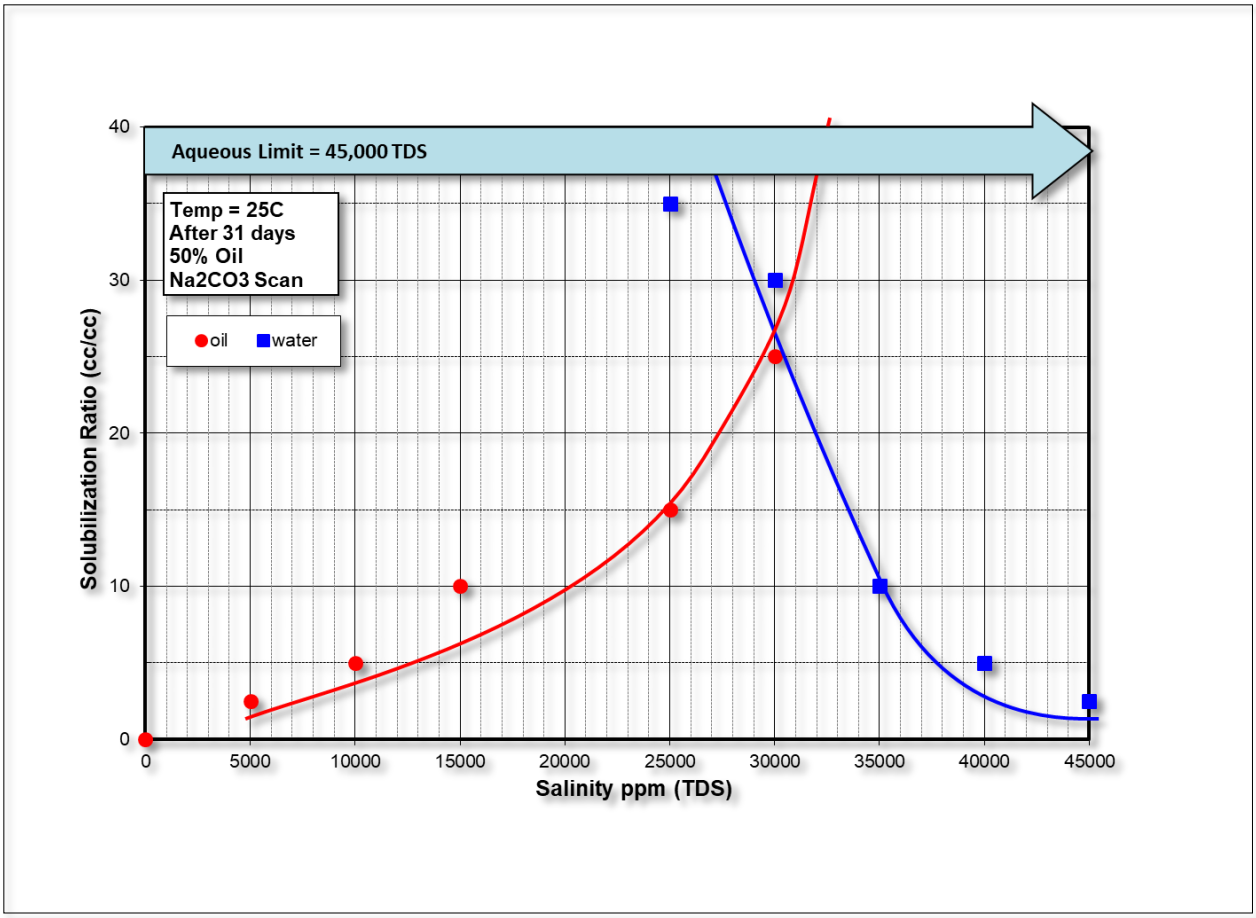

Figure 6.3: Oil and water solubilization ratio for surfactant formulation at an oil volume fraction of 50%

Figure 6.4 shows the activity diagram where the microemulsion phase behavior is plotted as a function of oil volumetric fraction of 10%, 30%, and 50%. As the oil fraction increases, the three-phase salinity window moves to lower salinity, and thus, the optimum salinity decreases. For inactive oils, the optimum salinity does not change with the oil fraction. If the oil is active, soap forms by the reaction of oil and Na_2CO_3; as the oil fraction increases the amount of soap increases. Thus, the soap to synthetic surfactant ratio increases. Since the soap is usually more hydrophobic than the added surfactants, the optimal salinity decreases, as shown in Figure 6.4. During the ASP flood, the salinity of the ASP slug is often in the type III region (~30,000ppm) (or slightly into type II), and the salinity of the polymer slug is in the range of type-I salinity (~15,000ppm). In general, the negative slope of the optimum salinity line in the activity diagram

is preferred because it ensures that the composition path (the dashed line) during an ASP flood would cross the type III salinity region where ultralow tension can be achieved.

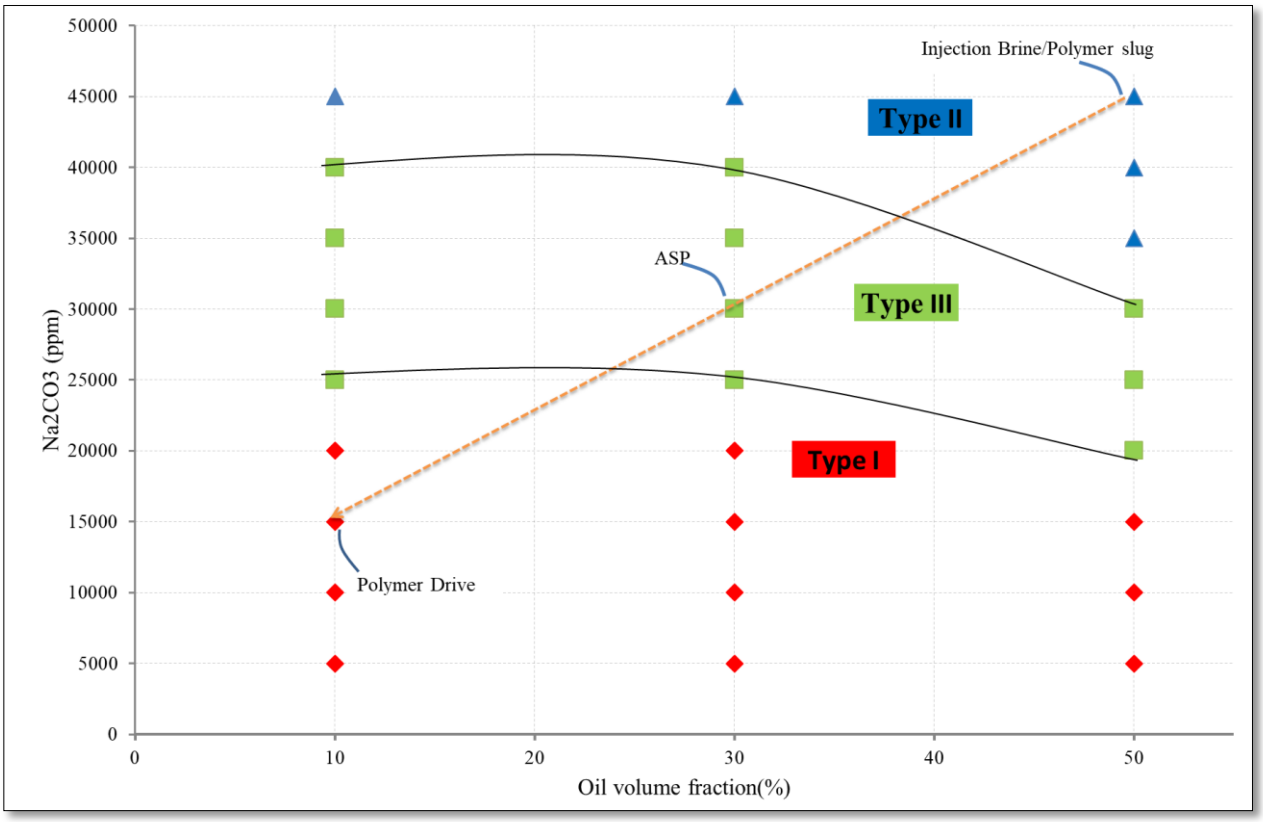

Figure 6.4: Activity diagram showing the phase behavior of viscous oil and the ASP solution at varying oil volume fractions and Na2CO3 concentration with 27cp oil.

6.2.2 HETEROGENEOUS QUARTER 5-SPOT ASP FLOODS

A heterogeneous quarter 5-spot sand pack of size 10” x 10” x 1” was constructed. Two sands with a permeability contrast of 10:1 were packed into a 2D square steel cell, as shown in the Figure 6.2. Surfactant, oil and brine were mixed to study phase behavior and interfacial tension. An alkali-surfactant formulation was identified that produced ultra-low interfacial tension with the reservoir oil (27 cp). ASP flood was performed in tertiary modes. In one tertiary experiment, waterflood was conducted first followed by the ASP flood. In a second experiment, polymer

flood was conducted first followed by the ASP flood. The ASP formulation and slug size were kept the same. The oil recovery, oil cut, and pressure drop were measured. The effluent properties were monitored and the surfactant retention was calculated. Images were taken during flooding and were digitally analyzed to estimate the areal sweep efficiency. The main goal of this work is to compare WF-ASP with PF-ASP and study the transport of ASP processes in heterogeneous rocks.

Post-Waterflood Heterogeneous Quarter 5-spot ASP Flood

Initially, the heterogeneous sand pack was completely saturated with oil (So = 100%). Water was injected first for 2.4 PV. Then the ASP slug was injected for about 0.5 PV followed by the polymer slug of the same viscosity, as listed in Table 6.1. The ASP slug viscosity was ~50 cp and the polymer slug viscosity was 50 cp. Figure 6.5 shows total relative mobility and apparent viscosity for the oil bank at different saturations. The minimum total relative mobility was calculated to be 0.02 cp^{-1}. The maximum apparent viscosity of oil bank, which is equal to the reciprocal of the minimum total relative mobility, was 48 cp. The viscosities of ASP slug and polymer drive was chosen to be above 48 cp for a stable displacement of the oil bank.

Figure 6.6 shows the cumulative oil recovery, the oil cut, the remaining oil saturation and the pressure drop in the waterflood and the subsequent ASP flood. The waterflood was stopped after 2.4 pore volumes injected when the oil cut went below 2%. The water breakthrough occurred early only after 0.097 pore volumes. The waterflood recovered 22% of the original oil in place (OOIP) and decreased the oil saturation from the initial oil saturation of 100% to 78%. The pressure drop decreased from initial 0.5 psi to 0.2 psi.

During the ASP flood, the oil cut started increasing after 0.2 PV of ASP injection and reached its peak of 75% after 0.35 PV injection. Most of the oil was recovered within 1 PV after

the surfactant injection, but oil recovery increased slowly until the end of 2 PV polymer drive. The ASP flood and subsequent polymer drive in total recovered an extra 32% of OOIP and increased the overall recovery to 53% of OOIP. Furthermore, the oil saturation decreased from 78% to 46%.The tertiary recovery was able to recover 45% of the remaining oil in place (ROIP). After the start of the ASP injection, the pressure drop gradually increased and reached a maximum value of 2 psi at the end of polymer flood.

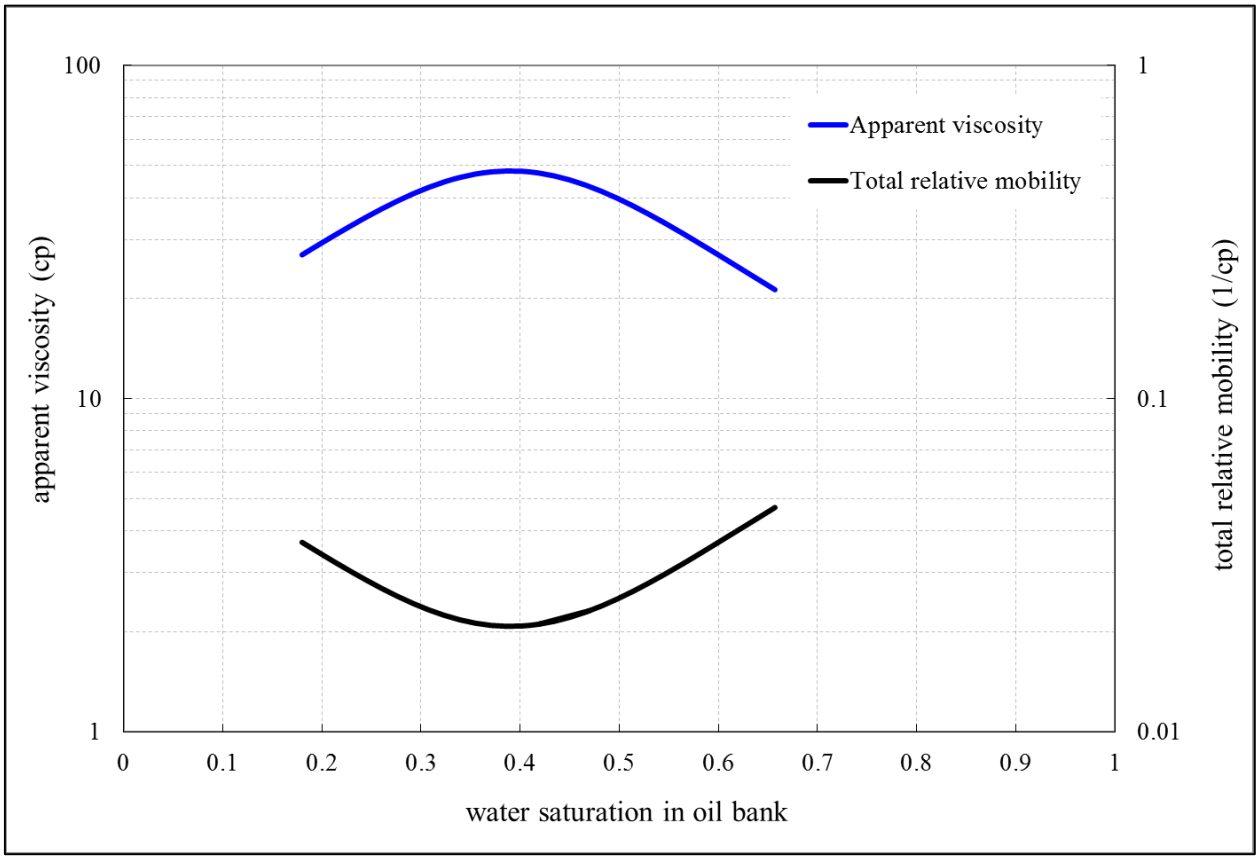

Figure 6.5: Total relative mobility and apparent viscosity of oil water bank (water and oil)

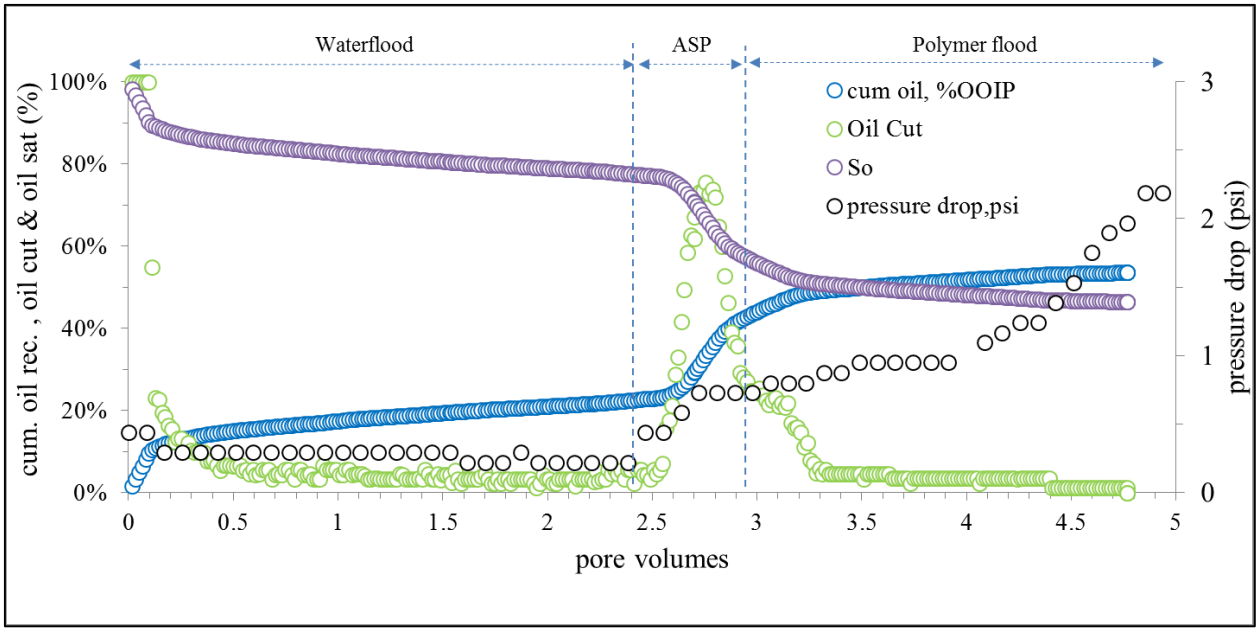

Figure 6.6: Cumulative oil recovery, the oil cut, the oil saturation and the pressure drop for post-waterflood ASP flood

Post-Polymer Flood Heterogeneous Quarter 5-spot ASP Flood

Initially, the heterogeneous sand pack was completely saturated with oil (So = 100%). Polymer solution (5 cp viscosity) was injected first for 2.4 PV. Then the ASP slug was injected for about 0.5 PV followed by the polymer slug of the same viscosity, as listed in Table 6.1. The ASP slug viscosity was ~50 cp and the polymer slug viscosity was 50 cp. Figure 6.7 shows total relative mobility and apparent viscosity for the oil bank at different saturations where oil bank consists of differing saturations of 5cp polymer and oil. The 5cp polymer viscosity was chosen so that the initial polymer flood would be stable. The minimum total relative mobility was calculated to be 0.007 cp^{-1}. The maximum apparent viscosity of oil bank, which is equal to the reciprocal of the minimum total relative mobility, was 140 cp. In theory, for ASP flood to be stable after initial polymer flooding the viscosity of ASP slug must be at least 140 cp. Nevertheless, one of the main goals of these experiments was to compare WF-ASP with PF-ASP

and study the transport of ASP processes in heterogeneous rocks. Therefore, the viscosities of ASP and polymer drive were 50 cp, similar to post-waterflood ASP case.

Figure 6.8 shows the cumulative oil recovery, the oil cut, the remaining oil saturation and the pressure drop for the polymer flood and subsequent ASP flood. The polymer breakthrough occurred after 0.2 pore volumes. The polymer flood was continued for 2.4 PV (similar to the water flood case). The polymer flood recovered 50% of the original oil in place (OOIP) and decreased the oil saturation from the initial oil saturation of 100% to 50%. This oil recovery is a lot higher than that for the waterflood (which was only 22% OOIP).

During the ASP flood, oil cut started increasing after 0.25 PV of ASP injection and reached its peak of 75% after 0.45 pore volume injection. Interestingly, other than arriving slightly later by 0.1 pore volume, the post-polymer ASP oil cut was very similar to post-waterflood ASP oil cut. Most of the oil was recovered by 1 pore volume after the surfactant injection. The ASP flood and subsequent polymer drive in total recovered an extra 32% of OOIP and increased the overall recovery to 82% of OOIP. Furthermore, the oil saturation decreased from 50% to 18%.The tertiary recovery was able to recover 64% of the remaining oil in place (ROIP). After the start of the ASP injection, the pressure drop gradually increased and reached a maximum value of 5 psi at the end of polymer flood.

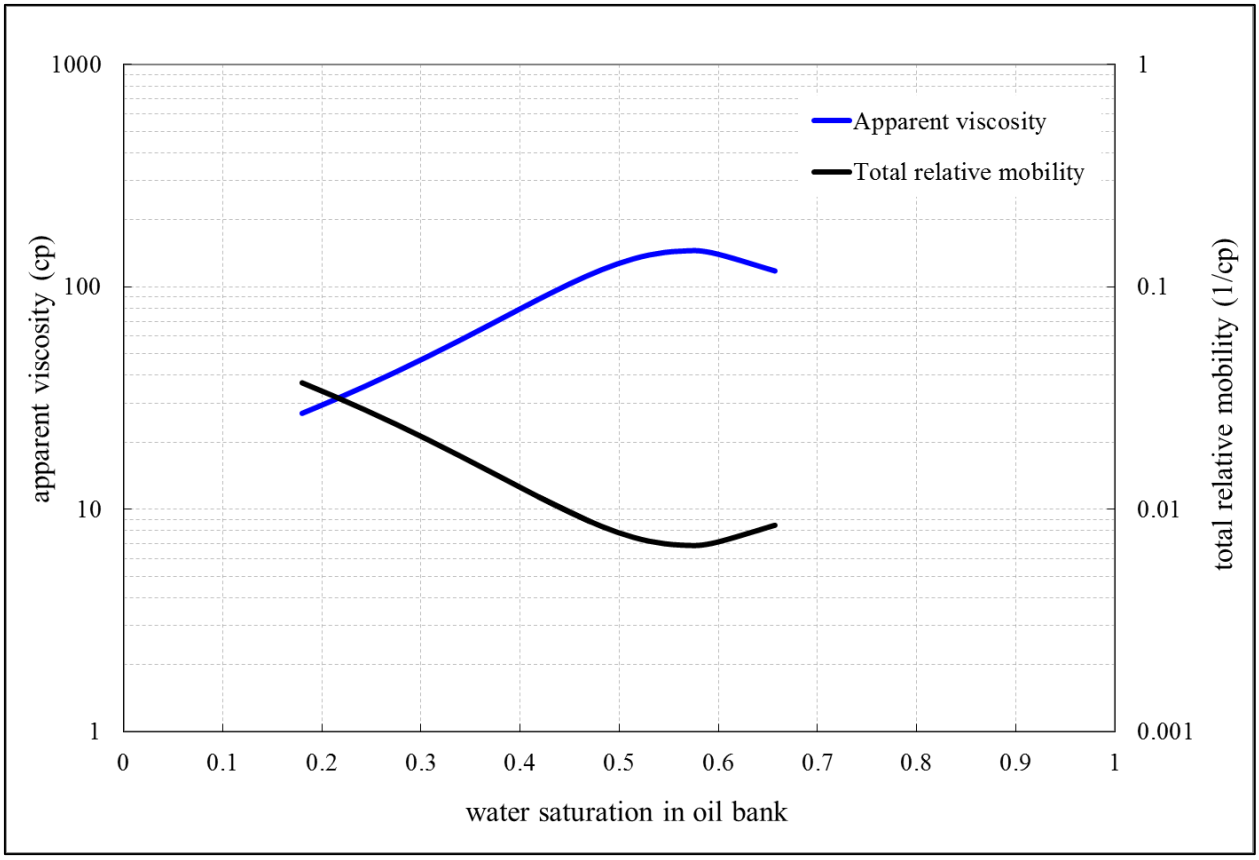

Figure 6.7: Total relative mobility and apparent viscosity of oil water bank (5 cp polymer and oil)

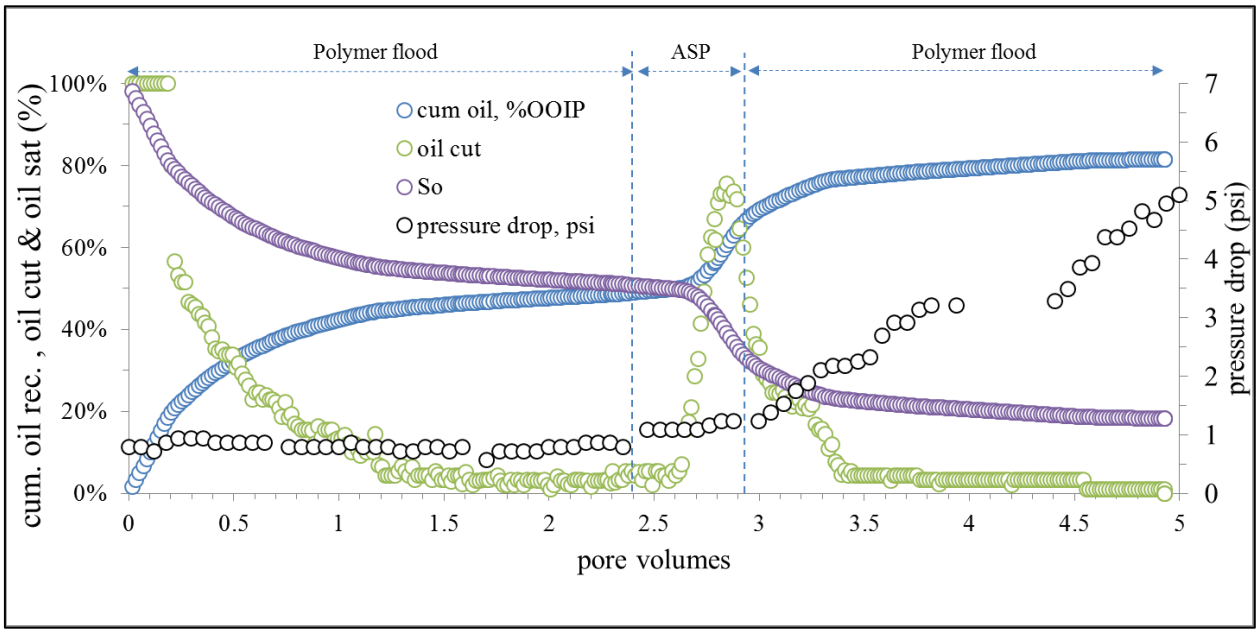

Figure 6.8: Cumulative oil recovery, the oil cut, the oil saturation and the pressure drop for post-polymer ASP flood

Effluent analysis

Figure 6.9 shows the normalized surfactant effluent concentration and pH for both the floods in the heterogeneous sand pack. The pH increased from 7 to 10.5 after surfactant came out. The normalized surfactant effluent concentration represents the percentage of total injected surfactant that came out with the effluents. The unrecovered percentage of surfactant was mostly retained due to heterogeneity of the flood. The post-polymer ASP flood had a retention of 0.43 mg/g of rock; 62% of injected surfactant was recovered. The retention in the post-waterflood ASP flood was 0.691 mg/g of rock or 39% was recovered back. The peak surfactant slug came out after 0.5 pore volumes injected for post-polymer case compared to the post-waterflood case where the surfactant slug came out after 0.8 pore volumes of injection. The surfactant effluent came out much later for post-waterflood case compared to post-polymer flooding case due to higher retention.

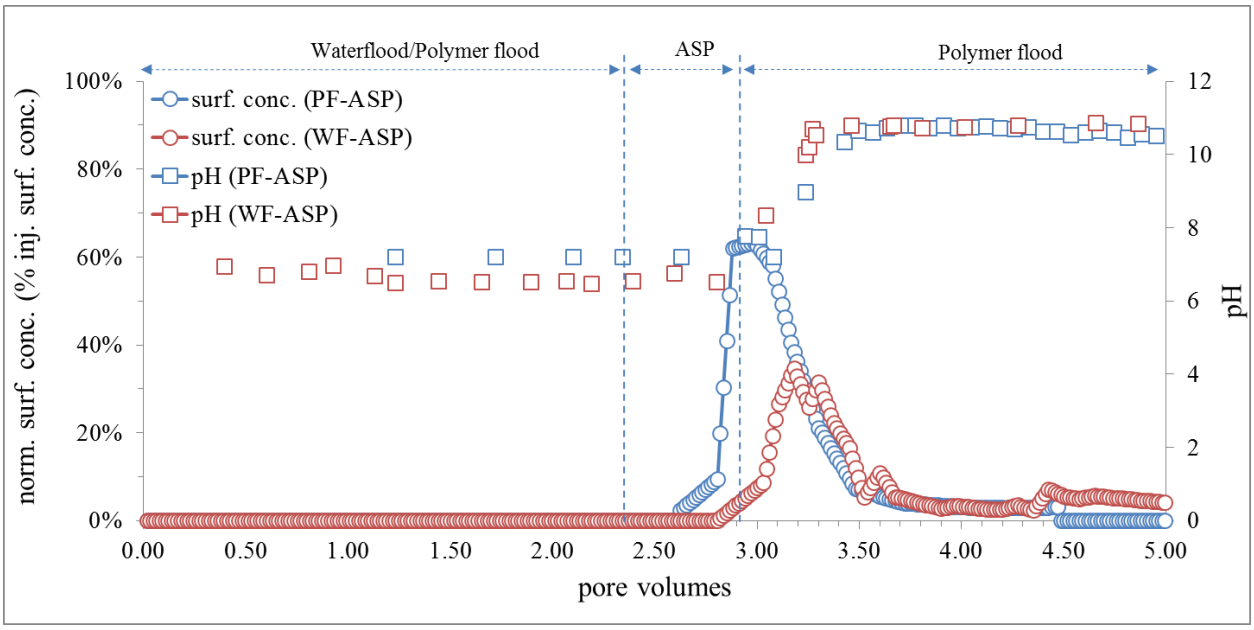

Figure 6.9: Effluent surfactant and pH for heterogeneous ASP floods

6.2.3 Sweep Efficiency of Heterogeneous ASP Floods

Post-Waterflood Heterogeneous Quarter 5-spot ASP Flood

Figures 6.10 and 6.11 show the flood progression at different pore volumes at the bottom of the sandpack. Injection port is located at the top left corner of each picture and production port is on the right bottom corner of each picture. Right half of the sandpack picture along the diagonal is high permeability zone and left half is the low permeability zone. Figure 6.10 shows color pictures while Figure 6.11 shows black-and-white pictures. The light color in Figure 6.10 represents the injectants and dark color represents oil. Oil in general is the darkest phase, however, it may look brown if it is partly swept or water invades the bottom of the sandpack. Therefore, the black and white pictures are also presented to differentiate between settled oil and swept areas because it clearly shows where the oil and aqueous phase are.

Waterflood sweeps only high permeability zone initially during 0-0.54 pore volumes injected. In addition to channeling though high permeability layer, the viscous fingering and oil bypassing can be easily observed. Flood front gets narrower towards producer and tends to be close to diagonal as expected with much of the oil left unswept in the low perm sand. Figure 6.10 shows the increase in areal sweep efficiency at the bottom of the sand pack during the flood .The water breakthrough occurs at 0.097 pore volumes injected. The areal sweep efficiency at the water breakthrough was equal to 35%. Between 0.54 and 2.4 PV during the waterflood, about 18% of the low perm near the diagonal also gets swept. The final waterflood areal sweep efficiency reaches 68% at 2.4 pore volumes injected (before switching to ASP flood).

Between 2.4 and 2.9 PV, ASP sweeps only the high perm region. Between 2.9 and 4.7 PV, it looks like a lot of low perm gets swept by ASP, but that is just at the bottom. In the presence of surfactant, gravity segregation occurs and the later pictures are not representative of the whole cross-section. Furthermore, the low permeability zone is markedly darker and some of the

microemulsion is trapped in the low perm region which decreases the flood's displacement efficiency.

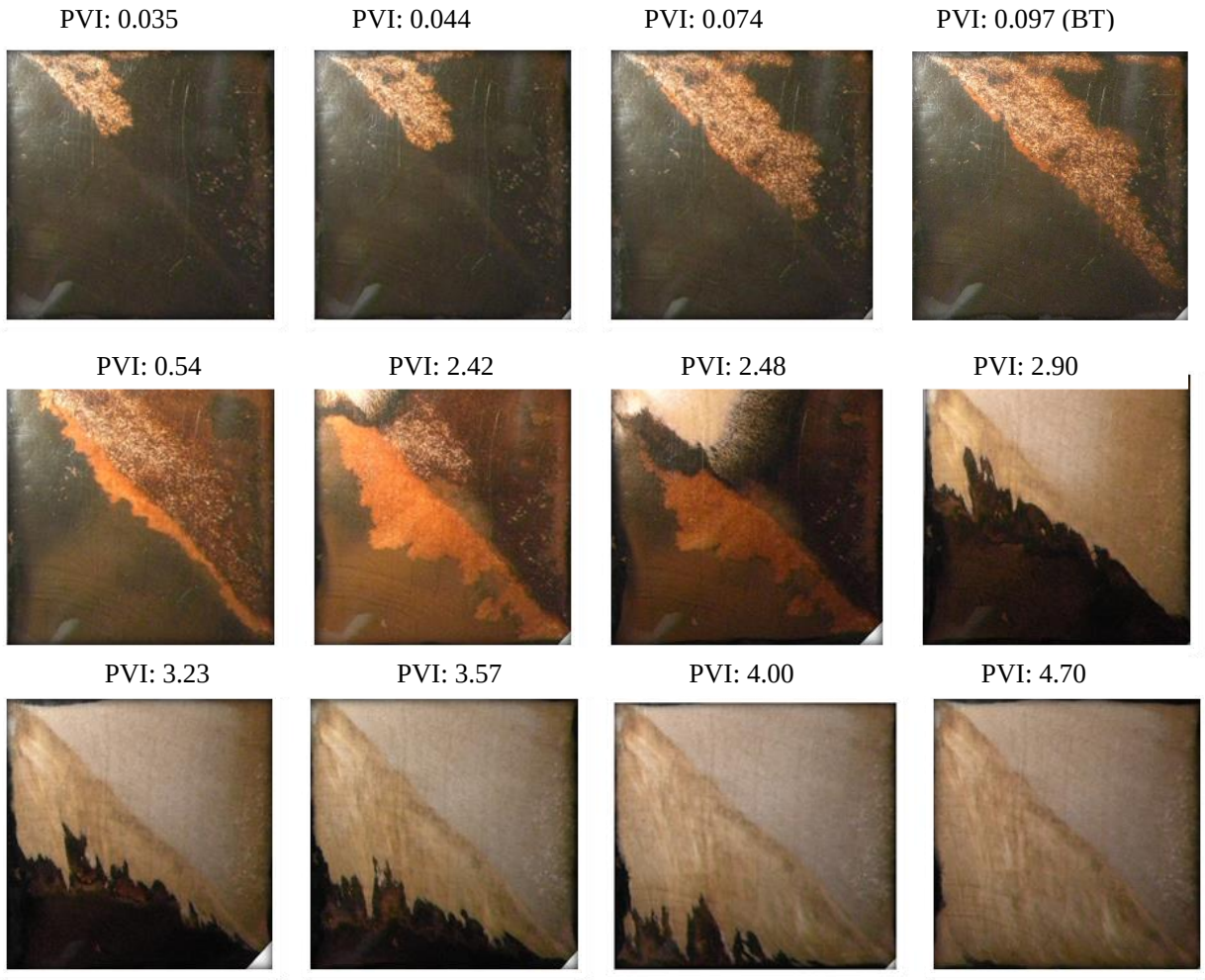

Figure 6.10: Areal sweep progression at different times during waterflood-ASP case (colored)

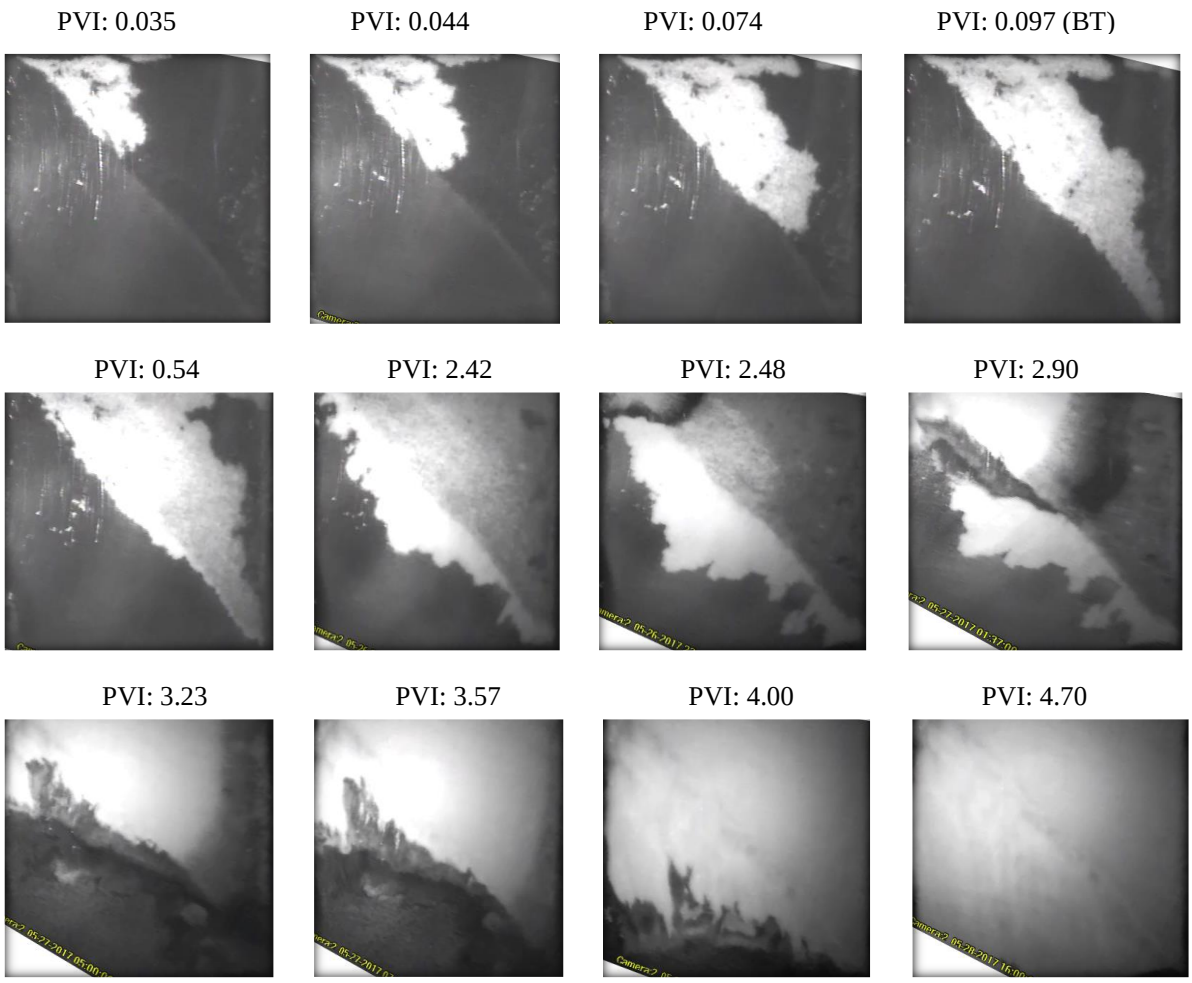

Figure 6.11: Areal sweep progression at different times during waterflood-ASP case (black and white)

Post-Polymer Flood Heterogeneous Quarter 5-spot ASP Flood

Figures 6.12 and 6.13 show the picture of the bottom of the sand pack during PF-ASP flood. The high perm zone is on the left side in these pictures. Polymer flood sweeps only the high permeability zone initially during 0-0.2 pore volumes injected. The viscous fingering and oil bypassing is not as obvious as in waterflooding case. The flood front seems very stable and high permeability zone was swept evenly. Figure 6.14 shows the higher areal sweep efficiency compared to waterflooding .The polymer breakthrough occurs after 0.194 pore volumes injected.

The areal sweep efficiency at the water breakthrough was equal to 53% compared to waterflooding case of 35%. Between 0.194 and 2.4 PV during polymer flood, about 37% of the low permeability zone also gets swept compared to only 18% for waterflooding case. The final polymer flood areal sweep efficiency reaches 87% at 2.4 pore volumes injected before switching to ASP flood.

Between 2.4 and 2.9 PV, ASP sweeps both high permeability and some of the low permeability zones compared. Between 2.9 and 4.7 PV, it looks like a lot of low permeability gets swept by ASP polymer, but that is just at the bottom. In the presence of surfactant, gravity segregation occurs and the later pictures are not representative of the whole cross-section. Furthermore, the low permeability zone markedly darker and full of microemulsion that decreases the flood's displacement efficiency. Therefore, further analysis performed to find local oil saturation as shown in Figure 6.15.

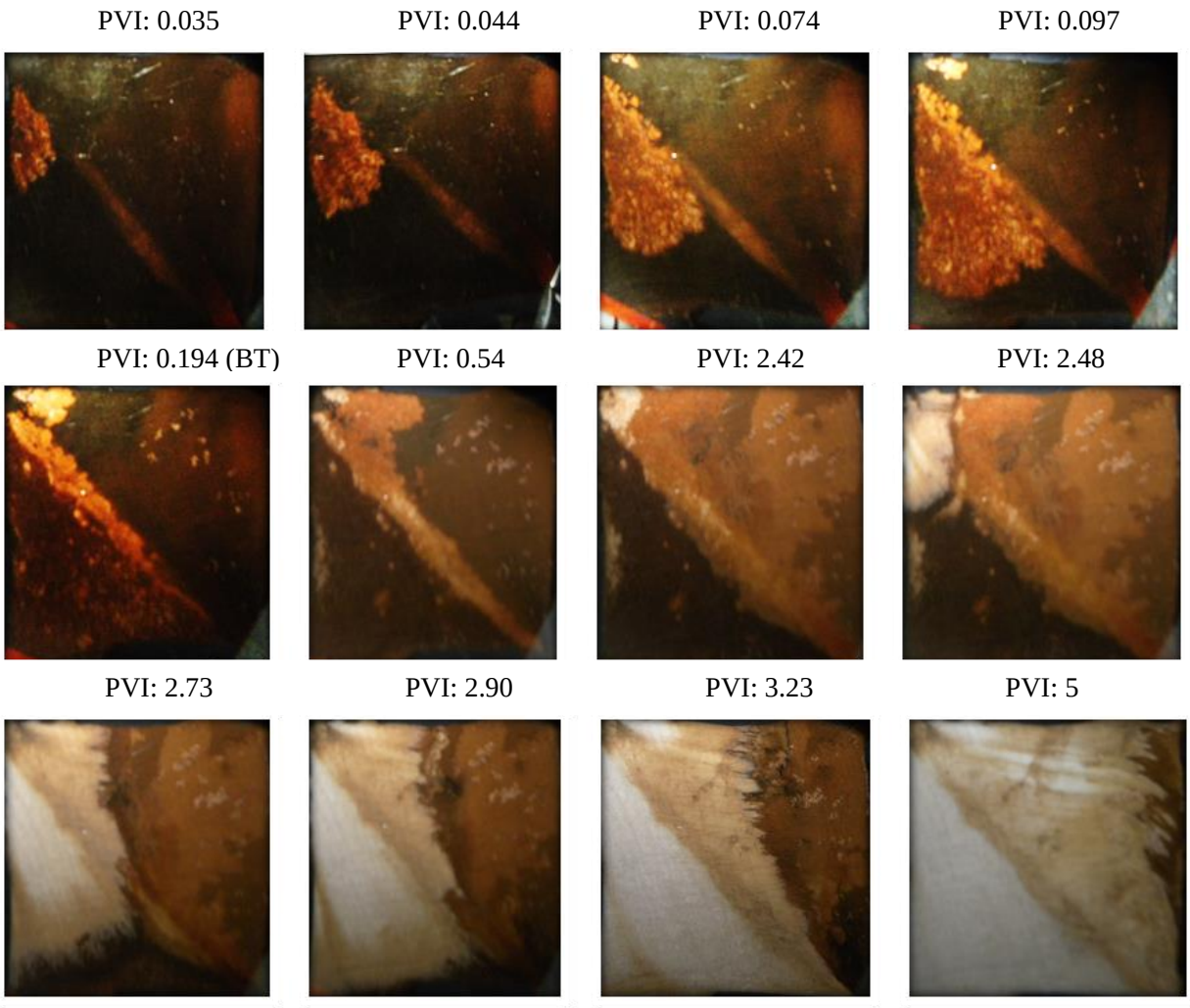

Figure 6.12: Areal sweep progression at different times during polymer-ASP case (colored)

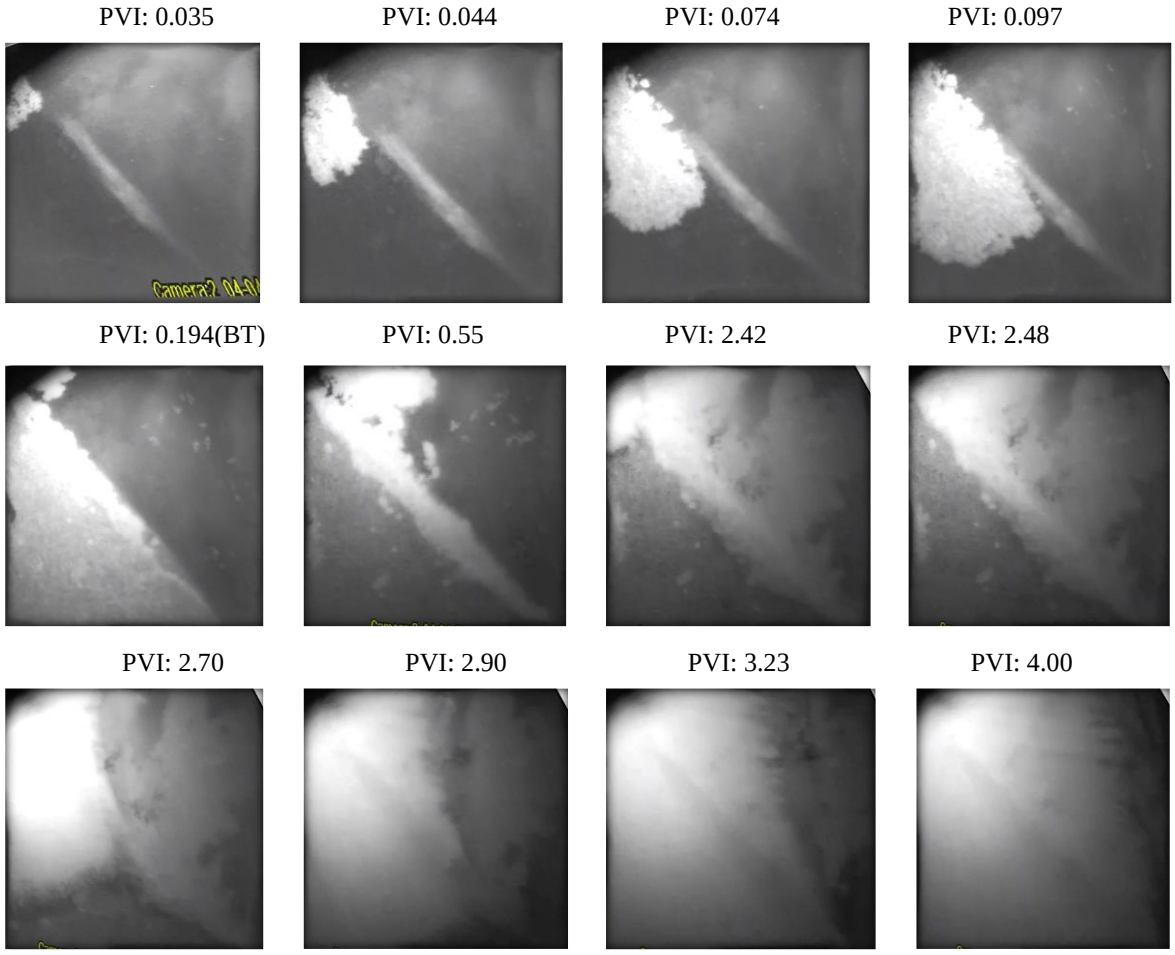

Figure 6.13: Areal sweep progression at different times during polymer-ASP case (colored)

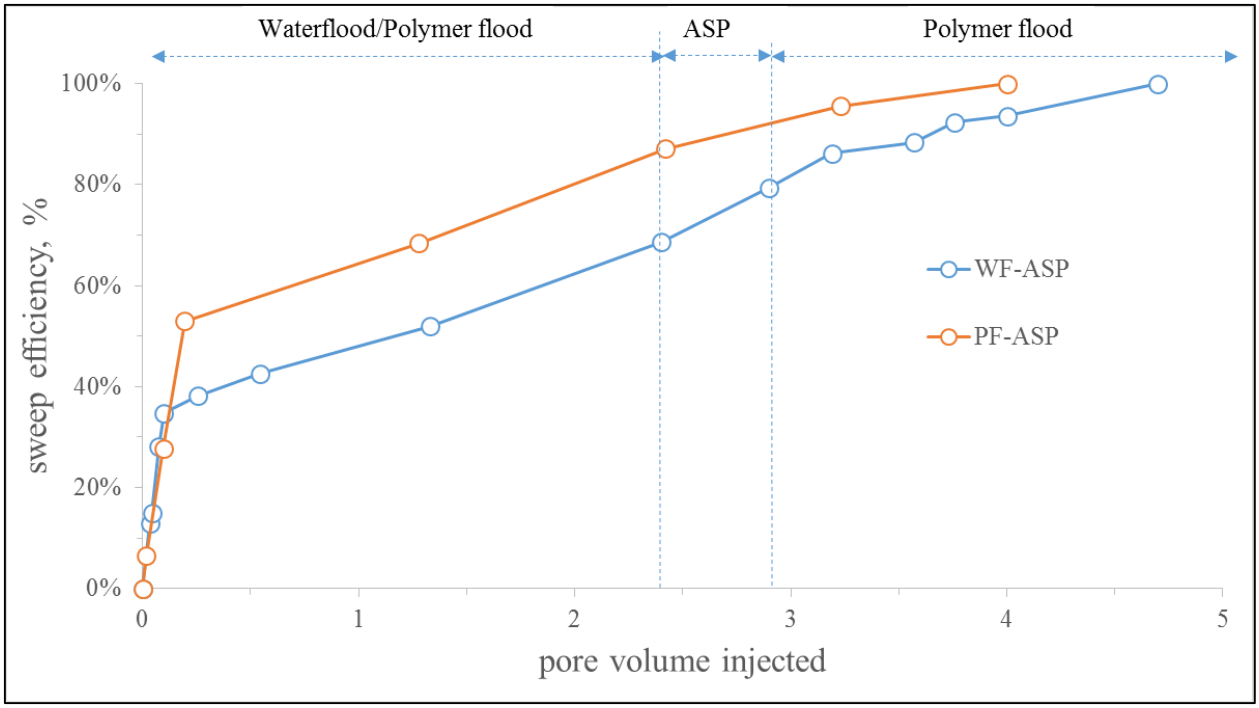

Figure 6.14: Areal sweep efficiency for heterogeneous tertiary ASP floods

Figure 6.15 shows final local oil saturation values. C and D pictures represents post-waterflooding ASP case and A and B represents post-polymer ASP case. High permeability zone for post-waterflooding is located at the upper right half and lighter side and for post polymer case in the lower left and lighter side. Even though, at the end of the ASP flooding the areal sweep both pictures look like well swept, the vertical heterogeneity affects final recovery efficiency significantly. Post-waterflooding ASP and post-polymer flooding ASP cases look very similar, however, the have very different local recovery efficiencies. For post-waterflooding ASP case the final average saturation was ~43% (slightly lower than 46% obtained from material balance) with 39% average oil saturation for high permeability zone and 46% average oil saturation for low permeability zone. Furthermore, it can be seen that low saturation values occur along the diagonal and closer towards high perrmability zone. Thus, even though the areal sweep efficiency was high for both floods the combination of gravity segregation and high surfactant

retention cause the displacement and vertical sweep efficiency to be low for the post-waterlfooding ASP case.

For post-polymer ASP case the final average saturation was ~18% with 11% average oil saturation for high permeability zone and 24% average oil saturation for low permeability zone. Figure 6.15 shows that high oil concentration is mostly in low permeability zone and along the wall. Nevertheless, compared to post-waterflooding case, the local oil saturations are much lower and have typical high displacement efficiency that is observed during homogenous ASP floods.

Thus, the displacement efficiencies are very different for two cases. Initial idea based on total relative mobility estimation suggested that post-polymer flooding ASP would perform worse compared to post-waterflooding ASP due to mobility ratio requirement being much higher for ASP flooding to be stable after polymer compared to waterflood. Nevertheless, the these series of experiments clearly demonstrated performing polymer flooding before ASP flood is clearly more beneficial compared to starting ASP flooding after waterflooding.

A)

13%	16%	17%	13%	28%
13%	5%	5%	9%	56%
7%	8%	11%	7%	60%
4%	10%	6%	10%	56%
5%	10%	18%	20%	39%

B)

C)

31%	10%	18%	60%	97%
15%	15%	9%	40%	87%
71%	23%	14%	7%	80%
50%	23%	27%	6%	36%
97%	98%	96%	27%	19%

D)

Figure 6.15: Final recovery factors for heterogeneous floods. C and D are for post-waterflooding ASP and A-B are for post-polymer flooding ASP.

CHAPTER 7: CONCLUSIONS AND RECOMMENDATIONS FOR FUTURE RESEARCH

7.1 Conclusions

In this dissertation, alkaline-surfactant-polymer (ASP) and alkaline-cosolvent-polymer (ACP) floods were studied in two-dimensional sand packs. This research is the first of a kind ASP/ACP study in a multidimensional medium. There are currently no published work available that focuses on studying ASP and ACP in a two-dimensional porous medium. Two kinds of sand packs were developed: homogeneous and heterogeneous with a permeability contrast of 10:1. ASP formulations were developed for a 100 cp and a 27 cp oil. An ACP formulation was developed for a 300 cp oil. In Chapter 4, ASP flood was studied in a homogeneous sand pack at different viscosity ratios and ASP injection start times. In Chapter 5, ACP flood was studied in a homogeneous sand pack at different viscosity ratios and ACP injection start times. In Chapter 6, ASP flood was studied in a heterogeneous sand pack. The following conclusions can be drawn from this study.

- Mixture of surfactants (0.75% Alfoterra S2313S-90 and 0.25% Enordet IOS C15-18), alkali (32,500 ppm Na_2CO_3), and co-solvent (1% IBA) show high solubilization ratio and ultralow IFT with a viscous reservoir oil (100 cp) at 25 ºC. These chemicals develop microemulsions, not macroemulsions, with the viscous oil. ASP formulations can recover most of the oil remaining after a waterflood in a linear sandpack if enough polymer is used and chemical slug viscosity is higher than the oil viscosity.
- ASP floods in quarter 5-spot 2D sandpacks showed cumulative oil recovery in the range of 60 to 98% OOIP depending on the viscosity of the chemical slug. The 2D tertiary ASP flood recovered most of the oil (~98% of OOIP) when the ASP slug viscosity exceeded the oil viscosity,

but pressure gradients were high at ~ 1ft/d injection. When the ASP slug viscosity was lowered to about 1/3 of the oil viscosity, the oil recovery dropped slightly to 90% OOIP, but the pressure gradient decreased significantly. The viscosity ratio of 3 appeared to be the optimum where the oil recovery is high (90% OOIP) and the pressure gradient is feasible (5.4 psi/ft) in the quarter 5-spot sandpack. This optimum needs to be re-evaluated at the field scale for the specific reservoir heterogeneity.

- Sweep efficiency was reduced due to gravity segregation because gravitational forces become important when capillarity disappears due to low interfacial tension.

- As the extent of waterflood preceding the ASP flood became shorter, the oil was recovered faster for the same pore volumes injected. The ultimate recovery was independent of the extent of waterflood. These findings imply that the timing of the flood has a significant impact on the production acceleration, which also has an economic impact.

- The tertiary ASP floods in the 2D laboratory model were simulated by the simulator UTCHEM. The calibrated simulation model can be used at the field scale to determine the optimum viscosity ratio and timing of ASP floods. Alkaline-surfactant-polymer (ASP) process is a very attractive process to maximize viscous oil recovery.

- Three-phase microemulsion behavior can be developed between an active viscous oil (330 cp) and alkaline-cosolvent mixtures (30,000 ppm Na_2CO_3 and 1 % IBA-30EO) without using any synthetic surfactant. ACP formulations can recover all the oil remaining after a waterflood in a linear sandpack if enough polymer is used and chemical slug viscosity is higher than the oil viscosity.

- ACP floods in quarter 5-spot sandpacks showed cumulative oil recovery in the range of 60 to 90% OOIP. As the chemical slug viscosity decreased, oil recovery and pressure gradient both

decreased. The viscosity ratio of 4 appeared to be the optimum where the oil recovery is high (75% OOIP) and the pressure gradient is feasible (4.5 psi/ft) in the quarter 5-spot sandpack. This optimum needs to be evaluated at the field scale for the specific reservoir heterogeneity.

- The ultimate recovery was slightly higher for tertiary ACP floods compared to the secondary ACP flood, but a delayed start led to a delayed oil recovery.

- Experimental results were numerically simulated and matched using an in-house simulator UTCHEM. 3D simulations in UTCHEM can match the ACP floods in the quarter 5-spot sandpacks. The calibrated simulation model can be used at the field scale to determine the optimum viscosity ratio and timing of ACP floods.

- Alkaline-cosolvent-polymer (ACP) process is a very attractive alternative to alkaline-surfactant-polymer (ASP) processes for active oils since it avoids the complexity and the cost of using a surfactant.

- A visual 5-spot sandpack model was developed by using a transparent polymer plate at the bottom of the model. Overburden pressure could be applied only on one side of the sand pack. The two diagonal halves of the model were packed with different sands to achieve a permeability contrast of 10:1.

- A mixture of surfactants (0.75% Alfoterra S2313S-90 and 0.25% Enordet IOS C15-18), alkali (30,000 ppm Na_2CO_3), and co-solvent (1% IBA) showed high solubilization ratio and ultralow IFT with a viscous reservoir oil (27 cp) at 25 ^oC. This system was used for heterogeneous post-waterflood and post-polymer flood tertiary ASP flooding.

- Secondary water flood (45,000 ppm NaCl) of a 27 cp oil in the heterogeneous quarter 5-spot recovered 22% OOIP. Post-waterflood ASP flood recovered 30% OOIP additional oil with a cumulative (WF+ASP) oil recovery of 52%. Secondary polymer (785 ppm HPAM 3630S and

45,000 ppm NaCl) flood of the same heterogeneous quarter 5-spot yielded 50% OOIP. Post-polymer flood ASP flood recovered 30% OOIP additional oil with a cumulative (PF+ASP) oil recovery of 80% OOIP. The cumulative oil recovery was much higher in the case of post-polymer flood ASP.

- The maximum oil cut of 75% was the same for both post-waterflood and post-polymer ASP floods.

- Visual observations of these floods in this quarter 5-spot show the evolution of sweep efficiency. In the post-water flood ASP case, the water flood swept mostly the high permeability region. The following ASP flood followed the water swept region because of the higher effective water permeability and bypassed the lower permeability region. The polymer drive moved some oil from the low permeability region to the high permeability region. In the post-polymer flood ASP case, the polymer flood swept both high and low permeability regions. The subsequent ASP flood also swept both high and low permeability regions.

- In the post-water flood ASP case, the final average oil saturation was 43% (slightly lower than 48% obtained from material balance) with 39% average oil saturation for high permeability zone and 46% average oil saturation for low permeability zone. In the post-polymer flood ASP case the final average oil saturation was ~18% with 11% average oil saturation for high permeability zone and 24% average oil saturation for low permeability zone.

- These series of experiments demonstrates the interaction of sweep efficiency and displacement efficiency of ASP flooding through visual observations. It demonstrates that the polymer flood - ASP flood combination is more effective than the water flood - ASP flood combination.

7.2 Recommendations

Based on the present study, further research in the following area is recommended:

- Conduct more transparent heterogeneous 2D ASP and ACP experiments using different flow patterns in the sandpack. It is recommended adding more realistic areal heterogeneity.
- Conduct transparent heterogeneous 2D ASP and ACP experiments in secondary mode.
- Conduct optimum viscosity and timing experiments under constant differential pressure condition.
- Conduct experiments with 2D ASP/ACP core slab experiments to see the effect of permeability
- Using modeling, develop 'viscous fingering number' that achieves mechanistically sound history match of unstable ASP/ACP floods.
- Simulate realistic field case unstable ASP/ACP floods in order to see the field response

NOMENCLATURE

ASP-Alkaline-Surfactant-Polymer

ASP HET1 - Alkaline-Surfactant-Polymer Heterogeneous Flood #1

ASP HET2 - Alkaline-Surfactant-Polymer Heterogeneous Flood #2

ACP-Alklaine-Colsolvent-Polymer

DOE-Department of Energy

DI-Deionized

EOR-Enhanced Oil Recovery

PF-Polymer Flood

PV-Pore Volume

PVI-Pore Volumes Injected

RPM-Revolutions per minute

SRB-Synthetic Reservoir Brine

So- Oil Saturation

VR-Viscosity Ratio

WF-Waterflooding

APPENDIX

The input files are presented in this section. The first section shows ASP UTCHEM simulation input files. The second section gives the ACP flood UTCHEM input file.

A.1 Unstable ASP Simulation of 100 cp Oil in a Quarter 5-spost Sandpack

The simulation of quarter 5-spot sandpack ASP flood at Oil/ASP viscosity ratio of 3 after 1 pore volume waterflood is presented below. The simulation was conducted using UTCHEM.

```
CC**********************************************************************
CC *
CC BRIEF DESCRIPTION OF DATA SET : UTCHEM (VERSION 9.9) *
CC *
CC**********************************************************************
CC *
CC History match of ASP quarter 5-spot sandpack at VR=3  *
CC *
CC LENGTH (FT) : PROCESS : A/S/P FLOODING *
CC THICKNESS (FT) : INJ. PRESSURE (PSI) : *
CC WIDTH (FT) : COORDINATES : CARTESIAN *
CC POROSITY : *
CC GRID BLOCKS : 50X50X1 *
CC DATE : *
CC *
CC**********************************************************************
CC
CC**********************************************************************
CC *
CC RESERVOIR DESCRIPTION *
CC *
CC**********************************************************************
CC
CC
*----RUNNO
R03-20
CC
CC
*----HEADER
ASP quarter 5-spot hisotry match tertiary VR=3 case
Experiment
```

```
**********************************************************
CC
CC SIMULATION FLAGS
*---- IMODE IMES IDISPC ICWM ICAP IREACT IBIO ICOORD ITREAC ITC IGAS IENG
ILGR IBLACK
      1   7   0     0   0    3   0    1     0    0  0   0   1     0
CC
CC NUMBER OF GRID BLOCKS AND FLAG SPECIFIES CONSTANT OR VARIABLE
GRID SIZE
*----NX   NY    NZ IDXYZ IUNIT  N_WELLMAX
   50   50    1    0    0     2
CC
CC CONSTANT GRID BLOCK SIZE IN X, Y, AND Z
*----DX    DY      DZ
  0.0166 0.0166 0.083
CC
CC TOTAL NO. OF COMPONENTS, NO. OF TRACERS, NO. OF GEL COMPONENTS
*----N no NTw nta ngc ng noth
   12 0  0   0   4   0   0
CC
CC
*---- SPNAME(I),I=1,N
WATER
OIL
SURFACTANT
POLYMER
ANION
CALCIUM
alc1
alc2
CARBONATE
SODIUM
HYDROGEN
pet acid
CC
CC FLAG INDICATING IF THE COMPONENT IS INCLUDED IN CALCULATIONS OR
NOT
*----ICF(KC) FOR KC=1,N
    1  1  1  1  1  0   1  0  1  1  1   1
CC
CC*****************************************************************
CC *
CC OUTPUT OPTIONS *
CC *
CC*****************************************************************
CC
```

```
CC
CC FLAG FOR PV OR DAYS FOR OUTPUT AND STOP THE RUN
*----ICUMTM ISTOP IOUTGMS
     1    1    0      0
CC
CC FLAG INDICATING IF THE PROFILE OF KCTH COMPONENT SHOULD BE
WRITTEN
*----IPRFLG(KC),KC=1,N
    1  1   1   1  1  0  0  0  1  1  1   1
CC
CC FLAG FOR PRES,SAT.,TOTAL CONC.,TRACER CONC.,CAP.,GEL, ALKALINE
PROFILES
*----IPPRES IPSAT IPCTOT IPBIO IPCAP IPGEL IPALK ITEMP IPOBS  IPATERN
    1     1    1      0    0     0    1  0     0    0
CC
CC FLAG FOR WRITING SEVERAL PROPERTIES
*----ICKL IVIS IPER ICNM ICSE IFOAM IHYST INONEQ
     1    1   1  1   1   0    0    0
CC
CC FLAG FOR WRITING SEVERAL PROPERTIES TO PROF
*----IADS IVEL IRKF IPHSE  ISHC
     1   0   1    1  0
CC
CC*****************************************************************
CC *
CC RESERVOIR PROPERTIES *
CC *
CC*****************************************************************
CC
CC
CC MAX. SIMULATION TIME ( PV)
*---- TMAX   NSTRTDATE
      4.6    20150101
CC
CC ROCK COMPRESSIBILITY (1/PSI), STAND. PRESSURE(PSIA)
*----COMPR PSTAND
     0.   14.7
CC
CC FLAGS INDICATING CONSTANT OR VARIABLE POROSITY, X,Y,AND Z
PERMEABILITY
*----IPOR1 IPERMX IPERMY IPERMZ IMOD ITRANZ INTG   IACTNUM ICUTOFF
     0    4        3    3     0  0     0      0       0
CC
CC CONSTANT POROSITY
*----PORC1
    .354
```

```
CC
CC Y DIRECTION PERMEABILITY IS DEPENDENT ON X DIRECTION PERMEABILITY
*---- CONSTANT PERMEABILITY MULTIPLIER FOR Y DIRECTION PERMEABILITY
   1
CC
CC Z DIRECTION PERMEABILITY IS DEPENDENT ON X DIRECTION PERMEABILITY
*---- CONSTANT PERMEABILITY MULTIPLIER FOR Z DIRECTION PERMEABILITY
   1
CC
CC FLAG FOR CONSTANT OR VARIABLE DEPTH, PRESSURE, WATER SATURATION
*----IDEPTH IPRESS ISWI ICWI   IPORINTERP
      0      0     0  -1     1
CC
CC CONSTANT DEPTH (FT)
*----D111
      0.
CC
CC INITIAL PRESSURE (PSIA)
*----PINIT DEPTH
    14.7   0.0
CC
CC CONSTANT INITIAL WATER SATURATION (residual oil)
*----SWI
    0.16
CC
CC CONSTANT CHLORIDE AND CALCIUM CONCENTRATIONS (MEQ/ML)
*----C50   C60
   0.054  0.0
CC
CC*****************************************************************
CC *
CC PHYSICAL PROPERTY DATA *
CC *
CC*****************************************************************
CC
CC 3.4.1 OIL CONC. AT PLAIT POINT FOR TYPE II(+)AND TYPE II(-), CMC
CC CMC
*---- c2plc c2prc epsme ihand
      0     1     0.002    0
CC
CC 3.4.2 flag indicating type of phase behavior parameters
*---- ifghbn=0 for input height of binodal curve; =1 for input sol. ratio
      0
```

```
    CC 3.4.3 SLOPE AND INTERCEPT OF BINODAL CURVE AT ZERO, OPT., AND 2XOPT
SALINITY
    CC FOR ALCOHOL 1
    *---- hbns70 hbnc70 hbns71 hbnc71 hbns72 hbnc72
          0    0.05    0     0.041   0     0.0472
    CC 3.4.5 SLOPE AND INTERCEPT OF BINODAL CURVE AT ZERO, OPT., AND 2XOPT
SALINITY
    CC FOR ALCOHOL 2
    *---- hbns80 hbnc80 hbns81 hbnc81 hbns82 hbnc82
         0       0.0     0     0.0    0     0.0
    CC
    CC 3.4.6 LOWER AND UPPER EFFECTIVE SALINITY FOR ALCOHOL 1 AND
ALCOHOL 2
    *---- csel7 cseu7 csel8 cseu8
         0.5    1.1   0     0
    CC 3.4.7 THE CSE SLOPE PARAMETER FOR CALCIUM AND ALCOHOL 1 AND
ALCOHOL 2
    CC Ca Alcohol#1 Alcohol#2
    *---- beta6 beta7 beta8
          0     0      0
    CC
    CC 3.4.8 FLAG FOR ALCOHOL PART. MODEL AND PARTITION COEFFICIENTS
    *---- ialc opsk7o opsk7s opsk8o opsk8s
          0    0      0       0     0
    CC these are used only for alcohol partitioning in a two alcohol system:
    CC 3.4.9 NO. OF ITERATIONS, AND TOLERANCE
    *---- nalmax epsalc
           20   0.0001
    CC 3.4.10 ALCOHOL 1 PARTITIONING PARAMETERS IF IALC=1
    CC aq-oleic aq-oleic surf-oleic
    *---- akwc7   akws7    akm7     ak7     pt7
         4.671    1.79     48      35.31   0.222
    CC
    CC 3.4.11 ALCOHOL 2 PARTITIONING PARAMETERS IF IALC=1
    *---- akwc8 akws8 akm8 ak8 pt8
         0      0     0    0   0
    CC
    CC 3.4.22 ift model flag
    *---- ift=0 for Healy&Reed; =1 for Chun Huh correl.
         1
    CC 3.4.24 INTERFACIAL TENSION PARAMETERS
    CC typ=.1-.35 typ=5-20
    *---- chuh ahuh
         0.3   10
    CC 3.4.25 LOG10 OF OIL/WATER INTERFACIAL TENSION
    CC units of log 10 dynes/cm = mN/m
```

```
*---- xiftw
      1.3
CC 3.4.26 ORGANIC MASS TRANSFER FLAG
CC imass=0 for no oil sol. in water. icorr=0 for constant MTC
*---- imass icor
      0     0
CC
CC
*----
      0      0
CC 3.4.31 CAPILLARY DESATURATION PARAMETERS FOR PHASE 1, 2, AND 3
CC AQ OLEIC ME
*---- itrap t11   t22  t33
      2    565   874 364.2
CC
CC 3.4.32 FLAG FOR RELATIVE PERMEABILITY AND CAPILLARY PRESSURE MODEL
*---- iperm=0 IRTYPE
      0       0
CC
CC 3.4.35 FLAG FOR CONSTANT OR VARIABLE REL. PERM. PARAMETERS
*---- isrw iprw iew
      0    0    0
CC
CC CONSTANT RES. SATURATION OF PHASES 1,2,AND 3 AT LOW CAPILLARY NO.
*----S1RWC S2RWC S3RWC
     .16   .26   .16
CC
CC CONSTANT ENDPOINT REL. PERM. OF PHASES 1,2,AND 3 AT LOW CAPILLARY NO.
*----P1RW P2RW P3RW
    .025  0.95 .025
CC
CC CONSTANT REL. PERM. EXPONENT OF PHASES 1,2,AND 3 AT LOW CAPILLARY NO.
*----E1W   E2W    E3W
    2.5    2.2     2.5
CC
CC RES. SATURATION OF PHASES 1,2,AND 3 AT HIGH CAPILLARY NO.
*----S1RC S2RC S3RC
     .0   .0   .0
CC
CC ENDPOINT REL. PERM. OF PHASES 1,2,AND 3 AT HIGH CAPILLARY NO.
*----P1RC P2RC P3RC
   1.0   1.0  1.0
CC
```

```
CC REL. PERM. EXPONENT OF PHASES 1,2,AND 3 AT HIGH CAPILLARY NO.
*----E13CW   E23C E31C
      1.0   1.0    1.0
CC 3.4.61 WATER AND OIL VISCOSITY , RESERVOIR TEMPERATURE
CC water oil =0 for isothermal modeling
*---- VIS1 VIS2 TSTAND
     1.0   100   0
CC
CC 3.4.80 COMPOSITIONAL PHASE VISCOSITY PARAMETERS for microemulsion
*----IMEVIS  ALPHAV1  ALPHAV2  ALPHAV3  ALPHAV4  ALPHAV5   ALPHAV6
ALPHAV7  ALPHAV8
      4    1.55    9.    0.      0.49    1.      0      1        20
CC
CC 3.4.81 PARAMETERS TO CALCULATE POLYMER VISCOSITY AT ZERO SHEAR
RATE
*----   AP1 AP2 AP3
       80 200 23000
CC
CC 3.4.82 PARAMETER TO COMPUTE CSEP,MIN. CSEP, AND SLOPE OF LOG VIS.
VS. LOG CSEP
*---- BETAP CSE1 SSLOPE
       1 0.01 -0.2
CC
CC 3.4.83 PARAMETER FOR SHEAR RATE DEPENDENCE OF POLYMER VISCOSITY
*---- GAMMAC GAMHF POWN IPMOD  ISHEAR  RWEFF   GAMHF2   IGAMC
       1.2    .3    1.6    0     0      0.25     0      0
CC
CC 3.4.84 FLAG FOR POLYMER PARTITIONING, PERM. REDUCTION PARAMETERS
*---- IPOLYM EPHI3 EPHI4 BRK  CRK  RKCUT
       1     1.    1.   100  0.05   1
CC 3.4.85 SPECIFIC WEIGHT FOR COMPONENTS 1,2,3,7,8 ,Coeffient of oil and
GRAVITY FLAG
CC if IDEN=1 ignore gravity effect; =2 then include gravity effect
*---- DEN1 DEN2 DEN23 DEN3 DEN7 DEN8 IDEN
     0.44 0.44 0.44 0.44 0.44   0    1
CC ISTB=0:BOTTOMHOLE CONDITION , 1: STOCK TANK
CC 3.4.93 FLAG FOR CHOICE OF UNITS when printing
*----- ISTB
       0
CC
CC 3.4.95 COMPRESSIBILITY FOR VOL. OCCUPYING COMPONENTS 1,2,3,7,AND 8
*---- COMPC(1) COMPC(2) COMPC(3) COMPC(7) COMPC(8)
       0.00000   0.0000    0      0        0
CC IOW=0 water wet, =1 oil wet, =2 mixed wet
CC 3.4.99 CONSTANT OR VARIABLE PC PARAM., WATER-WET OR OIL-WET PC
CURVE FLAG
```

```
*---- ICPC IEPC IOW
      0    0    0
CC
CC 3.4.100 CAPILLARY PRESSURE PARAMETER, CPC0
*---- CPC0
      0
CC
CC 3.4.103 CAPILLARY PRESSURE PARAMETER, EPC0
*---- EPC0
     2.0
CC
CC 3.4.117 MOLECULAR DIFFUSION COEF. KCTH COMPONENT IN PHASE 1
*---- D(KC,1),KC=1,N
 0 0 0 0 0 0 0 0 0 0 0 0
CC
CC 3.4.118 MOLECULAR DIFFUSION COEF. KCTH COMPONENT IN PHASE 2
*---- D(KC,2),KC=1,N
  0 0 0 0 0 0 0 0 0 0 0 0
CC
CC 3.4.119 MOLECULAR DIFFUSION COEF. KCTH COMPONENT IN PHASE 3
*---- D(KC,3),KC=1,N
  0 0 0 0 0 0 0 0 0 0 0 0
CC
CC 3.4.121 LONGITUDINAL AND TRANSVERSE DISPERSIVITY OF PHASE 1
*---- ALPHAL(1) ALPHAT(1)
     0.005   0.001
CC
CC 3.4.122 LONGITUDINAL AND TRANSVERSE DISPERSIVITY OF PHASE 2
*---- ALPHAL(2) ALPHAT(2)
     0.005    0.001
CC
CC 3.4.124 LONGITUDINAL AND TRANSVERSE DISPERSIVITY OF PHASE 3
*---- ALPHAL(3) ALPHAT(3)
      0.005    0.001
CC
CC 3.4.125 flag to specify organic adsorption calculation
*---- iadso=0 if organic adsorption is not considered
       0
CC
CC 3.4.130 SURFACTANT AND POLYMER ADSORPTION PARAMETERS
*---- AD31 AD32 B3D   AD41 AD42 B4D IADK IADS1 FADS REFK   IADSP IADSS
     1.   0.0 1000. 1.0  0.1  300   0    0     0     50    0     0
2 0 800
.4 0.5
0
 5 10  0  2  0  1
```

```
 5  1  4  6
 3  2  0  0  1
 0  0  0
 4
CARBON (AS CARBOBATES)          -2.00
SODIUM                           1.00
HYDROGEN (REACTIVE)              1.00
Oleic acid                      -1.00
chlorine (* ELEMNT *)           -1.00
 HYDROGEN ION
 SODIUM ION
 CARBONATE ION
 HAo
 WATER
 A-
 OH-
 HCO3-
 H2CO3
 HAw (* FLDSPS *)
 SORBED HYDROGEN ION
 SORBED SODIUM ION (* SORBSPS *)
 2
 0.  0.  1.  0.  0.  0.  0.  1.  1.  0.
 0.  1.  0.  0.  0.  0.  0.  0.  0.  0.
 1.  0.  0.  1.  2.  0.  1.  1.  2.  1.
 0.  0.  0.  1.  0.  1.  0.  0.  0.  1.
 0.  0.
 0.  1.
 1.  0.
 0.  0.
 1.0  0.0  0.0  0.0  0.0  0.0  0.0
 0.0  1.0  0.0  0.0  0.0  0.0  0.0
 0.0  0.0  1.0  0.0  0.0  0.0  0.0
 0.0  0.0  0.0  1.0  0.0  0.0  0.0
 0.0  0.0  0.0  0.0  1.0  0.0  0.0
-1.0  0.0  0.0  1.0  0.0  0.0  0.0
-1.0  0.0  0.0  0.0  0.0  0.0  0.0
 1.0  0.0  1.0  0.0  0.0  0.0  0.0
 2.0  0.0  1.0  0.0  0.0  0.0  0.0
 0.0  0.0  0.0  1.0  0.0  0.0  0.0
 0.0  0.0  0.0  0.0  0.0  1.0  0.0
 0.0  0.0  0.0  0.0  0.0  0.0  1.0
 1.0  1.0 -2.0  0.0  0.0 -1.0 -1.0 -1.0  0.0  0.0
 1.0  1.0
0.1000000000000E+01 0.1000000000000E+01 0.1000000000000E+01
0.1000000000000E+01 0.1000000000000E+01 0.5004112152846E-11
```

```
0.1000000000000E-13 0.2680000000000E+11 0.7030000000000E+17
0.5004112152846E-03
0.2700000000000E+07
-1.0  1.0  0.0  0.0  0.0  1.0 -1.0
 0.0
0.7999933060370E-03
0.5400000000000E-01 0.0000000000000E+00
0.2000000000000E-02
0.5500641497917E-01
0.1109993935850E+03
0.2091880952015E-04
0.1532738206478E-01
0.5789192104459E-08 0.5500641497917E-01 0.6308892128399E-05
0.7997908119048E-01 0.5545919827264E+02
0.1770249154077E-03 0.6229683906293E-03
0.9999916325462E+00 0.9939064067071E+00
0.1000000000000E-07 0.4000000000000E+03
CC
CC**********************************************************************
CC *
CC WELL DATA *
CC *
CC**********************************************************************
CC
CC
CC FLAG FOR PRESSURE CONST. BOUNDARIES
*---- IBOUND IZONE
      0     0
CC
CC TOTAL NUMBER OF WELLS, WELL RADIUS FLAG, FLAG FOR TIME OR COURANT NO.
*----NWELL IRO ITIME NWREL  IFLAGN ISOLVER
     2    2    1    2 0    0
CC
CC WELL ID,LOCATIONS,AND FLAG FOR SPECIFYING WELL TYPE, WELL RADIUS, SKIN
*----IDW IW JW IFLAG RW  SWELL IDIR IFIRST ILAST IPRF
     1  1  1  1 .001  0.   3   1     1  0
CC
CC WELL NAME
*---- WELNAM
  INJECTOR
CC
CC ICHEK MAX. AND MIN. ALLOWABLE BOTTOMHOLE PRESSURE AND RATE
*----ICHEK PWFMIN PWFMAX QTMIN QTMAX
      0   0.0     5000. 0.0 50000.
```

```
CC
CC WELL ID, LOCATION, AND FLAG FOR SPECIFYING WELL TYPE, WELL RADIUS, SKIN
*----IDW IW JW IFLAG RW    SWELL IDIR IFIRST ILAST IPRF
     2  50 50  2   .001   0.    3    1      1     0
CC
CC WELL NAME
*---- WELNAM
   PRODUCER
CC
CC MAX. AND MIN. ALLOWABLE BOTTOMHOLE PRESSURE AND RATE
*----ICHEK PWFMIN PWFMAX QTMIN QTMAX
     0      0.0    5000. 0.0 50000.
CC
CC ID,INJ. RATE AND INJ. COMP. FOR RATE CONS. WELLS FOR EACH PHASE (L=1,3)
*----ID QI(M,L) C(M,KC,L)
1 0.0254 1.0 0. 0. 0. 0.054 0. 0. 0. 0.0001 0.05401 110.996 1e-7
1 0. 0. 0. 0. 0. 0. 0. 0. 0. 0. 0. 0. 0.
1 0. 0. 0. 0. 0. 0. 0. 0. 0. 0. 0. 0. 0.
CC
CC ID,
*----ID PWF
  2 14.7
CC
CC CUM. INJ. TIME , AND INTERVALS (PV OR DAY) FOR WRITING TO OUTPUT FILES
*----TINJ CUMPR1 CUMHI1 WRHPV WRPRF RSTC
    1.04 0.03   0.03   0.03  0.03   1.04
CC
CC FOR IMES=2 ,THE INI. TIME STEP,CONC. TOLERANCE,MAX.,MIN. COURANT NO.
*---- DT   DCLIM  CNMAX  CNMIN
  0.000001  12*0.05 0.7 0.01
CC
CC
*---- IBMOD
0
CC
CC IRO, ITIME, NEW FLAGS FOR ALL THE WELLS
*---- IRO ITIME IFLAG
     2    1     1   2
CC
CC NUMBER OF WELLS CHANGES IN LOCATION OR SKIN OR PWF
*---- NWEL1
     0
```

```
CC
CC NUMBER OF WELLS WITH RATE CHANGES, ID
*---- NWEL2 ID
      1    1
CC
CC ID,INJ. RATE AND INJ. COMP. FOR RATE CONS. WELLS FOR EACH PHASE (L=1,3)
*---- ID QI(M,L) water oil surf polymer Chlor divalent
1 0.0254 0.98 0.0 0.01 0.18 .054 0. 0.01 0. 0.61 0.62 110.996 1e-7
1 0. 0. 0. 0. 0. 0. 0. 0. 0. 0. 0. 0. 0.
1 0. 0. 0. 0. 0. 0. 0. 0. 0. 0. 0. 0. 0.
CC
CC CUM. INJ. TIME , AND INTERVALS (PV) FOR WRITING TO OUTPUT FILES
*---- TINJ CUMPR1 CUMHI1 WRHPV WRPRF RSTC
      1.67    0.03   0.03  0.03  0.03  1.67
CC
CC FOR IMES=4 ,THE INI. TIME STEP,CONC. TOLERANCE,MAX.,MIN. TIME STEPS
*---- DT   DCLIM   CNMAX CNMIN
  0.000001 12*0.05  0.7  0.05
CC
CC
*---- IBMOD
    0
CC
CC IRO, ITIME, NEW FLAGS FOR ALL THE WELLS
*---- IRO ITIME IFLAG
      2    1     1    2
CC
CC NUMBER OF WELLS CHANGES IN LOCATION OR SKIN OR PWF
*---- NWEL1
     0
CC
CC NUMBER OF WELLS WITH RATE CHANGES, ID
*---- NWEL2 ID
      1     1
CC
CC ID,INJ. RATE AND INJ. COMP. FOR RATE CONS. WELLS FOR EACH PHASE (L=1,3)
*---- ID QI(M,L) water oil surf polymer Chlor divalent
1 0.0254 1. 0.0 0.0  0.18 .054 0. 0.0 0. 0.43 0.46 110.996 1e-7
1 0. 0. 0. 0. 0. 0. 0. 0. 0. 0. 0. 0. 0.
1 0. 0. 0. 0. 0. 0. 0. 0. 0. 0. 0. 0. 0.
CC
CC CUM. INJ. TIME , AND INTERVALS (PV) FOR WRITING TO OUTPUT FILES
*---- TINJ CUMPR1 CUMHI1 WRHPV WRPRF RSTC
      2.63    0.03   0.03  0.03  0.03  2.63
```

```
CC
CC FOR IMES=4 ,THE INI. TIME STEP,CONC. TOLERANCE,MAX.,MIN. TIME STEPS
*---- DT      DCLIM CNMAX CNMIN
   0.000001 12*0.05 0.7 0.05
CC
CC
*---- IBMOD
     0
CC
CC IRO, ITIME, NEW FLAGS FOR ALL THE WELLS
*---- IRO ITIME IFLAG
      2    1     1   2
CC
CC NUMBER OF WELLS CHANGES IN LOCATION OR SKIN OR PWF
*---- NWEL1
0
CC
CC NUMBER OF WELLS WITH RATE CHANGES, ID
*---- NWEL2 ID
1 1
CC
CC ID,INJ. RATE AND INJ. COMP. FOR RATE CONS. WELLS FOR EACH PHASE (L=1,3)
*---- ID QI(M,L) water oil surf polymer Chlor divalent
1 0.0254 1. 0.0 0.0  0. .054 0. 0.0 0. 0.0001 0.0541 110.996 1e-7
1 0. 0. 0. 0. 0. 0. 0. 0. 0. 0. 0. 0. 0.
1 0. 0. 0. 0. 0. 0. 0. 0. 0. 0. 0. 0. 0.
CC
CC CUM. INJ. TIME , AND INTERVALS (PV) FOR WRITING TO OUTPUT FILES
*---- TINJ CUMPR1 CUMHI1 WRHPV WRPRF RSTC
      4.6    0.03   0.03  0.03  0.03  100000
CC
CC FOR IMES=4 ,THE INI. TIME STEP,CONC. TOLERANCE,MAX.,MIN. TIME STEPS
*---- DT    DCLIM  CNMAX  CNMIN
     0.000001 12*0.05 3 0.05
```

A.2 Unstable ACP Simulation of 100 cp Oil in a Quarter 5-spost Sandpack

The simulation of quarter 5-spot sandpack ACP flood at Oil/ACP viscosity ratio of 2 after 1 pore volume waterflood is presented below. The fine grid simulation was conducted using UTCHEM.

```
CC*************************************************************
```

```
CC *
CC BRIEF DESCRIPTION OF DATA SET : UTCHEM (VERSION 2016)*
CC *
CC*********************************************************************
CC *
CC History match of ACP quarter 5-spot flood *
CC *
CC LENGTH (FT) : PROCESS : A/S/P FLOODING *
CC THICKNESS (FT) : INJ. PRESSURE (PSI) : *
CC WIDTH (FT) : COORDINATES : CARTESIAN *
CC POROSITY : *
CC GRID BLOCKS : 50X50X5 *
CC DATE : *
CC *
CC*********************************************************************
CC
CC*********************************************************************
CC *
CC RESERVOIR DESCRIPTION *
CC *
CC*********************************************************************
CC
CC
*----RUNNO
R03-20
CC
CC
*----HEADER
ACP 5-spot sandpack
Experiment
************************************************************
CC
CC SIMULATION FLAGS
*---- IMODE IMES IDISPC ICWM ICAP IREACT IBIO ICOORD ITREAC ITC IGAS IENG
ILGR IBLACK
      1   7   0     0   0    3   0    1      0    0  0   0   0    0
CC
CC NUMBER OF GRID BLOCKS AND FLAG SPECIFIES CONSTANT OR VARIABLE
GRID SIZE
*----NX   NY    NZ IDXYZ IUNIT  N_WELLMAX
   50   50    5   0    0     2
CC
CC CONSTANT GRID BLOCK SIZE IN X, Y, AND Z
*----DX    DY      DZ
  0.016664 0.016664 0.0168
CC
```

```
CC TOTAL NO. OF COMPONENTS, NO. OF TRACERS, NO. OF GEL COMPONENTS
*----N no NTw nta ngc ng noth
   12 0 0  0  4  0  0
CC
CC
*---- SPNAME(I),I=1,N
WATER
OIL
SURFACTANT
POLYMER
ANION
CALCIUM
alc1
alc2
CARBONATE
SODIUM
HYDROGEN
pet acid
CC
CC FLAG INDICATING IF THE COMPONENT IS INCLUDED IN CALCULATIONS OR
NOT
*----ICF(KC) FOR KC=1,N
    1 1 1 1 1 0  1 0 1 1 1  1
CC
CC*********************************************************************
CC *
CC OUTPUT OPTIONS *
CC *
CC*********************************************************************
CC
CC
CC FLAG FOR PV OR DAYS FOR OUTPUT AND STOP THE RUN
*----ICUMTM ISTOP IOUTGMS
     1    1    0      0
CC
CC FLAG INDICATING IF THE PROFILE OF KCTH COMPONENT SHOULD BE
WRITTEN
*----IPRFLG(KC),KC=1,N
    1  1   1   1  1  0  0  0  1  1  1   1
CC
CC FLAG FOR PRES,SAT.,TOTAL CONC.,TRACER CONC.,CAP.,GEL, ALKALINE
PROFILES
*----IPPRES IPSAT IPCTOT IPBIO IPCAP IPGEL IPALK ITEMP IPOBS  IPATERN
    1    1    1      0    0     0    1  0     0    0
CC
CC FLAG FOR WRITING SEVERAL PROPERTIES
```

```
*----ICKL IVIS IPER ICNM ICSE IFOAM IHYST INONEQ
     1    1   1  1    1    0    0    0
CC
CC FLAG FOR WRITING SEVERAL PROPERTIES TO PROF
*----IADS IVEL IRKF IPHSE  ISHC
     1   0   1    1  0
CC
CC*****************************************************************
CC *
CC RESERVOIR PROPERTIES *
CC *
CC*****************************************************************
CC
CC
CC MAX. SIMULATION TIME ( PV)
*---- TMAX   NSTRTDATE
     3    20150101
CC
CC ROCK COMPRESSIBILITY (1/PSI), STAND. PRESSURE(PSIA)
*----COMPR PSTAND
     0.   14.7
CC
CC  FLAGS  INDICATING  CONSTANT  OR  VARIABLE  POROSITY,  X,Y,AND  Z
PERMEABILITY
*----IPOR1 IPERMX IPERMY IPERMZ IMOD ITRANZ INTG   IACTNUM ICUTOFF
     0    4       3    3     0  0     0      0      0
CC
CC CONSTANT POROSITY
*----PORC1
    .354
CC
CC  Y  DIRECTION  PERMEABILITY  IS  DEPENDENT  ON  X  DIRECTION
PERMEABILITY
*---- CONSTANT PERMEABILITY MULTIPLIER FOR Y DIRECTION PERMEABILITY
    1
CC
CC  Z  DIRECTION  PERMEABILITY  IS  DEPENDENT  ON  X  DIRECTION
PERMEABILITY
*---- CONSTANT PERMEABILITY MULTIPLIER FOR Z DIRECTION PERMEABILITY
    1
CC
CC  FLAG  FOR  CONSTANT  OR  VARIABLE  DEPTH,  PRESSURE,  WATER
SATURATION
*----IDEPTH IPRESS ISWI ICWI   IPORINTERP
     0      0     0  -1     1
CC
```

```
CC CONSTANT DEPTH (FT)
*----D111
      0.
CC
CC INITIAL PRESSURE (PSIA)
*----PINIT DEPTH
    14.7   0.0
CC
CC CONSTANT INITIAL WATER SATURATION (residual oil)
*----SWI
    0.06
CC
CC CONSTANT CHLORIDE AND CALCIUM CONCENTRATIONS (MEQ/ML)
*----C50   C60
   0.684  0.0
CC
CC*************************************************************************
CC *
CC PHYSICAL PROPERTY DATA *
CC *
CC*************************************************************************
CC
CC 3.4.1 OIL CONC. AT PLAIT POINT FOR TYPE II(+)AND TYPE II(-), CMC
CC CMC
*---- c2plc  c2prc   epsme   ihand
      0     1     0.0024    0
CC
CC 3.4.2 flag indicating type of phase behavior parameters
*---- ifghbn=0 for input height of binodal curve; =1 for input sol. ratio
      0
CC 3.4.3 SLOPE AND INTERCEPT OF BINODAL CURVE AT ZERO, OPT., AND 2XOPT
SALINITY
CC FOR ALCOHOL 1
*---- hbns70 hbnc70 hbns71 hbnc71 hbns72 hbnc72
       0    0.035    0     0.025   0     0.035
CC 3.4.5 SLOPE AND INTERCEPT OF BINODAL CURVE AT ZERO, OPT., AND 2XOPT
SALINITY
CC FOR ALCOHOL 2
*---- hbns80 hbnc80 hbns81 hbnc81 hbns82 hbnc82
      0      0.0     0     0.0    0     0.0
CC
CC 3.4.6 LOWER AND UPPER EFFECTIVE SALINITY FOR ALCOHOL 1 AND
ALCOHOL 2
*---- csel7 cseu7 csel8 cseu8
      0.5    0.8   0     0
```

```
CC 3.4.7 THE CSE SLOPE PARAMETER FOR CALCIUM AND ALCOHOL 1 AND ALCOHOL 2
CC Ca Alcohol#1 Alcohol#2
*---- beta6 beta7 beta8
      0     0      0
CC
CC 3.4.8 FLAG FOR ALCOHOL PART. MODEL AND PARTITION COEFFICIENTS
*---- ialc opsk7o opsk7s opsk8o opsk8s
      0    0      0       0     0
CC these are used only for alcohol partitioning in a two alcohol system:
CC 3.4.9 NO. OF ITERATIONS, AND TOLERANCE
*---- nalmax epsalc
       20   0.0001
CC 3.4.10 ALCOHOL 1 PARTITIONING PARAMETERS IF IALC=1
CC aq-oleic aq-oleic surf-oleic
*---- akwc7   akws7    akm7     ak7     pt7
     4.671    1.79     48      35.31   0.222
CC
CC 3.4.11 ALCOHOL 2 PARTITIONING PARAMETERS IF IALC=1
*---- akwc8 akws8 akm8 ak8 pt8
      0      0     0    0   0
CC
CC 3.4.22 ift model flag
*---- ift=0 for Healy&Reed; =1 for Chun Huh correl.
      1
CC 3.4.24 INTERFACIAL TENSION PARAMETERS
CC typ=.1-.35 typ=5-20
*---- chuh ahuh
     0.3   10
CC 3.4.25 LOG10 OF OIL/WATER INTERFACIAL TENSION
CC units of log 10 dynes/cm = mN/m
*---- xiftw
      1.3
CC 3.4.26 ORGANIC MASS TRANSFER FLAG
CC imass=0 for no oil sol. in water. icorr=0 for constant MTC
*---- imass icor
       0     0
CC
CC
*----  iwalt  iwalf  ivfm
       0      0      0
CC 3.4.31 CAPILLARY DESATURATION PARAMETERS FOR PHASE 1, 2, AND 3
CC          AQ   OLEIC   ME
*---- itrap  t11     t22    t33
       2    1000    2000    800
CC
```

```
   CC 3.4.32 FLAG FOR RELATIVE PERMEABILITY AND CAPILLARY PRESSURE
MODEL
   *---- iperm=0 IRTYPE
         0       0
   CC
   CC 3.4.35 FLAG FOR CONSTANT OR VARIABLE REL. PERM. PARAMETERS
   *---- isrw iprw iew
         0   0   0
   CC
   CC CONSTANT RES. SATURATION OF PHASES 1,2,AND 3 AT LOW CAPILLARY NO.
   *----S1RWC S2RWC S3RWC
        .06  .36  .06
   CC
   CC CONSTANT ENDPOINT REL. PERM. OF PHASES 1,2,AND 3 AT LOW CAPILLARY
NO.
   *----P1RW   P2RW   P3RW
       .16    0.5   0.5
   CC
   CC CONSTANT REL. PERM. EXPONENT OF PHASES 1,2,AND 3 AT LOW
CAPILLARY NO.
   *----E1W    E2W    E3W
      2.2    2.2   2.2
   CC
   CC RES. SATURATION OF PHASES 1,2,AND 3 AT HIGH CAPILLARY NO.
   *----S1RC S2RC S3RC
        .0   .0   .0
   CC
   CC ENDPOINT REL. PERM. OF PHASES 1,2,AND 3 AT HIGH CAPILLARY NO.
   *----P1RC P2RC P3RC
     1.0   1.5  1.5
   CC
   CC REL. PERM. EXPONENT OF PHASES 1,2,AND 3 AT HIGH CAPILLARY NO.
   *----E13CW   E23C E31C
         1.0   1.0    1.0
   cc
   CC 3.4.61 WATER AND OIL VISCOSITY , RESERVOIR TEMPERATURE
   CC water oil =0 for isothermal modeling
   *---- VIS1 VIS2 TSTAND
         0.9  320   0
   CC
   CC 3.4.80 COMPOSITIONAL PHASE VISCOSITY PARAMETERS for microemulsion
   *----IMEVIS  ALPHAV1  ALPHAV2  ALPHAV3  ALPHAV4  ALPHAV5   ALPHAV6
ALPHAV7  ALPHAV8
         3     1.5     9.     0.      0.49     2.       0       1.5        10
   CC
```

```
    CC 3.4.81 PARAMETERS TO CALCULATE POLYMER VISCOSITY AT ZERO SHEAR
RATE
    *----   AP1   AP2 AP3
          60   100  2500
    CC
    CC 3.4.82 PARAMETER TO COMPUTE CSEP,MIN. CSEP, AND SLOPE OF LOG VIS.
VS. LOG CSEP
    *---- BETAP  CSE1  SSLOPE
          0    0.64  -0.53
    CC
    CC 3.4.83 PARAMETER FOR SHEAR RATE DEPENDENCE OF POLYMER VISCOSITY
    *---- GAMMAC GAMHF POWN IPMOD  ISHEAR  RWEFF   GAMHF2    IGAMC
          1    10    1.5     0     2      0.25      0       0
    CC
    CC 3.4.84 FLAG FOR POLYMER PARTITIONING, PERM. REDUCTION PARAMETERS
    *---- IPOLYM EPHI3  EPHI4  BRK    CRK    RKCUT
           1     1.    1.    100     0.05   1
    CC 3.4.85 SPECIFIC WEIGHT FOR COMPONENTS 1,2,3,7,8 ,Coeffient of oil and
GRAVITY FLAG
    CC if IDEN=1 ignore gravity effect; =2 then include gravity effect
    *---- DEN1   DEN2 DEN23 DEN3  DEN7 DEN8 IDEN
         0.44   0.4  0.42  0.44  0.44   0    2
    CC ISTB=0:BOTTOMHOLE CONDITION , 1: STOCK TANK
    CC 3.4.93 FLAG FOR CHOICE OF UNITS when printing
    *----- ISTB
          0
    CC
    CC 3.4.95 COMPRESSIBILITY FOR VOL. OCCUPYING COMPONENTS 1,2,3,7,AND 8
    *---- COMPC(1) COMPC(2) COMPC(3) COMPC(7) COMPC(8)
          0.00000   0.0000    0      0        0
    CC IOW=0 water wet, =1 oil wet, =2 mixed wet
    CC 3.4.99 CONSTANT OR VARIABLE PC PARAM., WATER-WET OR OIL-WET PC
CURVE FLAG
    *---- ICPC IEPC IOW
          0    0    0
    CC
    CC 3.4.100 CAPILLARY PRESSURE PARAMETER, CPC0
    *---- CPC0
          0
    CC
    CC 3.4.103 CAPILLARY PRESSURE PARAMETER, EPC0
    *---- EPC0
         2.0
    CC
    CC 3.4.117 MOLECULAR DIFFUSION COEF. KCTH COMPONENT IN PHASE 1
    *---- D(KC,1),KC=1,N
```

```
  0 0 0 0 0 0 0 0 0 0 0 0
CC
CC 3.4.118 MOLECULAR DIFFUSION COEF. KCTH COMPONENT IN PHASE 2
*---- D(KC,2),KC=1,N
  0 0 0 0 0 0 0 0 0 0 0 0
CC
CC 3.4.119 MOLECULAR DIFFUSION COEF. KCTH COMPONENT IN PHASE 3
*---- D(KC,3),KC=1,N
  0 0 0 0 0 0 0 0 0 0 0 0
CC
CC 3.4.121 LONGITUDINAL AND TRANSVERSE DISPERSIVITY OF PHASE 1
*---- ALPHAL(1) ALPHAT(1)
      0.00   0.00
CC
CC 3.4.122 LONGITUDINAL AND TRANSVERSE DISPERSIVITY OF PHASE 2
*---- ALPHAL(2) ALPHAT(2)
      0.00    0.00
CC
CC 3.4.124 LONGITUDINAL AND TRANSVERSE DISPERSIVITY OF PHASE 3
*---- ALPHAL(3) ALPHAT(3)
       0.00    0.00
CC
CC 3.4.125 flag to specify organic adsorption calculation
*---- iadso=0 if organic adsorption is not considered
        0
CC
CC 3.4.130 SURFACTANT AND POLYMER ADSORPTION PARAMETERS
*---- AD31 AD32 B3D   AD41 AD42 B4D IADK IADS1 FADS REFK   IADSP IADSS
      1.   0.0 1000. 2     2   100   0    0     0   4000    0     0
  2 0 800  0
 .14 0.7
0
 5 10  0  2  0  1
 5  1  4  6
 3  2  0  0  1
 0  0  0
 4
CARBON (AS CARBOBATES)           -2.00
SODIUM                            1.00
HYDROGEN (REACTIVE)               1.00
Oleic acid                       -1.00
chlorine (* ELEMNT *)            -1.00
 HYDROGEN ION
 SODIUM ION
 CARBONATE ION
 HAo
```

WATER
A-
OH-
HCO3-
H2CO3
HAw (* FLDSPS *)
SORBED HYDROGEN ION
SORBED SODIUM ION (* SORBSPS *)
2
0. 0. 1. 0. 0. 0. 0. 1. 1. 0.
0. 1. 0. 0. 0. 0. 0. 0. 0. 0.
1. 0. 0. 1. 2. 0. 1. 1. 2. 1.
0. 0. 0. 1. 0. 1. 0. 0. 0. 1.
0. 0.
0. 1.
1. 0.
0. 0.
1.0 0.0 0.0 0.0 0.0 0.0 0.0
0.0 1.0 0.0 0.0 0.0 0.0 0.0
0.0 0.0 1.0 0.0 0.0 0.0 0.0
0.0 0.0 0.0 1.0 0.0 0.0 0.0
0.0 0.0 0.0 0.0 1.0 0.0 0.0
-1.0 0.0 0.0 1.0 0.0 0.0 0.0
-1.0 0.0 0.0 0.0 0.0 0.0 0.0
1.0 0.0 1.0 0.0 0.0 0.0 0.0
2.0 0.0 1.0 0.0 0.0 0.0 0.0
0.0 0.0 0.0 1.0 0.0 0.0 0.0
0.0 0.0 0.0 0.0 0.0 1.0 0.0
0.0 0.0 0.0 0.0 0.0 0.0 1.0
1.0 1.0 -2.0 0.0 0.0 -1.0 -1.0 -1.0 0.0 0.0
1.0 1.0
0.1000000000000E+01 0.1000000000000E+01 0.1000000000000E+01
0.1000000000000E+01 0.1000000000000E+01 0.5004112152846E-11
0.1000000000000E-13 0.2680000000000E+11 0.7030000000000E+17
0.5004112152846E-03
0.2700000000000E+07
-1.0 1.0 0.0 0.0 0.0 1.0 -1.0
0.0
0.7999933060370E-03
0.68 0.0000000000000E+00
0.2000000000000E-02
0.68
0.1109993935850E+03
0.2091880952015E-04
0.43E-01
0.5789192104459E-08 0.68 0.6308892128399E-05

```
0.645 0.5545919827264E+02
0.1770249154077E-03 0.6229683906293E-03
0.9999916325462E+00 0.9939064067071E+00
0.1000000000000E-07 0.4000000000000E+03
CC
CC*****************************************************************
CC *
CC WELL DATA *
CC *
CC*****************************************************************
CC
CC
CC FLAG FOR PRESSURE CONST. BOUNDARIES
*---- IBOUND IZONE
      0     0
CC
CC TOTAL NUMBER OF WELLS, WELL RADIUS FLAG, FLAG FOR TIME OR COURANT NO.
*----NWELL IRO ITIME NWREL  IFLAGN ISOLVER
     2    2    1    2 0    0
CC
CC WELL ID,LOCATIONS,AND FLAG FOR SPECIFYING WELL TYPE, WELL RADIUS, SKIN
*----IDW IW JW IFLAG RW  SWELL IDIR IFIRST ILAST IPRF
     1  1  1  1 .001  0.   3   1     5   1
cc PERf
     0 0 1 0 0
cc
CC
CC WELL NAME
*---- WELNAM
  INJECTOR
CC
CC ICHEK MAX. AND MIN. ALLOWABLE BOTTOMHOLE PRESSURE AND RATE
*----ICHEK PWFMIN PWFMAX QTMIN QTMAX
      0   0.0     5000. 0.0 50000.
CC
CC WELL ID, LOCATION, AND FLAG FOR SPECIFYING WELL TYPE, WELL RADIUS, SKIN
*----IDW   IW   JW IFLAG  RW    SWELL IDIR IFIRST ILAST IPRF
      2   50  50   2   .001  0.   3   1     5    1
CC
cc PERf
     0 0 1 0 0
cc
CC WELL NAME
```

```
*---- WELNAM
   PRODUCER
CC
CC MAX. AND MIN. ALLOWABLE BOTTOMHOLE PRESSURE AND RATE
*----ICHEK PWFMIN PWFMAX QTMIN QTMAX
     0      0.0    5000. 0.0 50000.
CC
CC ID,INJ. RATE AND INJ. COMP. FOR RATE CONS. WELLS FOR EACH PHASE (L=1,3)
*----ID QI(M,L) C(M,KC,L)
1   0.0254  1.0   0.  0.   0.   0.68  1.e-8 0. 0. 0.0001 0.68   110.996 1e-7
1   0.      0.    0.  0.   0.   0.    0. 0. 0. 0.      0.       0.     0.
1   0.      0.    0.  0.   0.   0.    0. 0. 0. 0.      0.       0.     0.
CC
CC ID,
*----ID PWF
     2 14.7
CC
CC CUM. INJ. TIME , AND INTERVALS (PV OR DAY) FOR WRITING TO OUTPUT FILES
*----TINJ   CUMPR1 CUMHI1 WRHPV WRPRF RSTC
    1.0    0.05   0.05   0.05  0.05   1.0
CC
CC FOR IMES=2 ,THE INI. TIME STEP,CONC. TOLERANCE,MAX.,MIN. COURANT NO.
*---- DT      DCLIM   CNMAX  CNMIN
  0.000001  12*0.05   0.2   0.01
CC
CC
*---- IBMOD
0
CC
CC IRO, ITIME, NEW FLAGS FOR ALL THE WELLS
*---- IRO ITIME IFLAG
     2    1     1   2
CC
CC NUMBER OF WELLS CHANGES IN LOCATION OR SKIN OR PWF
*---- NWEL1
     0
CC
CC NUMBER OF WELLS WITH RATE CHANGES, ID
*---- NWEL2 ID
      1    1
CC
CC ID,INJ. RATE AND INJ. COMP. FOR RATE CONS. WELLS FOR EACH PHASE (L=1,3)
```

```
*---- ID QI(M,L) water oil surf polymer Chlor divalent alc1 alc2 CO3    Na   H      A0
1   0.0254  1  0.0  0.00  0.295  .085  1.e-8   0.0  0.        0.566 0.651  110.996 1e-7
1   0.      0. 0. 0. 0. 0. 0. 0. 0. 0. 0. 0. 0.
1   0.      0. 0. 0. 0. 0. 0. 0. 0. 0. 0. 0. 0.
CC
CC CUM. INJ. TIME , AND INTERVALS (PV) FOR WRITING TO OUTPUT FILES
*---- TINJ CUMPR1 CUMHI1 WRHPV WRPRF RSTC
    1.5    0.02   0.02  0.02  0.02  1.5
CC
CC FOR IMES=4 ,THE INI. TIME STEP,CONC. TOLERANCE,MAX.,MIN. TIME STEPS
*---- DT   DCLIM   CNMAX CNMIN
  0.000001 12*0.05  0.2  0.02
CC
CC
*---- IBMOD
   0
CC
CC IRO, ITIME, NEW FLAGS FOR ALL THE WELLS
*---- IRO ITIME IFLAG
      2    1     1    2
CC
CC NUMBER OF WELLS CHANGES IN LOCATION OR SKIN OR PWF
*---- NWEL1
     0
CC
CC NUMBER OF WELLS WITH RATE CHANGES, ID
*---- NWEL2 ID
      1     1
CC
CC ID,INJ. RATE AND INJ. COMP. FOR RATE CONS. WELLS FOR EACH PHASE
(L=1,3)
*---- ID QI(M,L) water oil surf polymer Chlor divalent  alc1  alc2 CO3     Na   H      Ao
1    0.0254       1.    0.0 0.0  0.27   .01     1.e-8     0.0   0.   0.377 0.377 110.996 1e-7
1    0. 0. 0. 0. 0. 0. 0. 0. 0. 0. 0. 0. 0.
1    0. 0. 0. 0. 0. 0. 0. 0. 0. 0. 0. 0. 0.
CC
CC CUM. INJ. TIME , AND INTERVALS (PV) FOR WRITING TO OUTPUT FILES
*---- TINJ CUMPR1 CUMHI1 WRHPV WRPRF RSTC
      2.5    0.02   0.02  0.02  0.02  2.5
CC
CC FOR IMES=4 ,THE INI. TIME STEP,CONC. TOLERANCE,MAX.,MIN. TIME STEPS
*---- DT      DCLIM CNMAX CNMIN
   0.000001 12*0.05 0.2 0.05
CC
CC
*---- IBMOD
```

```
      0
    CC
    CC IRO, ITIME, NEW FLAGS FOR ALL THE WELLS
    *---- IRO ITIME IFLAG
         2   1    1   2
    CC
    CC NUMBER OF WELLS CHANGES IN LOCATION OR SKIN OR PWF
    *---- NWEL1
    0
    CC
    CC NUMBER OF WELLS WITH RATE CHANGES, ID
    *---- NWEL2 ID
    1 1
    CC
    CC ID,INJ. RATE AND INJ. COMP. FOR RATE CONS. WELLS FOR EACH PHASE
(L=1,3)
    *---- ID QI(M,L) water oil surf polymer Chlor divalent
    1   0.0254          1.0   0.  0.   0.   0.68  0. 0. 0. 0.0001 0.68   110.996 1e-7
    1    0. 0. 0. 0. 0. 0. 0. 0. 0. 0. 0. 0. 0.
    1    0. 0. 0. 0. 0. 0. 0. 0. 0. 0. 0. 0. 0.
    CC
    CC CUM. INJ. TIME , AND INTERVALS (PV) FOR WRITING TO OUTPUT FILES
    *---- TINJ CUMPR1 CUMHI1 WRHPV WRPRF RSTC
         4.6    0.05   0.05  0.05  0.05  5
    CC
    CC FOR IMES=4 ,THE INI. TIME STEP,CONC. TOLERANCE,MAX.,MIN. TIME STEPS
    *---- DT    DCLIM      CNMAX  CNMIN
        0.000001 12*0.05  0.2 0.05
```

REFERENCES

Adkins, S., Liyanage, P., Pinnawala Arachchilage, G. W. P., Mudiyanselage, T., Weerasooriya, U., & Pope, G. (2010). A New Process for Manufacturing and Stabilizing High-Performance EOR Surfactants at Low Cost for High-Temperature, High-Salinity Oil Reservoirs. *Proceedings of SPE Improved Oil Recovery Symposium*. https://doi.org/10.2118/129923-MS

Adkins, S., Pinnawala Arachchilage, G. W. P., Solairaj, S., Lu, J., Weerasooriya, U., & Pope, G. A. (2012). Development of Thermally and Chemically Stable Large-Hydrophobe Alkoxy Carboxylate Surfactants. In *SPE Improved Oil Recovery Symposium*. Society of Petroleum Engineers. https://doi.org/10.2118/154256-MS

Bansal, V. K., & Shah, D. O. 1977. Microemulsions: Theory and Practice. New York, New York: Academic Press.

Bentsen, R. G., & Saeedi, J. (1981). Liquid-liquid Immiscible Displacement In Unconsolidated Porous Media. *Journal of Canadian Petroleum Technology*, *20*(1). https://doi.org/10.2118/81-01-04

Bourrel, M., Schechter, R.S., 1988. Microemulsions and related system, formulation, solvency, and physical properties. Marcel Dekker, Inc.

Brigham, W. E., & Smith, D. H. (1965). Prediction Of Tracer Behavior In Five-Spot Flow. In *Conference on Production Research and Engineering*. Society of Petroleum Engineers. https://doi.org/10.2118/1130-MS

Brownell, L.E. and Katz, D.L.: ‘‘Flow of Fluids Through Porous Media—Part II,’’ Chem. Eng. Prog. ~1947! 43, No. 11, 601

Bryan, J. L., & Kantzas, A. (2007). Enhanced Heavy-Oil Recovery by Alkali-Surfactant Flooding. In *SPE Annual Technical Conference and Exhibition*. Society of Petroleum Engineers. https://doi.org/10.2118/110738-MS

Buchgraber, M., Clemens, T., Castanier, L. M., & Kovscek, A. (2011). A Microvisual Study of the Displacement of Viscous Oil by Polymer Solutions. *SPE Reservoir Evaluation & Engineering*, *14*(3), 269–280. https://doi.org/10.2118/122400-PA

Carlisle, C., Al-Maraghi, E., Al-Saad, B., Britton, C., Fortenberry, R., & Pope, G. (2014). One-Spot Pilot Results in the Sabriyah-Mauddud Carbonate Formation in Kuwait Using a Novel Surfactant Formulation. In SPE Improved Oil Recovery Symposium. Society of Petroleum Engineers. https://doi.org/10.2118/169153-MS

Chuoke, R.L., van Meurs, P., and van der Poel, C. ―The Instability of Slow, Immiscible, Viscous Liquid-Liquid Displacments in Permeable Media,‖ Aime 216, 1959.

De Haan, J. (1959, January 1). 25. Effect of Capillary Forces in the Water-Drive Process. World Petroleum Congress.

Delamaide, E., Zaitoun, A., Renard, G., & Tabary, R. (2014). Pelican lake field: first successful application of polymer flooding in a heavy-oil reservoir. *SPE Reservoir Evaluation & Engineering*, *17*(3), 340–354. https://doi.org/10.2118/165234-PA

Delshad, M., Bhuyan, D., Pope, G. A., & Lake, L. W. (1986). Effect of Capillary Number on the Residual Saturation of a Three-Phase Micellar Solution. In *SPE Enhanced Oil Recovery Symposium*. Society of Petroleum Engineers. https://doi.org/10.2118/14911-MS

Delshad, M., Pope, G. A., & Sepehrnoori, K. (1996). A compositional simulator for modeling surfactant enhanced aquifer remediation, 1 formulation. Journal of Contaminant Hydrology, 23(4), 303–327. https://doi.org/10.1016/0169-7722(95)00106-9

Dombrowski, H. S., & Brownell, L. E. (1954). Residual Equilibrium Saturation of Porous Media. *Industrial & Engineering Chemistry*, *46*(6), 1207–1219. https://doi.org/10.1021/ie50534a037

Doorwar, S., & Mohanty, K. K. (2015). Fingering Function for Unstable Immiscible Flows. In *SPE Reservoir Simulation Symposium*. Society of Petroleum Engineers. https://doi.org/10.2118/173290-MS

Doorwar, S., & Mohanty, K. K. (2011). Viscous Fingering during Non-Thermal Heavy Oil Recovery. In *SPE Annual Technical Conference and Exhibition*. Society of Petroleum Engineers. https://doi.org/10.2118/146841-MS

Dyes, A. B., Caudle, B. H., & Erickson, R. A. (1954). Oil Production After Breakthrough as Influenced by Mobility Ratio. *Journal of Petroleum Technology*, *6*(4), 27–32. https://doi.org/10.2118/309-G

Engelberts, W. F., & Klinkenberg, L. J. (1951, May). Laboratory experiments on the displacement of oil by water from packs of granular material. In Proceedings 3rd World Petroleum Congress, The Hague (Vol. 2, pp. 544-554).

Flaaten, A. K., Nguyen, Q. P., Zhang, J., Mohammadi, H., & Pope, G. A. (2010). Alkaline/Surfactant/Polymer Chemical Flooding Without the Need for Soft Water. *SPE Journal*, *15*(1), 184–196. https://doi.org/10.2118/116754-PA

Flaaten, A., Nguyen, Q. P., Zhang, J., Mohammadi, H., & Pope, G. A. (2008). ASP Chemical Flooding Without the Need for Soft Water. In *SPE Annual Technical Conference and Exhibition*. Society of Petroleum Engineers. https://doi.org/10.2118/116754-MS

Flaaten, A.K.2007. Experimental Study of Microemuslion Characterization and Optimization in Enhanced Oil Recovery: A Design Approach for Resrvoirs with High Salinity and Hardness. MS Thesis, The University of Texas at Austin, Austin, Texas.

Flory, P. J. (1953). *Principles of polymer chemistry*. Cornell University Press. Retrieved from https://books.google.com/books/about/Principles_of_Polymer_Chemistry.html?id=CQ0EbEkT5R0C

Fortenberry P. R. Experimental Demonstration and Improvement of Chemical EOR Techniques in Heavy Oils. M.S Thesis, University of Texas at Austin, Austin, Texas, 2013.

Fortenberry, R., Kim, D. H., Nizamidin, N., Adkins, S., Arachchilage, G. W. P. P., Koh, H. S., … Pope, G. A. (2015). Use of Cosolvents To Improve Alkaline/Polymer Flooding. *SPE Journal*, *20*(2), 255–266. https://doi.org/10.2118/166478-PA

Gao, B., & Sharma, M. M. (2013). A New Family of Anionic Surfactants for Enhanced-Oil-Recovery Applications. *SPE Journal*, *18*(5), 829–840. https://doi.org/10.2118/159700-PA

Gogarty, W. B. (1967). Mobility Control With Polymer Solutions. *Society of Petroleum Engineers Journal*, *7*(2), 161–173. https://doi.org/10.2118/1566-B

Gogarty, W. B., Meabon, H. P., & Milton, H. W. (1970). Mobility Control Design for Miscible-Type Waterfloods Using Micellar Solutions. *Journal of Petroleum Technology*, *22*(2), 141–147. https://doi.org/10.2118/1847-E-PA

Green, D. W. and Willhite, G. P. 1998. Enhanced oil recovery, SPE Textbook Series, Volume 6, Society of Petroleum Engineers, Richardson, TX, USA.

Habermann, B. (1960). The Efficiency of Miscible Displacement as a Function of Mobility Ratio. 219. 264-72. Trans., AIME

Hallam, R. J., Piekenbrock, E. J., Abou-Sayed, A. S., Garon, A. M., Putnam, T. W., Weggeland, M. C., & Webb, K. J. (1992). Resource Description and Development Potential of the Ugnu Reservoir, North Slope, Alaska. *SPE Formation Evaluation*, *7*(3), 211–218. https://doi.org/10.2118/21779-PA

Healy, R. N., Reed, R. L., & Stenmark, D. G. (1976). Multiphase Microemulsion Systems. *Society of Petroleum Engineers Journal*, *16*(3), 147–160. https://doi.org/10.2118/5565-PA

Hirasaki, G., Miller, C. A., & Puerto, M. (2011). Recent Advances in Surfactant EOR. *SPE Journal*, *16*(4), 889–907. https://doi.org/10.2118/115386-PA

Hirasaki, G. J., van Domselaar, H. R., & Nelson, R. C. (1983). Evaluation of the Salinity Gradient Concept in Surfactant Flooding. *Society of Petroleum Engineers Journal*, *23*(3), 486–500. https://doi.org/10.2118/8825-PA

Hsieh, W. C., & Shah, D. O. (1976). The Effect of Chain Length of Oil and Alcohol As Well as Surfactant to Alcohol Ratio on the Solubilization, Phase Behavior and Interfacial Tension of Oil/Brine/Surfactant/Alcohol Systems. In *SPE International Oilfield and Geothermal Chemistry Symposium*. Society of Petroleum Engineers. https://doi.org/10.2118/6594-MS

Huh, C. (1979). Interfacial tensions and solubilizing ability of a microemulsion phase that coexists with oil and brine. *Journal of Colloid And Interface Science*, *71*(2), 408–426. https://doi.org/10.1016/0021-9797(79)90249-2

Huh, C. (1983). Equilibrium of a Microemulsion That Coexists With Oil or Brine. *Society of Petroleum Engineers Journal*, *23*(5), 829–847. https://doi.org/10.2118/10728-PA

Jang, S. H., Liyanage, P. J., Tagavifar, M., Chang, L., Upamali, K. A. N., Lansakara-P, D., … Pope, G. A. (2016). A Systematic Method for Reducing Surfactant Retention to Extremely Low Levels. In *SPE Improved Oil Recovery Conference*. Society of Petroleum Engineers. https://doi.org/10.2118/179685-MS

Koh H., (2015) Experimental Investigation of the Effect of Polymers on Residual Oil Saturation, PhD Dissertation, University of Texas at Austin

Koh, V.B. Lee, and G.A. Pope, "Experimental Investigation of the Effect of Polymers on Residual Oil Saturation," SPE 179683-PA, SPE Journal, preprint, https://doi.org/10.2118/179683-PA, August, 2017.

Kulawardana, E. U., Koh, H., Kim, D. H., Liyanage, P. J., Upamali, K., Huh, C., … Pope, G. A. (2012). Rheology and Transport of Improved EOR Polymers under Harsh Reservoir Conditions. In *SPE Improved Oil Recovery Symposium*. Society of Petroleum Engineers. https://doi.org/10.2118/154294-MS

Kumar, R., Dao, E., & Mohanty, K. (2012). Heavy-Oil Recovery by In-Situ Emulsion Formation. *SPE Journal*, *17*(2), 326–334. https://doi.org/10.2118/129914-PA

Kumar, R., & Mohanty, K. K. (2010). ASP Flooding of Viscous Oils. In *SPE Annual Technical Conference and Exhibition*. Society of Petroleum Engineers. https://doi.org/10.2118/135265-MS

Kumar, R.2013. Enhanced Oil Recovery of Heavy Oils by Non-Thermal Chemical Methods. PhD dissertation, University of Texas, Austin, TX USA

Lake, L. 1989. Enhanced Oil Recovery. Englewood Cliffs, New Jersey: Prentice Hall

Levitt, D., Jackson, A., Heinson, C., Britton, L. N., Malik, T., Dwarakanath, V., & Pope, G. A. (2009). Identification and Evaluation of High-Performance EOR Surfactants. *SPE Reservoir Evaluation & Engineering*, *12*(2), 243–253. https://doi.org/10.2118/100089-PA

Li, Y., Zhang, W., Kong, B., Puerto, M., Bao, X., Sha, O., … Hirasaki, G. J. (2014). Mixtures of Anionic-Cationic Surfactants: A New Approach for Enhanced Oil Recovery in Low-Salinity, High-Temperature Sandstone Reservoir. *SPE Improved Oil Recovery Symposium*, 1–19. https://doi.org/10.2118/169051-MS

Li, Z., Delshad, M., Lotfollahi, M., Koh, H., Luo, H., Chang, H. L., … Brennan, B. (2014). Polymer Flooding of a Heavy Oil Reservoir with an Active Aquifer. In *SPE Improved Oil Recovery Symposium*. Society of Petroleum Engineers. https://doi.org/10.2118/169149-MS

Liyanage, P. J., Lu, J., Arachchilage, G. W. P., Weerasooriya, U. P., & Pope, G. A. (2015). A novel class of large-hydrophobe tristyrylphenol (TSP) alkoxy sulfate surfactants for chemical enhanced oil recovery. *Journal of Petroleum Science and Engineering*, *128*, 73–85. https://doi.org/10.1016/J.PETROL.2015.02.023

Lu, J., Britton, C., Solairaj, S., Liyanage, P. J., Kim, D. H., Adkins, S., … Pope, G. A. (2012). Novel Large-Hydrophobe Alkoxy Carboxylate Surfactants for Enhanced Oil Recovery. In *SPE Improved Oil Recovery Symposium*. Society of Petroleum Engineers. https://doi.org/10.2118/154261-MS

Luo, H., Al-Shalabi, E. W., Delshad, M., Panthi, K., & Sepehrnoori, K. (2015). A Robust Geochemical Simulator to Model Improved Oil Recovery Methods. In *SPE Reservoir Simulation Symposium*. Society of Petroleum Engineers. https://doi.org/10.2118/173211-MS

Luo, H., Mohanty, K. K., Delshad, M., & Pope, G. A. (2016). Modeling and Upscaling Unstable Water and Polymer Floods: Dynamic Characterization of the Effective Finger Zone. In *SPE Improved Oil Recovery Conference*. Society of Petroleum Engineers. https://doi.org/10.2118/179648-MS

Maerker, J., & Gale, W. (1992). Surfactant Flood Process Design for Loudon. *SPE Eeservoir Engineering*, *7*(1), 36–44. Retrieved from https://www.onepetro.org/journal-paper/SPE-20218-PA

Meter, D. M., & Bird, R. B. (1964). Tube flow of non-Newtonian polymer solutions: PART I. Laminar flow and rheological models. *AIChE Journal*, *10*(6), 878–881. https://doi.org/10.1002/aic.690100619

Mohammadi, H., Delshad, M., & Pope, G. A. (2009). Mechanistic Modeling of Alkaline/Surfactant/Polymer Floods. *SPE Reservoir Evaluation & Engineering*, *12*(4), 518–527. https://doi.org/10.2118/110212-PA

Mohammadi, H. 2008. Mechanistic modeling, design, and optimization of alkaline / surfactant / polymer flooding. Ph.D. Dissertation, The University of Texas at Austin, TX.

Mohanty, K. K. (1983). Multiphase Flow in Porous Media: III. Oil Mobilization, Transverse Dispersion, and Wettability. *SPE Annual Technical Conference and Exhibition*. https://doi.org/10.2118/12127-MS

Moore, T. F., & Slobod, R. L. (1955). Displacement of Oil by Water-Effect of Wettability, Rate, and Viscosity on Recovery. *Fall Meeting of the Petroleum Branch of AIME*. https://doi.org/10.2118/502-G

Nelson, R. C., Lawson, J. B., Thigpen, D. R., & Stegemeier, G. L. (1984). Cosurfactant-Enhanced Alkaline Flooding. In *SPE Enhanced Oil Recovery Symposium*. Society of Petroleum Engineers. https://doi.org/10.2118/12672-MS

Nelson, R. C., & Pope, G. A. (1978). Phase Relationships in Chemical Flooding. *Society of Petroleum Engineers Journal*, *18*(5), 325–338. https://doi.org/10.2118/6773-PA

Panthi, K. K., Sharma, H., & Mohanty, K. K. (2013). ASP Flood of a Viscous Oil in a Carbonate Rock. In *SPE Annual Technical Conference and Exhibition*. Society of Petroleum Engineers. https://doi.org/10.2118/166230-MS

Peters, E. J., & Flock, D. L. (1981, April 1). The Onset of Instability During Two-Phase Immiscible Displacement in Porous Media. Society of Petroleum Engineers. doi:10.2118/8371-PA

Peyton, H. R. (1970). Arctic Engineering. *Journal of Petroleum Technology*, *22*(9), 1076–1082. https://doi.org/10.2118/2701-PA

Pope, G. A., & Nelson, R. C. (1978). A Chemical Flooding Compositional Simulator. *Society of Petroleum Engineers Journal*, *18*(5), 339–354. https://doi.org/10.2118/6725-PA

Pope, G. A., Tsaur, K., Schechter, R. S., & Wang, B. (1982). The Effect of Several Polymers on the Phase Behavior of Micellar Fluids. *Society of Petroleum Engineers Journal*, *22*(6), 816–830. https://doi.org/10.2118/8826-PA

Puerto, M. C., Hirasaki, G. J., Miller, C. A., Reznik, C., Dubey, S., & Barnes, J. R. (2014). Effects of Hardness and Cosurfactant on Phase Behavior of Alcohol-Free Alkyl Propoxylated Sulfate Systems. *SPE Improved Oil Recovery Symposium*, (April 2014), 1–23.

Puerto, M., Hirasaki, G. J., Miller, C. A., & Barnes, J. R. (2012). Surfactant Systems for EOR in High-Temperature, High-Salinity Environments. *SPE Journal*, *17*(1), 11–19. https://doi.org/10.2118/129675-PA

Puig, J. E., Franses, E. I., Davis, H. T., Miller, W. G., & Scriven, L. E. (1979). On Interfacial Tensions Measured With Alkyl Aryl Sulfonate Surfactants. *Society of Petroleum Engineers Journal*, *19*(2), 71–82. https://doi.org/10.2118/7055-PA

Rachford, H. H. (1964, June 1). Instability in Water Flooding Oil from Water -Wet Porous Media Containing Connate Water. Society of Petroleum Engineers. doi:10.2118/684-PA.

Riaz, A., & Tchelepi, H. A. (2006). Numerical simulation of immiscible two-phase flow in porous media. Physics of Fluids (1994-present), 18(1), 014104.

Rosen, M.J. 1989. Surfactants and Interfacial Phenomena. Second edition. New York. John Wiley and Sons.

Saffman, P.G. and Taylor, G. (1958). The Penetration of a Fluid into a Porous Medium or Hele-Shaw Cell Containing a More Viscous Liquid. Proc. R. Soc. Lond. 245 312-329.

Sahni, V., Dean, R. M., Britton, C., Kim, D. H., Weerasooriya, U., & Pope, G. A. (2010). The Role of Co-Solvents and Co-Surfactants in Making Chemical Floods Robust. In *SPE Improved Oil Recovery Symposium*. Society of Petroleum Engineers. https://doi.org/10.2118/130007-MS

Salter, S. J. (1977). The Influence of Type and Amount of Alcohol on Surfactant-Oil-Brine Phase Behavior and Properties. In *SPE Annual Fall Technical Conference and Exhibition*. https://doi.org/10.2118/6843-MS

Sanz, C., & Pope, G. (1995). Alcohol-Free Chemical Flooding: From Surfactant Screening to Coreflood Design. *Proceedings of SPE International Symposium on Oilfield Chemistry*, 117–128. https://doi.org/10.2523/28956-MS

Sharma, H., Weerasooriya, U., Pope, G. A., & Mohanty, K. K. (2014). SPE170825-MS Ammonia-Based ASP Processes for Gypsum-Containing Reservoirs. In *SPE Annual technical conference and exhibition*. https://doi.org/10.2118/170825-MS

Sheng, J. (2013). *Enhanced oil recovery field case studies*. Gulf Professional Publishing.

Sheng, J.J. Modern Chemical Enhanced Oil Recovery: Theory and Practice. Elsevier, Burlington, MA, 2011.

Solairaj S. 2011. New Method of Predicting Optimum Surfactant Structure for EOR. M.S Thesis, University of Texas at Austin, Austin, Texas.

Sorbie, K.S., 1991. Polymer-Improved Oil Recovery. CRC Press.

Stegemeier, G. L. (1977). MECHANISMS OF ENTRAPMENT AND MOBILIZATION OF OIL IN POROUS MEDIA. In *Improved Oil Recovery by Surfactant and Polymer Flooding* (pp. 55–91). https://doi.org/10.1016/B978-0-12-641750-0.50007-4

Taber, J. J., Martin, F. D., & Seright, R. S. (1997). EOR Screening Criteria Revisited - Part 1: Introduction to Screening Criteria and Enhanced Recovery Field Projects. *SPE Reservoir Engineering*, *12*(3), 189–198. https://doi.org/10.2118/35385-PA

Tagavifar, M., Fortenberry, R., de Rouffignac, E., Sepehrnoori, K., & Pope, G. A. (2016). Heavy-Oil Recovery by Combined Hot Water and Alkali/Cosolvent/Polymer Flooding. *SPE Journal*, *21*(1), 074–086. https://doi.org/10.2118/170161-PA

Tagavifar, M., Herath, S., Weerasooriya, U. P., Sepehrnoori, K., & Pope, G. (2016). Measurement of Microemulsion Viscosity and Its Implications for Chemical EOR. In *SPE Improved Oil Recovery Conference*. Society of Petroleum Engineers. https://doi.org/10.2118/179672-MS

Upamali, P.J. Liyanage, J. Cai, J. Lu, S.H. Jang, U.P.Weerasooriya, and G.A. Pope, "New Surfactants and Co-Solvents Increase Oil Recovery and Reduce Cost," SPE 179702-MS, presented at the SPE Improved Oil Recovery Conference, Tulsa, OK, April 11-13, 2016.

Van Meurs, P. (1957, January 1). The Use of Transparent Three-Dimensional Models for Studying the Mechanism of Flow Processes in Oil Reservoirs. Society of Petroleum Engineers.

Wade, W. H., Morgan, J. C., Jacobson, J. K., & Schechter, R. S. (1977). Low Interfacial Tensions Involving Mixtures of Surfactants. *Society of Petroleum Engineers Journal*, *17*(2), 7–8. https://doi.org/10.2118/6002-PA

Walker, D.L. Experimental Investigation of the Effect of Increasing the Temperature of ASP Flooding, M.S. Thesis, The University of Texas at Austin, Austin, Texas, 2011.

Walker, C. Britton, D.H. Kim, S. Dufour, U. Weerasooriya, and G.A. Pope, "The Impact of Microemulsion Viscosity on Oil Recovery," SPE 154275, presented at the Eighteenth SPE Improved Oil Recovery Symposium held in Tulsa, OK, April 14-18, 2012.

Wang, D., Liu, C., Wu, W., & Wang, G. (2010). Novel Surfactants that Attain Ultra-Low Interfacial Tension between Oil and High Salinity Formation Water without adding Alkali, Salts, Co-surfactants, Alcohols and Solvents. In *SPE EOR Conference at Oil & Gas West Asia*. Society of Petroleum Engineers. https://doi.org/10.2118/127452-MS

Wassmuth, F. R., Green, K., Arnold, W., & Cameron, N. (2009). Polymer Flood Application to Improve Heavy Oil Recovery at East Bodo. *Journal of Canadian Petroleum Technology*, *48*(2), 55–61. https://doi.org/10.2118/09-02-55

Winsor, P., 1954. Solvent Properties of Amphilic Compounds. Butterworths, London.

Worawutthichanyakul, T., & Mohanty, K. K. (2017). Unstable Immiscible Displacements in Oil-Wet Rocks. *Transport in Porous Media*, *119*(1), 205–223. https://doi.org/10.1007/s11242-017-0880-6

Yang, H., Britton, C., Liyanage, P. J., Solairaj, S., Kim, D. H., Nguyen, Q., Weerasooriya, U., Pope, G. A. (2010). Low-Cost , High-Performance Chemicals for Enhanced Oil Recovery. *Spe 129978*, (1998). https://doi.org/10.2118/129978-MS

Zhang, G., Yu, J., Du, C., & Lee, R. (2015). Formulation of Surfactants for Very Low/High Salinity Surfactant Flooding without Alkali. In *SPE International Symposium on Oilfield Chemistry*. Society of Petroleum Engineers. https://doi.org/10.2118/173738-MS

Zhang, J., Ravikiran, R., Freiberg, D., & Thomas, C. P. (2012). ASP Formulation Design for Heavy Oil. In *SPE Improved Oil Recovery Symposium*. Society of Petroleum Engineers. https://doi.org/10.2118/153570-MS

Zhao, P., Jackson, A. C., Britton, C., Kim, D. H., Britton, L. N., Levitt, D. B., & Pope, G. A. (2008). Development of High-Performance Surfactants for Difficult Oils. *Spe 113432*, (1992). https://doi.org/10.2118/113432-MS

VITA

Almas Aitkulov was born in Taraz, Kazakhstan. After completing his work at Physics-Mathematics School for Gifted Children, Almaty, Kazakhstan, in 2006, he entered Texas A&M University. In 2010, he transferred to the University of Texas at Austin, Austin, Texas. He received the degree of Bachelor of Science in Petroleum Engineering from the University of Texas at Austin, Austin in May 2012. In September, 2012, he entered the Graduate School at the University of Texas at Austin.

Address: almas.aitkulov@yahoo.com

This manuscript was typed by the author.